The role of the ammonia transporter RhCG in systemic acid-base homeostasis

Dissertation zur Erlangung der naturwissenschaftlichen
Doktorwürde (Dr. sc. nat.)
vorgelegt der Mathematisch-naturwissenschaftlichen Fakultät
der Universität Zürich

von

Lisa Bounoure

aus Frankreich

Promotionskomitee:

Prof. Dr. Carsten A. Wagner
Prof. Dr. med. Olivier Devuyst
Dr. Soline Bourgeois
Dr. Yves Colin

Zürich, 2013

TABLE OF CONTENTS

Summary

Several conditions, from dietary metabolism to various disease states, induce changes of systemic acid-base balance. Excretion of fixed acid or alkali equivalentsinto urine is directed by the kidneys and critically participates in the regulation of blood pH homeostasis. The ammonium (NH_4^+)/ ammonia (NH_3) buffering system plays a major role to correct an extra acid load. In the collecting duct (CD) of kidneys, type-A intercalated cells mediate the removal of acids in the form of NH_3 and protons (H^+) and produce new bicarbonate (HCO_3^-). Urinary H^+ secretion is mediated by active transport by vacuolar H^+-ATPases (H^+-ATPases). In the lumen,protonstrap NH3 molecules, resulting in NH_4^+ formation in urine. For long considered as a solely passive mechanism, the transport of NH_3 in thecollecting duct of kidney is critically mediated by the NH_3transporterRhCG.

In acid-loading conditions, mice deficient for *Rhcg* (*Rhcg*$^{-/-}$) are not able to excrete a proper amount of $NH_4^+$and show a more alkaline urine than wildtype animals.In humans, patients with impaired capacity to acidify urine develop distal renal tubular acidosis (dRTA). In particular, mutations affecting isoforms of the H^+-ATPase found in kidney CD type-A intercalated cells cause the development of inherited forms of dRTA in humans and rodents.After a chronic acid-loading period, an incomplete form of dRTA also appears in *Rhcg*$^{-/-}$ mice.

The present dissertation aimed to understand the importance of RhCG in controlling systemic acid-base homeostasis. To this end, three projects were developed.

First, using a novel model of *Rhcg*$^{+/+,\ +/-}$and $^{-/-}$ mice receiving a HCl diet for 2 or 7 days, we studied the effect of a single allele or complete deletion of *Rhcg* on acid-base status and NH_3 transport across CCD cells, in order to determine to which extend Rhcg deficiency can induce metabolic acidosis. To clarify the role of Rhcg on the basolateral side of the CD cells, we assessedthe basolateral transport of NH_3 inmicroperfused cortical collecting ducts of *Rhcg*$^{+/+,\ +/-}$and $^{-/-}$ mice.Finally, adaptation mechanisms occurring in

kidneys of *Rhcg*$^{+/+,+/-}$and $^{-/-}$ mice in response to the HCl acid-load were also inspected.

In a second project, we studied *Rhcg*$^{+/+,+/-}$and $^{-/-}$ mice to determine the role of Rhcg in conditions of a physiological requirement for enhanced NH_4^+ excretion into urine, such as the consumption of a high protein diet, which is typical of a western life style.

Finally, we examined the possibility of a functional interaction between Rhcg and vacuolar H^+-ATPases in type-A intercalated cells of kidneys in order to detail the molecular pathway responsible for urinary acidification in the collecting duct of kidneys.

While *Rhcg*$^{+/+}$ and *Rhcg*$^{+/-}$ were able to adapt a 2-days HCl acid-load in food, *Rhcg*$^{-/-}$mice developedmetabolic acidosis with lower urinary$NH_4^+$and more alkaline urine. In addition,*Rhcg*$^{+/-}$ micealso developed metabolic acidosis after 7 days of HCl diet and most of the *Rhcg*$^{-/-}$ animals died before the end of the acid-loading period.Microperfusion studies of kidney cortical collecting ducts (CCDs) demonstrated that NH_3 transepithelial permeability was reduced by 54% and 80% respectively in CCDs from *Rhcg*$^{+/-}$ and *Rhcg*$^{-/-}$ mice compared to wildtype, confirming that a 50% reduction of Rhcg activity is enough to impair the kidney collecting duct response to a strong acid-load, and result in chronic metabolic acidosis. The apical but also basolateral permeability of CCD cells of kidneys was reducedin *Rhcg* knockout mice, attesting for Rhcg function in basolateral transport of NH_3.*Rhcg*$^{+/-}$ mice exhibited a strong reduction in apical NH_3 permeability only. Finally, reduced protein expression levels of the $Na^+/K^+/2Cl^-$ isoform 2 (NKCC2) co-transporter expressed in the thick ascending limb of the loop of Henle (TAL) was paralleled by lower concentrations of NH_4^+ in the inner medullary tissue of *Rhcg*$^{-/-}$ mice, suggesting an influence of Rhcg on the NH_3/NH_4^+cortico-papillary gradient formation or maintenance.

High protein diets from animal sources, which characterize the typical western diet, increase urinary NH_4^+ excretion in kidneys. Harmfuleffects of protein-rich diets on bone and kidney function have been described in animal models and humans with normal and reduced kidney function. However,

mechanisms by which high protein diets act on renal acid excretion have not been examined in detail. We studied the impact ofanacid-loading high protein diet as casein (HC diet)on *Rhcg*$^{+/+}$, $^{+/-}$ and $^{-/-}$ mice. After a transient decrease of blood pH and HCO_3^- in all genotypes, we described a similaradaptation to 9 days HC diet in *Rhcg*$^{+/+}$and *Rhcg*$^{+/-}$ mice, which enhanced the Na^+/glutamine co-transporter SNAT3 and the ammoniagenic enzyme PDG (Phosphate Dependent Glutaminase) involved inNH_4^+ production in the proximal tubule.*Rhcg*$^{-/-}$mice displayed an even stronger enhancement of these mechanisms, possibly as compensation.Non-acidogenic high protein diet as soy (HS diet) was used as a control and did not induce an acid-load of*Rhcg*$^{+/+}$, $^{+/-}$ and $^{-/-}$animals. In *Rhcg*$^{+/+}$ mice,protein expression levels of NKCC2 and the H_2O channel isoform 2 (AQP2)were decreased by theacidogenic HC diet paralleled by increased urinary volume. In *Rhcg*$^{-/-}$ compared to *Rhcg*$^{+/+}$ mice, we observed higher NKCC2 protein expression as well as tissue NH_4^+ concentration in the inner medulla after 4 days HC diet, but both were lowered after 9 days of the HC diet when higher urinary volumes were also observed. Our data suggest an original adaptive process of the kidney to an acidogenic high protein diet, involving a direct elimination of NH_4^+ into urine, which seems to be exacerbated by the absence of Rhcg. Our data eventually showed increased signs of bone resorption in *Rhcg*$^{-/-}$in the form ofhypercalcemia, hypercalciuria, increased deoxypyrydinoline (Dpd) and reduced bone mineral density in the cortical femur layer affected by HC diet.This study demonstrated the importance of Rhcg in the management of a physiological acid-load and suggests extra-renal effects of Rhcg.

In addition to reduced urinary NH_4^+ excretion, *Rhcg*$^{-/-}$ mice had more alkaline urine. Accordingly, we observed in microperfused CCD from *Rhcg*$^{-/-}$ mice a defect in NH_3 transport and a decrease in H^+ secretion compared to wildtype mice. We thus aimed to study a potentialfunctional interaction between Rhcg andthe multi-unit protein vacuolar H^+-ATPase (H^+-ATPase), which constitutes the main H^+ transport system in the collecting ducttype-A intercalated cells.*Rhcg*$^{-/-}$compared to $^{+/+}$ did not display any differential mRNA expression regulation of various H^+-ATPase subunits, but increased protein levels of B1 and reduced levels of the B2 isoform.Moreover, immunogold

electron-microscopy demonstrated similar subcellular localization of the ubiquitous A subunit of the vacuolar H^+-ATPase. HEK293 cells overexpressing RhCG exhibited higher H^+ fluxes compared to mock transfected cells together with enhanced levels of ATP6V1B1 mRNA. Finally, we investigated whether an opposite regulation could also occur by using an H^+-ATPase inhibitor, concanamycin, and mice lacking the B1 subunit of the H^+-ATPase (*Atp6v1b1*$^{-/-}$) that display reduced H^+-ATPase activity in CCD type-A intercalated cells.The H^+-ATPase inhibitor concanamycin reduced both H^+-ATPase and Rhcg activity in microperfused CCDs. However, *Atp6v1b1*$^{-/-}$ mice receiving 2 days HCl diet had lower H^+-ATPase activity than wildtype, but revealedapical and basolateral NH_3membrane permeabilities in microperfused CCD cells comparableto wildtype animals,attesting that a reduced H^+-ATPase activityhad no impact on Rhcg activity. This study demonstrates a functional interaction where Rhcg is necessary forfullfunction of the vacuolar H^+-ATPase in the collecting duct, although further experiments are needed to characterize this interaction.

In conclusion, this work confirms and details the central role of Rhcg in the final step of NH_4^+excretion by the kidney and opens new perspectives regarding the role of Rhcg in the regulation of H^+ transport by the collecting duct.

Deutsche Zusammenfassung der Doktorarbeit

Multiple Faktoren, welche durch ein breites Kontinuum vom gesunden Metabolismus bis zu pathologischen Krankheitsbildern bedingt sind, können zu Veränderungen des systemischen Säure-Base-Gleichgewichts führen. Die Ausschüttung von fixen Säure- und Base-Anteilen in den Urin wird durch die Nieren gesteuert, damit spielen diese eine zentrale Rolle in der Regulierung der Homöostase des Blut pH-Wertes. Das Ammonium (NH_4^+) / Ammoniak (NH_3) Puffersystem ist bedeutend für die Korrektur von schwankenden Säureladungen. In den Sammelrohren der Nieren vermitteln Typ A Schaltzellen eine Reduktion von Säure indem sie NH_3 und Protonen (H^+) aus dem Blut entfernen, während sie gleichzeitig Bikarbonate (HCO_3^-) produzieren. Die H^+-Sekretion wird durch einen aktiven Transport durch die vakuolare H^+-ATPase vermittelt. Protonen werden durch NH_3 Moleküle im Lumen eingefangen, dabei wird NH_4^+ im Urin angereichert. Langezeit wurde angenommen, dass es sich dabei lediglich um einen passiven Mechanismus handelt, doch neuere Forschungsergebnisse zeigen, dass der NH_3-Transporter RhCG (Rhesus Blutgruppen-assoziiertes C Glykoprotein) eine wichtige Rolle für den Transport von NH_3 in den Sammelrohren der Nieren spielt.

In säuregeladenen Zuständen können Mäuse, die kein Rhcg ($Rhcg^{-/-}$) besitzen, nicht die nötige Menge an NH_4^+ ausscheiden und ihr Urin ist in der Folge stärker alkalisch als beim Wildtyp. Menschen, welche in der Fähigkeit den Urin anzusäuren, eingeschränkt sind, können an einer distalen renal-tubulären Azidose (dRTA) erkranken. Insbesondere Mutationen, welche die Isoform der H^+-ATPase der Typ A Schaltzellen im Sammelrohr der Niere betreffen, können in einer erblichen Form der dRTA bei Menschen und Nagern resultieren. Nach einer chronischen Säureanreicherungsperiode, kommt es auch bei $Rhcg^{-/-}$ Mäusen zu einer eingeschränkten Form der dRTA.

Das Ziel dieser Dissertation ist das Verständnis der Wichtigkeit von Rhcg für die Kontrolle der systemischen Säure-Base-Homöostase. Zu diesem Zweck wurden drei Projekte ins Leben gerufen.

Als erstes haben wir den Effekt der einzelnen und kompletten Deletion von Rhcg auf den Säure-Base-Haushalt und den NH_3-Transport durch Sammelrohrzellen untersucht. Wir haben dazu ein neues Model von Rhcg$^{+/+}$, $^{+/-}$ und $^{-/-}$ Mäusen, welche während 2 oder 7 Tagen eine HCl (Salzsäure) Diät erhielten, verwendet und analysiert inwiefern ein Rhcg Verlust zur metabolischen Azidose führt. Um sicherzustellen welche Rolle Rhcg auf der basolateralen Seite von Sammelrohrzellen spielt, haben wir den basolateralen Transport von NH_3 in mikroperfusionierten kortikalen Sammelrohren von Rhcg$^{+/+}$, $^{+/-}$ und $^{-/-}$ Mäusen beobachtet. Schliesslich haben wir auch Anpassungsmechanismen in den Nieren von Rhcg$^{+/+}$, $^{+/-}$ und $^{-/-}$ Mäusen an die HCl Säureladung untersucht.

In der Folge haben wir in einem zweiten Projekt an Rhcg$^{+/+}$, $^{+/-}$ und /- Mäusen die Rolle von Rhcg in einer physiologischen Situation in der eine vermehrte Ausscheidung von NH_4^+ in den Urin nötig wird, analysiert. Diese Erhöhung wird durch eine, für die westliche Lebensweise typische, proteinreiche Diät gefördert.

Schliesslich wurde die Möglichkeit einer Interaktion zwischen Rhcg und der vakuolaren H^+-ATPase in den Typ A Schaltzellen mit dem Ziel die unterliegenden molekularen Signalwege, welche für die Ansäuerung des Urins in den Sammelzellen der Nieren verantwortlich sind, zu verstehen, erforscht.

Während sich die Rhcg$^{+/+}$ und $^{+/-}$ Mäuse an die 2-tägige HCl Säurezufuhr in ihrer Nahrung anpassen konnten, entwickelten die Rhcg$^{-/-}$ Mäuse eine metabolische Azidose mit erniedrigter NH_4^+ Sekretion und sie produzierten einem stärker alkalischen Urin. Zusätzlich haben auch die Rhcg$^{+/-}$ Mäuse innerhalb von sieben Tagen der HCl Diät eine metabolische Azidose entwickelt und die meisten Rhcg$^{-/-}$ Mäuse starben vor Ende der Säurezufuhrperiode. Die Mikroperfusionsstudien der Sammelrohre der Nieren zeigten, dass die transepithelialen Durchlässigkeiten für NH_3 bei Rhcg$^{+/-}$ Tieren zu 54 % und bei Rhcg$^{-/-}$ zu 80 % reduziert wurden, wenn diese mit dem Wildtyp verglichen wurden. Damit bestätigten wir, dass eine 50 %-ige Reduktion der Rhcg Aktivität ausreicht um die Antwort der Sammelrohre auf eine starke Säureanreicherung zu minimieren, in welchem Fall es schliesslich

zu einer chronischen metabolischen Azidose kommt. Die apikalen und basalen Permeabilitäten der Sammelzellen der Nieren wurden bei Rhcg-Knockout Mäusen reduziert, was die Funktion von Rhcg im basolateralen Transport von NH_3 bestätigt. $Rhcg^{+/-}$ Mäuse zeigten lediglich eine starke Reduktion der apikalen NH_3 Permeabilität. Schliesslich stellten wir parallel mit einer verminderten Proteinexpression der $Na^+/K^+/2Cl^-$ Isoform 2 (NKCC2) des Ko-Transporters des dicken aufsteigenden Tubulus der Henle-Schleife, auch eine verminderte NH_4^+-Konzentration im inneren Markgewebe der $Rhcg^{-/-}$ Mäuse fest, was darauf hinweist, dass Rhcg einen Einfluss auf die Bildung oder Erhaltung des kortikopapillären NH_3/NH_4^+ Gradienten hat.

Proteinreiche Diäten tierischen Ursprungs, welche für den westlichen Lebensstil typisch sind, erhöhen in den Nieren die Ausscheidung von NH_4^+ in den Urin. Die schädlichen Effekte solcher Diäten, die insbesondere die Knochen und Nierenfunktion beeinträchtigen, wurden bereits in Tiermodellen und auch an Menschen mit normaler und reduzierter Nierenfunktion, untersucht. Die genauen Mechanismen, durch welche proteinreiche Ernährung sich auf die renale Säureausscheidung auswirkt, wurden bisher nicht im Detail etabliert. Wir haben den Einfluss einer säureanreichernden proteinreichen Ernährung wie Käsein auf $Rhcg^{+/+}$, $^{+/-}$ und $^{-/-}$ Mäuse erforscht. Nach einer vorübergehenden Senkung des Blut-pHs und HCO_3^- in allen Genotypen, haben wir eine ähnliche Adaptation von $Rhcg^{+/+}$ und $^{+/-}$ bei einer 9-tägigen proteinreichen Ernährung festgestellt. Die Funktionen des Na^+/Glutamin Kotransporters SNAT3 und des ammoniagenen Enzyms PDG (phosphate dependent glutaminase), welches in der Produktion von NH_4^+ im proximalen Tubulus involviert ist, wurden erhöht. $Rhcg^{-/-}$ Mäuse haben dabei sogar eine stärkere Erhöhung dieser Mechanismen aufgezeigt, was möglicherweise der Kompensation dient. Eine nicht-säurehaltige proteinreiche Ernährung auf der Basis von Soja wurde als Kontrolle verwendet und hat keine Säureladung bei $Rhcg^{+/+}$, $^{+/-}$ und $^{-/-}$ Mäusen induziert. Bei den $Rhcg^{+/+}$ Mäusen wurde während einer säurehaltigen Diät, welche auf Käsein basierte, die Expression von NKCC2 und die Isoform 2 des H_20-Kanals (AQP2) herunterreguliert, während das Volumen des Urins zunahm. Im Vergleich von $Rhcg^{-/-}$ Mäusen mit $Rhcg^{+/+}$ Tieren zeigte sich, dass die NKCC2 Protein

Expression, sowie die NH_4^+ Konzentration im Gewebe der inneren Medulla nach 4 Tagen der Käsein-Diät zunahmen, wobei die Expression bei beiden Gruppen nach 9 Tagen abnahm und wiederum höhere Urinvolumen beobachtet wurden. Unsere Ergebnisse deuten darauf hin, dass die Nieren anfänglich mit einem Anpassungsprozess auf die proteinreiche Diät reagieren, wobei NH_4^+ direkt in den Urin ausgeschieden wird, diese Anpassung ist bei einem Fehlen von Rhcg eingeschränkt. Schliesslich haben wir bei den $Rhcg^{-/-}$ Mäusen auch erhöhte Zeichen von Knochenresorption in Form von Hyperkalzämie, Hyperkaliurie, und erhöhter Deoxypyridinoline (Dpd) und verminderter Knochendichte in der kortikalen Schicht des Femurs der Versuchstiere als Folge der proteinreichen Diät beobachtet. Diese Ergebnisse unterstreichen die Wichtigkeit von Rhcg in der Regulierung des physiologischen Säure-Base-Haushalts und lassen uns vermuten, dass Rhcg auch ausserhalb der Niere Einflüsse hat.

Nebst der reduzierten NH_4^+ Exkretion werden die $Rhcg^{-/-}$ Tiere auch durch einen basischeren Urin charakterisiert. In diesem Zusammenhang konnten wir bei den $Rhcg^{-/-}$ Tieren im Vergleich mit dem Wildtyp auch einen Defekts des NH_3 Transports und eine gleichzeitige Verminderung der H^+ Sekretion beobachten. Aufgrund dieser Feststellungen wollten wir eine potentielle funktionelle Interaktion zwischen Rhcg und der vakuolaren Multi-Unit-Protein H^+-ATPase (H^+-ATPase) untersuchen. Die H^+-ATPase ist das Haupttransportsystem in den Typ A Schaltzellen der Sammelrohre. Beim Vergleich von $Rhcg^{-/-}$ und $^{+/+}$ konnten wir keinen Unterschied in der mRNA Expression der Regulation der verschiedenen Untereinheiten der H^+-ATPase feststellen, doch die Proteinmenge von B1 war erhöht, während die B2-Isoform durch eine verminderte Proteinmenge charakterisiert wurde. Schliesslich zeigte die Immunogold-Elektronenmikroskopie eine ähnliche intrazelluläre Lokalisation der A-Untereinheit der vakuolaren H^+-ATPase. HEK293 Zellen, welche vermehrt RhCG expressionierten, zeichneten sich durch höhere H^+-Ströme aus, wenn wie mit Zellen, welche nur vorgetäuscht transfizierten wurden, verglichen wurden und auch die Menge an ATP6V1B1 mRNA war in den Rhcg Zellen erhöht. Schliesslich haben wir auch untersucht, ob der Gebrauch eines H^+-ATPase Inhibitors, Cocanamycin, zu

einer entgegengesetzten Regulation führen könnte und ob Mäuse, die keine B1-Untereinheit der H^+-ATPase (Atp6v1b1$^{-/-}$) besitzen, eine reduzierte H^+-ATPase Aktivität in den Typ A Schaltzellen des Sammelrohres aufzeigen. Der H^+-ATPase Inhibitor Concanamycin reduzierte gleichzeitig die Aktivität der H^+-ATPAse und Rhcg in mikroperfundierten Sammelrohren. Atp6v1b1$^{-/-}$ Mäuse, welche während 2 Tagen eine HCl Diät erhielten, zeigten im Vergleich mit dem Wildtyp, eine verminderte H^+-ATPase Aktivtät, doch die apikale und basolaterale NH_3 Permeabilität der Membranen der mikroperfundierten Schaltzellen in den Sammelrohren blieb unverändert, was zum Schluss führt, dass die Reduktion der H^+-ATPase Aktivität keinen Einfluss auf die Aktivität von Rhcg hat. Diese Arbeit enthüllt damit eine funktionelle Interaktion, welche von Rhcg abhängig ist. Rhcg ist bedeutend für die volle Funktion der vakuolaren H^+-ATPase des Sammelrohrs. Für eine genauere Charakterisierung dieser Interaktion sind weitere Experimente notwendig.

Diese Dissertation bestätigt und erläutert die zentrale Rolle von Rhcg im letzten Schritt der NH_4^+ Sekretion in den Nieren und eröffnet gleichzeitig neue Perspektiven bezüglich der Rolle von Rhcg in der Regulation des H^+-Transports im Sammelrohr der Niere.

I Introduction

Although ammonia (NH_3) was not characterized as a gas before 1774[1], as early as in the Middle Ages, the presence of ammonium (NH_4^+) in urine was known. Textile dyers used natural dyes from plant and animal sources to obtain colored fabric. The majority of those dyes required the use of a "mordant", a chemical entity enabling the fixation of the dye to the fabric, like urinary $NH_4^+$from fermented urine[2].

More than 1000 years later, in 1921, the physiological role of urinary NH_4^+ started to be elucidated by Nash and Benedict who proved that NH_3 is produced by the kidney and serves as a blood acidity buffering system[3]. In 1945, Robert Pitts described the role of NH_4^+ excretion in renal acid elimination, postulating that NH_3 diffuses across the luminal membrane of epithelial cells following a passive diffusion process[4,5]. This knowledge remained unchanged until 2000 when Marini *et al.* provided the first experimental evidences for a proteindirectly responsible for NH_3transport across cells in humans[6].

In 2008, Biver and co-workers characterized*in vivo* the first and so far only protein known to be responsible for NH_3 passage in the kidney collecting duct: the Rhesus factor glycoprotein C, RhCG[7]. This dissertation presents the main findings following this seminal study and clarifies the role of RhCG in systemic acid-base homeostasis maintenance.

I.1 The role of the kidneys in acid-base balance

In a normal subject, acid-base balance is permanently challenged by respiratory and metabolic alterations. Respiration discharging CO_2 or dietary intake and metabolism constantly modify blood chemical composition, and, in particular, blood pH homeostasis. A tight control of systemic acid-base status plays a critical role in maintaining a stable state of the entire body and individual cells to ensure the essential living functions[8]. Outside an acceptable range of pH, proteins are denaturated and enzymes loose their ability to

function. To maintain a proper digestive function, the gastric acid pH must range from 1.5 to 3.5. With a pH of 4.8, the intracellular organelles lysosomes are able to properly break down waste material and cellular debris.
In physiological conditions, the respiratory system gives the fastest response to prevent dramatic changes of the normal blood pH value (7.4). To regulate p_{CO2},the lungs are responsible for the exhalation of CO_2 through the lung epithelium. When ventilation problems occur and blood p_{CO2} cannot be properly controlled, increased p_{CO2} leads to respiratory acidosis where the blood pH value drops belowpH 7.4. A reduced p_{CO2} would increase blood pH above the value of 7.4, therefore inducing respiratory alkalosis[9].

Despite the critical action of the respiratory system in maintaining proper acid and base levels of the inner compartment, the equilibrium would be precarious without the non-volatile organism buffering system. The major blood buffering entity is bicarbonate (HCO_3^-). While HCO_3^- is permanently produced and regenerated, extra acid or alkaline loads are cleared from the blood. The kidney is the organ responsible for this maintenance of the organisms buffering power. Kidneys are also responsible for other essential processes: blood filtration, eliminationof toxic substances and returning of the useful ones, and blood pressure management. They also secrete different hormones involved in erythropoiesis, calcium absorption and blood pressure regulation[10]. The functional unit of kidneys, the nephron, consists of a glomerulus and a tubule. Blood is first filtrated through the glomerulus and the filtrate reaches later the tubular compartment. The tubule is an epithelial structure shaped of many subdivisions designed to convert the glomerular filtrate into urine. The composition of the glomerular filtrate shows the same solute concentrations than plasma with similar amounts of low molecular weight proteinsand less high molecular weight compounds and protein-bound solutes. The kidney requires a large glomerular filtration rate (GFR) of 125mL/min in order to eliminate rapidly body wastes present in the plasma and potential toxic materials[9].

At the level of the tubule, three interrelated mechanisms take place to cope with either excess acid loads produced by metabolism, diet and

intestinal losses or to handle an alkaline charge: the reabsorption of HCO_3^- filtered from the blood, the *de novo*formation of HCO_3^- and the elimination of excess acid or alkali into urine via the production and excretion of protons and protons-binding buffers in different parts of the nephron.

Almost 80% of the filtered HCO_3^- is reclaimed virtually along the proximal tubule. Most of the protons (H^+) that the proximal tubule secretes via the Na^+/H^+ exchanger isoform 3 NHE3 and vacuolar H^+-ATPases titrate the filtered HCO_3^-forming H_2CO_3, which is, in turn, dissociated by the membrane-bound enzyme carbonic anhydrase IV to yield CO_2 and H_2O. The water channel Aquaporine isoform 1 (AQP1) is then responsible for the apical transport of CO_2 and H_2O into the proximal tubule cells. The cytoplasmic carbonic anhydrase II enzyme catalyzes the formation of $H_2CO_3$from CO_2 and H_2O, which, ultimately, dissociates into H^+ and HCO_3^-[11]. The HCO_3^-ions produced are reabsorbed by the basolateral electrogenic Na^+/HCO_3^- co-transporter isoform 1(NBCe1) and replace the consumed molecules.The remaining HCO_3^- is reabsorbed by the thick ascending limb of the Loop of Henle (TAL) and, to a smaller extent, by the distal nephron.

Excess acids are buffered by ammonium (NH_4^+) and titratable acids before their excretion into urine[12]. The kidney filters titratable acids, mostly represented by phosphate, creatinine and urate, which bind protons and trap them in urine. The NH_3/NH_4^+ system is more complex and plays a major role in renal acid-base regulation. NH_3 is generated by the kidney andbinds protons at the level of the proximal tubule to form NH_4^+, which is excreted in the lumen and later reabsorbed by the TAL into the renal interstitium where it accumulates to create a cortico-papillary gradient of NH_3/NH_4^+. Finally, NH_3 is excreted into the lumen of the collecting duct where H^+ are trapped, leading to the excretion of acid in the form of NH_4^+. Protons not buffered by titratable acids and NH_3cause urinary acidification.

I.2 Regulation of renal ammoniummetabolism

$NH_4^+$is first produced in the proximal tubule cellsessentially by the metabolism of amino acids and mainly glutamine. In the proximal tubule, glutamine enters the epithelial cells through the Na^+/glutamine co-transporter SNAT3, and, later on, enters the mitochondria. NH_3 is then produced from glutamine by a cascade of deaminations involving the mitochondrial enzymes PDG (Phosphate Dependent Glutaminase) and GDH (Glutamine dehydroxylase) and producing α-ketoglutarate[13,14].Inside the cytoplasm of the proximal tubule cells, the NH_3 molecules produced bind protons to form NH_4^+. α-Ketoglutarate is ultimately converted to oxaloacetate, which in turn is converted to phosphoenolpyruvate and carbon dioxide via the action of phosphoenolpyruvate carboxykinase (PEPCK), a cytosolic gluconeogenic enzyme. These reactions ultimately lead to HCO_3^- generation and glucose production in the proximal tubule cells[15,16]. On the apical pole of the proximal tubule cells, the Na^+/H^+ exchanger isoform 3, NHE3, drives most of the NH_4^+produced in the cells into the lumen, the remaining part reaching the renal vein where NH_4^+will be detoxified by the liver to urea and glutamine[17].

After its production and active secretion into the luminal fluid, most of luminal NH_4^+ is then reabsorbed into the interstitium by the thick ascending limb (TAL) of the Loop of Henle to create a cortico-papillary gradient of NH_3 and NH_4^+[18]. Transcellular pathways chiefly reabsorb the bulk of NH_4^+ in this segment. On the luminal side, the main mechanism is achieved by the apical $Na^+/K^+/2Cl^-$isoform 2 NKCC2 co-transporter[19]while the basolateral Na^+/H^+ exchanger isoform 4 NHE4[20] and the electroneutral Na^+/HCO_3^- coptransporter isoform 1 (NBCn1, not represented in Figure 1) are involved in the NH_4^+ reabsorption and final accumulation in the interstitial tissue[21].

The final step of the NH_4^+ route along the nephron occurs in the distal nephron segments. An increasing gradient of NH_4^+ is formed in the connecting tubule (CNT), the cortical collecting duct (CCD), the outer medullary collecting duct (OMCD) and the inner medullary collecting duct

(IMCD). In the collecting duct, type-A intercalated cells mediate acid secretion and bicarbonate reabsorption. Acids are excreted in urine the form of protons by active transport of H^+ mostly operated by vacuolar H^+-ATPases (H^+-ATPases)[22]. The titration of protons in the form of NH_4^+in the final urine result from NH_3diffusion and, more importantly, from NH_3 transport into the lumen by the Rhesus factor glycoprotein C (RhCG)[23,24].

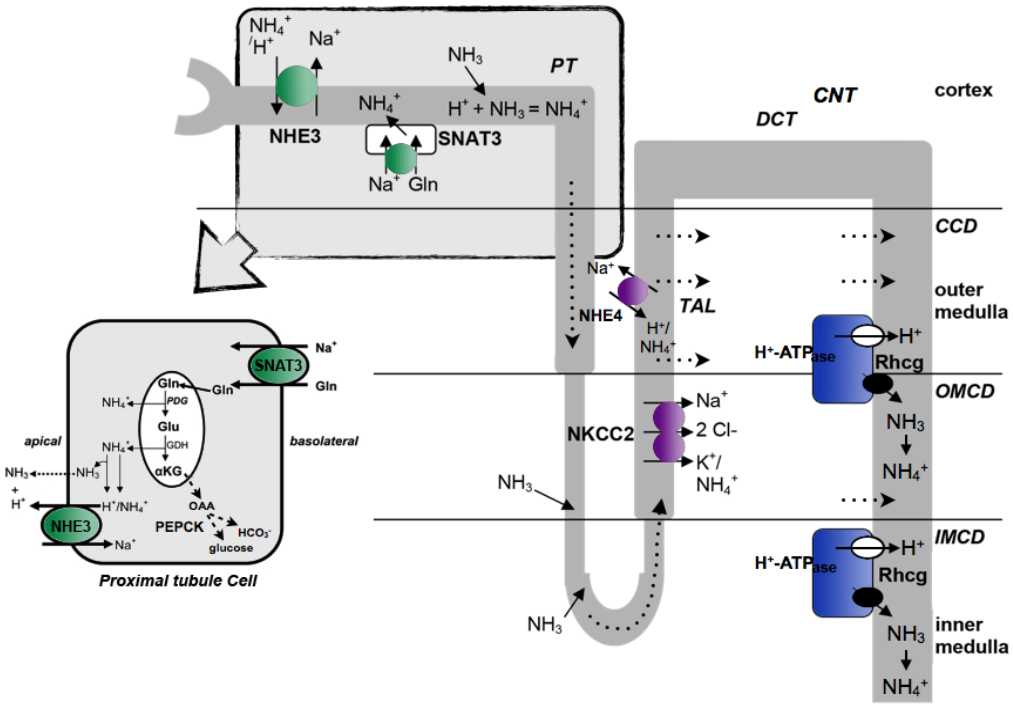

***Figure 1.*Mechanisms of NH_4^+ synthesis and transport in the kidney**

*Proximal tubule cell model.*From glutamine entering inside the cell via SNAT3, the mitochondrial ammoniagenic enzymes PDG and GDH allow the production ofα-ketoglutarate and NH_4^+.Alpha-ketoglutarate is converted to oxaloacetate, which is ultimately transformed to glucose and HCO_3^-bythe gluconeogenic enzyme PEPCK.NH_4^+ passage into the luminal fluid results from NH_3 diffusion and NHE3-driven NH_4^+ and H^+secretion. Glutamine (Gln); Phosphate-dependent glutaminase (PDG); Glutamate (Glu); Glutamine dehydrogenase (GDH); α-ketoglutarate (αKG); Oxaloacetate (OAA); Phosphoenolpyruvate carboxykinase (PEPCK); Na^+/H^+ exchanger isoform 3 (NHE3).

In the TAL, NH_4^+ reabsorption involving NKCC2 at the apical membrane and NHE4 on the basolateralside concentrates NH_4^+ in the medullary tissue. In the final step of renal NH_4^+ handling, RhCG transports NH_3 while H^+-ATPases mediate H^+ excretion. This process is critical in the kidney CD (CCD, OMCD and IMCD) to eliminate urinary NH_4^+. Thick ascending limb (TAL); $Na^+/K^+/2Cl^-$ co-transporter (NKCC2); Na^+/H^+ exchanger isoform 4 (NHE4); Rhesus factor glycoprotein C (RhCG); Cortical collecting duct (CCD); Outer medullary collecing duct (OMCD); Inner medullary collecting duct (IMCD). Modified from reference25.

I.3 The renalammoniumtransporter RhCG

Ammonia transport into urine has been for long considered as a passive diffusion mechanism. In the recent years of physiology history, this paradigm has been however challenged by the characterization of a protein involved in urinary NH_4^+excretion, the Rhesus factor protein RhCG. Rhesus glycoproteins are the animal equivalents of the bacteria, archea and plants Ammonia transport proteins (Amt) and Methylammonium permeases (Mep) in yeast. Amt and Mep proteins supply nitrogen to the cell in its bio-available form (NH_4^+ or NH_3), which is required for the synthesis of molecules such as amino acids or nucleic acids[26,27].In animals, the Rhesus family is composed of the RhAG[28], RhCE[29] and RhD[30] proteins found in erythrocytes and responsible for blood group identity, and the RhBG and RhCG homologous non-erythroid glycoproteins, which are expressed in a wide variety of tissues including kidneys.

In mouse and rat kidney RhBG is localized at the basolateral side of the distal convoluted tubule (DCT),the connecting segment (CNT) and the collecting duct cells. In the collecting duct, principal and type-A intercalated cells express RhBG, except for the IMCD where the protein is not detected in principal cells[31]. RhBG has also been recently reported in human kidney at the basolateral side ofthe CNT and in the cortical and outer medullary collecting ducts where the protein is only detected in type-A intercalated cells[32].Heterologous studies have shown that RhBG is able to transport NH_3[33].Mice with global Rhbgdeletion have normal basal acid–base parameters, normal responses to NH_4Cl-induced metabolic acidosis, and normal basolateral NH_3 and NH_4^+ transport in microperfused CCD segments[34]. A more recent study performed on mice with intercalated cell-specific Rhbg deletion showed that basal NH_3 excretion of these mice was not altered, whereas an increase in glutamine synthetase expression was detected,suggesting that higher production of NH_4^+in the proximal tubule may compensate for a NH_4^+excretion in this mouse model in baseline conditions. However, in the same mouse model, urinary NH_4^+excretion was impaired

following an acid-load[35]. Under specific conditions, RhBG may contribute to renal NH_4^+excretion.

The RhCG protein is expressed in mouse and humans in the late DCT, in the CNT andall along the collecting duct of kidneys (CCD, OMCD and IMCD) in principal and type-A intercalated cells[31,36,]. In principal cells, which are not primarily involved in renal acid excretion, the role of RhCG is not elucidated. The basolateral and apical membrane of principal cells are permeable to NH_3,with higherapical permeability, as revealedby confocal fluorescence imaging studies performed in perfused rabbit CCDs[37]. Although principal cells express less Rhcg than intercalated cells, increased principal cell Rhcg expression occurs in mice under chronic metabolicacidosis[38].

First studies of Rhcg and Rhbg localization in mice described an opposite polarity of the proteins in the collecting duct with Rhbg expression at the basolateral side and Rhcg expression at the apical side[31]. Immunogold stainings performed later in mouse collecting duct cells revealed that Rhcg is expressed at both apical and basolateral poles ofCD type-A intercalated cells[39]. The crystallographic structure of the human RhCG protein has been resolved in 2010, and RhCG, like Amt and Mep proteins, has been characterized as a gas channel permeable to NH_3[40]. On the basolateral side of type-A intercalated cells, RhCG is expressed together with other proteins that are able to transport NH_4^+ into epithelial cells: the Na^+/K^+-ATPases[41] and the $Na^+/K^+/2Cl^-$ cotransporter isoform 1 (NKCC1)[42].The anion exchanger isoform 1 protein (AE1) is also found at the basolateral pole and absorbs HCO_3^- produced inside the cells together with $H^+$from the action of carbonic anhydrase II (CAII)[43]. In the apical membrane, H^+/K^+-ATPases are able to transport NH_4^+, but RhCG is responsible for most of NH_4^+secretion. RhCG drives NH_3 into urine while H^+ pumps (H^+/K^+-ATPases and mostly vacuolar H^+-ATPases) are responsible for H^+ exit, their combined action generating urinary NH_4^+.

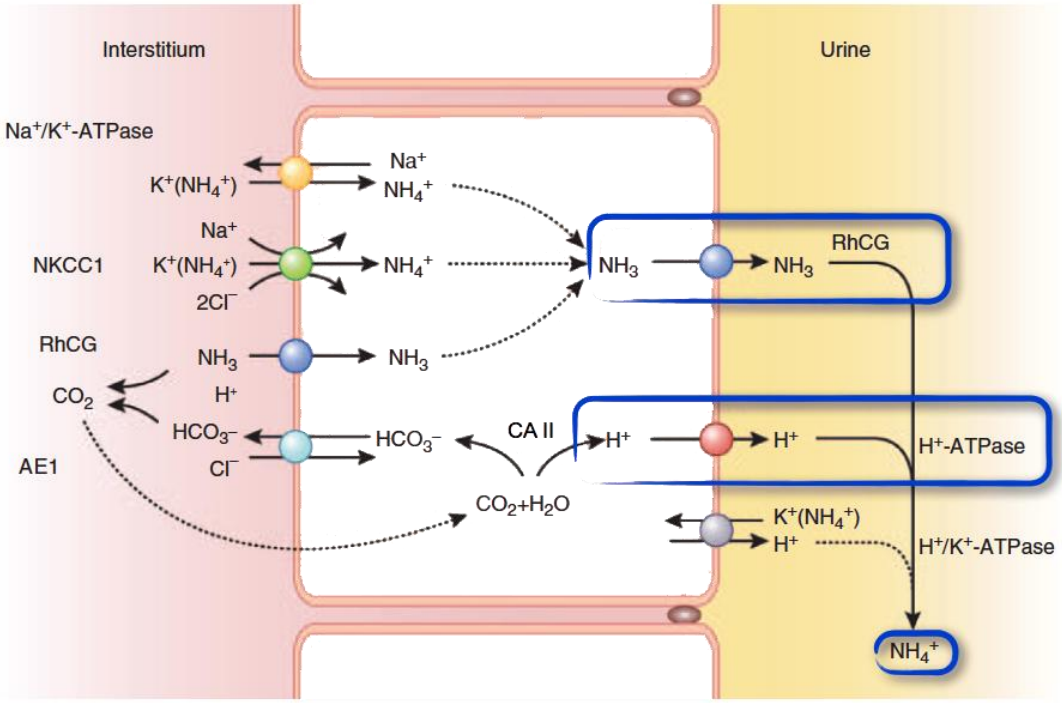

Figure 2. **Collecting duct typeA-intercalated cell model**

On the basolateral side of type-A intercalated cells, Na^+/K^+-ATPases and NKCC1 mediate NH_4^+ uptake while NH_3 enters the cell by diffusion and RhCG transport. AE1 absorbs HCO_3^- against Cl^- intake. Urinary NH_4^+ excretion results mostlyfrom NH_3 passage mediated by RhCG and H^+ active transport by H^+/K^+-ATPases and mostly, vacuolar H^+-ATPases. $Na^+/K^+/2Cl^-$ isoform 1 (NKCC1); Rhesus glycoprotein C (RhCG). Modified from reference 44.

In 2008, Biver and coworkers described *RhCG* as a new candidate gene for human distal renal tubular acidosis (dRTA)[7]. Both acute and chronic forms of metabolic acidosis have considerable adverse effects on renal cellular functions, impairing other cellular process implicated in different functions of the organism, like the cardiovascular system[45]. Renal tubular acidosis can be either proximal, due to impaired bicarbonate reabsorption, or distal, because of abnormal function of type-A intercalated cells and subsequent impairment of urine acidification[46]. The dRTA syndrome is characterized by normal anion gap metabolic acidosis with abnormally alkaline urine, hypokalemia, hypercalciuria and nephrocalcinosis[47]. dRTA patients present with a failure in NH_4^+ secretion secondary to reduced urinary acidification by the collecting duct into the tubular lumen which

compromisesrenal acid excretionand acid-base homeostasis[47].In human and rodent models, several genes have been linked to dRTA. Dominant forms of dRTA are generally less severe than recessive and have been associated with mutations of AE1[48]. Two genes coding for 2 different subunits of the vacuolar H^+-ATPase, *ATP6V0A4*[49] and *ATP6V1B1*[50] are linked with recessive dRTA. This later pathological condition appears in early infancy or early childhood with severe metabolic acidosis, growth retardation, and, if untreated, rickets[47]. In both cases of *ATP6V0A4* and *ATP6V1B1* mutations, dRTA is accompanied by the progressive apparition of sensorineural hearing loss[50,51].

In their study, Biver et al. targeted the *Rhcg*gene in mice, disrupting it by homologous recombination deleting 2 exons. After obtaining a full *Rhcg* knockout mouse (*Rhcg*$^{-/-}$),the metabolic status of *Rhcg*$^{+/+}$ and *Rhcg*$^{-/-}$ animals wasfirst investigated following an acid-load using 300mM NH_4Cl in drinking water for 2 and 6 days. Inwild-type mice, the NH_4Clacid-load induced a transient decrease of bloodpHand HCO_3^-levels with partial recovery at day 6,while *Rhcg*$^{-/-}$ mice could not adapt and showed decreased blood pH and HCO_3^-levels during the entire treatment, indicatingan impaired ability to cope with the acid-load. In addition, reduced urinary NH_4^+ excretion and more alkaline urine were observed in *Rhcg*$^{-/-}$ mice, features signing for dRTA.In *Rhcg*$^{-/-}$ mice receiving 200mM HCl diet during 7 days, a more severe metabolic acidosis, and impaired capacity to acidify urine accompanied by weight loss were found. Moreover, microperfusion experiments on outer medullary collecting ducts (OMCDs) and CCDs showed reduced apical permeability to NH_3 and transepithelial NH_3 transport in *Rhcg*$^{-/-}$, attesting tothe critical role of Rhcg in epithelial NH_3 transport and renal NH_4^+ excretion.

I.4 Aims of the dissertation

I.4.1 Determination of the phenotype of Rhcg$^{+/-}$ mice, role of Rhcg in basolateral NH_3 transport andrenal mechanisms of the adaptation to the lack of Rhcg

After the first *in vivo* characterization of the role of RhCG by Biver and colleagues,we aimed to perform a complementary study conducted on another model of *Rhcg*knockout mice. The first goal of this study was to determine whether or not a single deletion of *Rhcg* would affect the phenotype of *Rhcg*$^{+/-}$. With this question, we tried to understand if heterozygous abnormalities of Rhcg would lead to dRTA similarly to what was observed previously in *Rhcg*$^{-/-}$ mice.

Some studies have demonstrated an exclusive expression of Rhcg at the apical membrane of the collecting duct cells[31] whereas others detected the protein at both cellular sides[52]. Therefore, our second goal consisted of elucidating the controversial role of Rhcg in basolateral NH_3 transport.

Finally, the renal mechanisms of the adaptation to the lack of *Rhcg* remained unknown. Consequently, the last goal of our study was to assess how $NH_4^+$is accumulated in the medullary tissue as well as the regulation ofproteins involved in the NH_4^+management of other nephron segments in partial or complete absence of Rhcg.

I.4.2 Characterization of the response of Rhcg$^{+/+}$, Rhcg$^{+/-}$ and Rhcg$^{-/-}$ mice to high protein diet

In physiological conditions, various conditions are known to affect renal NH_4^+ excretion. Dietary K^+ depletion has been linked to development of a mild alkalosis-like state resulting from enhanced renal ammoniagenesis and NH_4^+ excretion in both animals and humans[53-56]. In the ammoniagenic pathway, the expression of SNAT3 is increased by K^+ depletion, has shown recently[57]. Studies on rats have also demonstrated that Rhcg expression and apical versus basolateral abundance in OMCD intercalated cells increase in

response to low K^+ diet, most probably contributing to increased NH_4^+ excretion and alkalosis[58].

Glucocorticoid and mineralocorticoid hormones, chiefly represented by cortisol and aldosterone, respectively, are also involved in acid-base homeostasis via regulation of renal NH_4^+metabolism. Both hormones are produced by the adrenal gland. Cortisol is the major glucocorticoid hormone produced by the *zona fasciculata* of the adrenal cortex regulating gluconeogenesis and involved in suppression of the immune system and metabolism[58]. In the proximal tubule of kidneys, glucocorticoids stimulate ammoniagenesis[60], an effect occurring through binding of the hormone to glucocorticoid receptors rather than mineralocorticoid receptors[61]. The mineralocorticoid hormone aldosterone is produced by the *zona glomerulosa* of the adrenal cortex and plays a central role in blood pressure regulation. Aldosterone acts on the distal convolutedtubule and collecting ducts by increasing the reabsorption of ions and water in the kidney in order to enhance the reabsorption of Na^+, secretion of K^+ andincrease water retention[62]. Known molecular targets of aldosterone action include the basolateral Na^+-K^+-ATPase and the apical epithelial sodium channel (ENaC), which are both critical for Na^+ reabsorption. During the distal acidification process, aldosterone enhances Na^+reabsorption but also H^+-ATPases activity, leading to increased H^+ excretion and luminal electronegativity[63].

Protein-rich diets are known to induce a systemic acid load to which the kidney responds by increasing the net acid excretion and mainly urinary NH_4^+ release[64,65]. Rich in sulphuric amino acids (SAA), methionine and cysteine, high protein diets from animal source induce an elevated production of H^+ and sulphate (SO_4^{2-}) when they are metabolised by the liver, resulting in increased blood acidity. To bring back a normal blood pH value, respiratory compensation occurs resulting in enhanced CO_2 exhalation through the lungs while the kidneys play a critical role filtering and clearing SO_4^{2-} from the blood, paralleled with increased urinary NH_4^+ excretion[64].

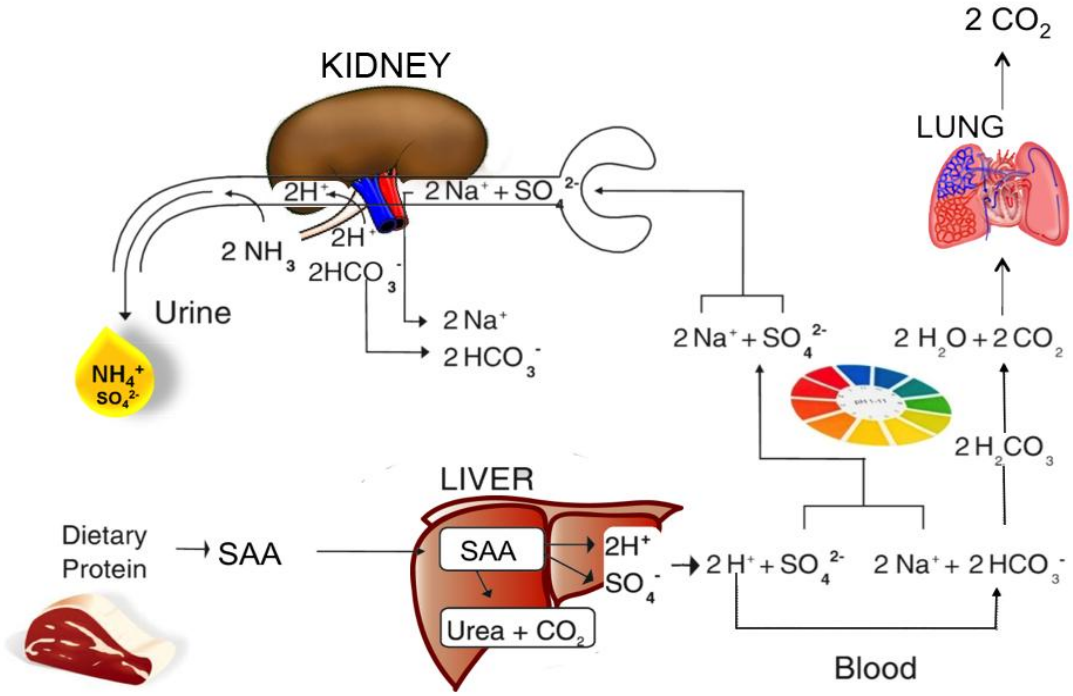

Figure 3. **The metabolism of proteins from animal source increases urinary NH_4^+ excretion**

Highly containing sulphuric amino acids (SAA), the consumption and metabolism of proteins from animal source by the liver induces a drop of blood pH that will be corrected by exhalation of CO_2 through the lung and the critical action of the kidney via augmented excretion of NH_4^+ into urine. Modified from reference 64.

The typical western diet contains high proportions of animal proteins and, in the recent years, high protein diets have become popular to fight excess weight and obesity. Therefore, the question of the impact of high dietary proteins on human health, especially on kidneys has become particularly relevant[65-67]. Detrimental effects of high protein consumption on chronic kidney disease (CKD) patients are clearly established[68]and the current protocol for these patients includes a reduction of proteins from animal sources to prevent a potential acceleration of renal function decline[69,70]. The normal functioning of kidneys is also modified by high protein diets. Rats fed high dietary protein as casein develop tubule-interstitial injury as a consequence of augmented intrinsic acid production provoked by endothelin-stimulated enhanced aldosterone activity[71-74]. Moreover, high protein intake is also suspected to affect bone health[75]. Several clinical studies have

interestingly linked the consumption of high animal protein diets with enhanced bone resorption[76].

The second part of the dissertation aimed at characterizing the effect of an acidogenic versus non-acidogenic diet on normal kidneys as well as understanding whether the lack of Rhcg induced a different response to those diets. Our first goal was to determine the impact of a high protein acid-load on metabolic parameters, and particularly urinary NH_4^+excretion of *Rhcg*$^{+/+}$, *Rhcg*$^{+/-}$ *and Rhcg*$^{-/-}$mice. Our second aim consisted of searching for which mechanisms, renal or extra-renal, were responsible for the response to a dietary acid-load.

I.4.3 Identification of a potential partnership between RhCG and the renal vacuolar H^+-ATPase

In the collecting duct of kidney, type-A intercalated cells are primarily involved in renal acid excretion. In these cells, NH_3 is mainly transported by facilitated diffusion through RhCG while protons are actively secreted into urine. H^+ are formed inside the epithelial cells by the conversion of CO_2 and H_2O into HCO_3^- and H^+ resulting from the action of carbonic anhydrase II (CAII) (see figure 2). Two types of H^+ pumps with ATPase activity are then responsible for H^+ transport across the apical membrane: the H^+/K^+-ATPase and the vacuolar H^+-ATPase (H^+-ATPase)[22]. However, the role of H^+/K^+-ATPase in H^+ secretion across the CD membrane is minor compared to H^+-ATPases[77].

Found ubiquitously in the organism vacuolar H^+-ATPases play a large variety of roles depending where they are expressed. They regulate the pH of intracellular organelles such as lysosome, the Golgi apparatus, secretory vesicles and endosomes, allowing their proper functioning. H^+-ATPases are also involved in synaptic transmission of neuronal cells[78], they are found in osteoclasts, in macrophages, and regulate the extracellular pH of closed compartments in the inner ear[79] and epididymis[80]. Eventually, they are found

in kidneys where they play a critical role in acid excretion. Renal vacuolar H^+-ATPases are found at the apical membrane of the proximal tubule, the TAL, the DCT and the type-A intercalated cells of the CCD, IMCD and OMCD where they allow H^+ secretion. In the distal nephron, H^+-ATPases are additionally present at the basolateral membrane of type-B intercalated cells where H^+ absorption takes place[22].

The vacuolar H^+-ATPase is composed of 22 subunits consisting of two connected domains. The peripheral catalytic V_1 domain contains 8 subunits,named A-H, and converts ATP to ADP and inositol phosphate. The membrane-bound V_0 domain contains 6 different subunits, a, d, c, c', c'', and e and acts as a proton translocating channel. In the V1 domain, disruption of the B subunit in yeast leads to a conditional lethal phenotype, suggesting its essential role in H^+-ATPase function[81]. Some subunits of H^+-ATPases are expressed in a restricted number of organs and among them, B1, C2 and G3 belonging to the V_1 domain and a1, a2 and a4 form the V_0 domain, are found in kidneys[82].

In rat and mouse intercalated cells of the kidney CD, the B1 isoform of vacuolar H^+-ATPases colocalizes with Rhcg[36]. Furthermore, in mouse and human, mutations of the genes coding for the a4 and B1 subunits of the vacuolar H^+-ATPase cause inherited forms of dRTA[49-51], a syndrome which also develops incompletely in *Rhcg* knockout mice[7].

A **B**

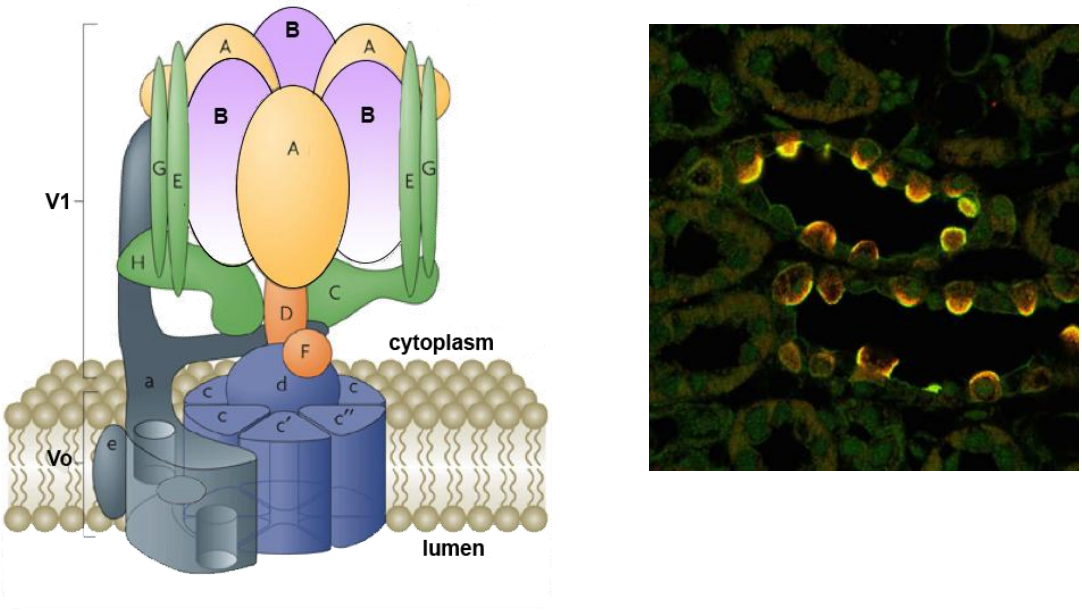

Figure 4. **The vacuolar H^+-ATPase is a multimeric protein expressing the B1 isoform in Rhcg positive type-A intercalated cells of kidney CCDs**

(A) Schematic structure of the vacuolar H^+-ATPase. The H^+-ATPase comprises 6 subunits (a, d, c, c', c'', e) in the V0 domain dedicated to H^+ secretion and 8 subunits (A-H) in the cytoplasmic domain V1 mediating ATP hydrolysis. Modified from reference 83.

(B) Immunostaings of Rhcg and B1 in rat OMCD cells. Among the 8 subunits (A-H) of the V1 domain, the B1 isoform of H^+-ATPases is found specifically in intercalated cells of the kidney CD where Rhcg is also expressed. Vacuolar H^+-ATPase (red), Rhcg (green), Merge (yellow). Taken from reference 36.

In the kidney type-A intercalated cells of kidneys, RhCG and H^+-ATPases display a coordinated action in order to eliminate NH_4^+ into urine. At baseline conditions[7] and following a 2 daysHCl acid-load[39], *Rhcg*$^{-/-}$mice show a more alkaline urine than *Rhcg*$^{+/+}$ under the same conditions.Thus, our third goal was first to investigate the capacity of *Rhcg*$^{-/-}$ to excrete protons in urine. Reciprocally, we aimed to investigate the influence of an impaired proton excretion capacity by the vacuolar H^+-ATPase on Rhcg mediated NH_3 excretion in the collecting duct of kidneys. We hypothesized that a potential functional interaction between RhCG and H^+-ATPases may occur.

II Haploinsufficiency of the ammonia transporter Rhcg predisposes to chronic acidosis - Rhcg is critical for apical and basolateral ammonia transport in the mouse collecting duct

***Article published**: J. Biol. Chem.*, vol 288, N° 8, pp. 5518–5529, February 22, 2013, DOI10.1074/jbc.M112.441782

Own contribution to the publication:

The qRT-PCR evaluating *Rhcg* mRNA level in *Rhcg*$^{+/+}$, $^{+/-}$ and $^{-/-}$ mice was performed and appears in **Figure 1B**.

Western blotting analysis was conducted on *Rhcg*$^{+/+}$, $^{+/-}$ and $^{-/-}$ mice receiving 2 days of HCl acid-load to evaluate the expression levels of various proteins involved in ammoniagenesis and NH_4^+ transport. **Figure 8** shows PEPCK (**Figure 8A**), PDG (**Figure 8B**), NKCC2 (**Figure 8C**) and NHE3 (**Figure 8D**) protein levels measured and compared between *Rhcg*$^{+/+}$, $^{+/-}$ and $^{-/-}$ mice.

THE JOURNAL OF BIOLOGICAL CHEMISTRY VOL. 288, NO. 8, pp. 5518–5529, February 22, 2013

Haploinsufficiency of the Ammonia Transporter Rhcg Predisposes to Chronic Acidosis

*Rhcg IS CRITICAL FOR APICAL AND BASOLATERAL AMMONIA TRANSPORT IN THE MOUSE COLLECTING DUCT**

Received for publication, December 3, 2012 Published, JBC Papers in Press, December 31, 2012, DOI 10.1074/jbc.M112.441782

Soline Bourgeois[‡], Lisa Bounoure[‡], Erik I. Christensen[§], Suresh K. Ramakrishnan[¶‖1], Pascal Houillier[¶‡‡], Olivier Devuyst[‡], and Carsten A. Wagner[‡2]**

*From the [‡]Institute of Physiology and Zurich Center for Integrative Human Physiology, University of Zurich, CH-8057 Zurich, Switzerland, the [§]Department of Biomedicine, University of Aarhus, 8000 Aarhus C, Denmark, [¶]INSERM, Centre de Recherche des Cordeliers, UMRS872, 75270 Paris, France, the [‖]Faculté de Médecine, Université Pierre et Marie Curie, F-75015 Paris, France, the **Université Paris-Descartes, F-75015 Paris, France, and the [‡‡]Hôpital Européen Georges Pompidou, Département de Physiologie, Assistance Publique-Hôpitaux de Paris, F-75015 Paris, France*

Background: Rhesus proteins transport NH_3 and/or NH_4^+ in heterologous expression systems.
Results: Heterozygous Rhcg mice develop delayed metabolic acidosis, whereas homozygous KO mice display severe metabolic acidosis. RhCG functions as an NH_3 transporter on apical and basolateral membranes.
Conclusion: RhCG is an NH_3 but not NH_4^+ transporter.
Significance: Loss or reduced expression of *RhCG* may underlie inherited or acquired forms of human acidosis.

Ammonia secretion by the collecting duct (CD) is critical for acid-base homeostasis and, when defective, causes distal renal tubular acidosis (dRTA). The Rhesus protein RhCG mediates NH_3 transport as evident from cell-free and cellular models as well as from *Rhcg*-null mice. Here, we investigated in a *Rhcg* mouse model the metabolic effects of Rhcg haploinsufficiency, the role of Rhcg in basolateral NH_3 transport, and the mechanisms of adaptation to the lack of Rhcg. Both $Rhcg^{+/+}$ and $Rhcg^{+/-}$ mice were able to handle an acute acid load, whereas $Rhcg^{-/-}$ mice developed severe metabolic acidosis with reduced ammonuria and high mortality. However, chronic acid loading revealed that $Rhcg^{+/-}$ mice did not fully recover, showing lower blood HCO_3^- concentration and more alkaline urine. Microperfusion studies demonstrated that transepithelial NH_3 permeability was reduced by 80 and 40%, respectively, in CDs from $Rhcg^{-/-}$ and $Rhcg^{+/-}$ mice compared with controls. Basolateral membrane permeability to NH_3 was reduced in CDs from $Rhcg^{-/-}$ mice consistent with basolateral Rhcg localization. $Rhcg^{-/-}$ responded to acid loading with normal expression of enzymes and transporters involved in proximal tubular ammoniagenesis but reduced abundance of the NKCC2 transporter responsible for medullary accumulation of ammonium. Consequently, tissue ammonium content was decreased. These data demonstrate a role for apical and basolateral Rhcg in transepithelial NH_3 transport and uncover an incomplete dRTA phenotype in $Rhcg^{+/-}$ mice. Haploinsufficiency or reduced expression of RhCG may underlie human forms of (in)complete dRTA.

Ammonium (NH_4^+) is the main component of urinary acid excretion. Renal synthesis and excretion of NH_4^+ rise in response to an acid load, allowing kidneys to regenerate bicarbonate and increase net acid excretion (1, 2). Impaired renal acid excretion characterizes type I distal renal tubular acidosis (dRTA)[3] with low urinary ammonium and inappropriately alkaline urinary pH (3).

Ammonium is formed in the proximal tubule from the metabolism of glutamine and added to the luminal fluid. It is reabsorbed into the medullary interstitium in the thick ascending limb creating a cortico-papillary NH_3/NH_4^+ gradient (4, 5). The final step of NH_3/NH_4^+ excretion is achieved by the CD (6). The high tissue concentration of NH_3/NH_4^+ and the pH gradient between interstitium and urine provide the driving forces for NH_4^+ excretion into urine. NH_4^+ secretion results from the trapping of NH_3 in the tubular lumen after being titrated by H^+ ions stemming from active secretion by V-type H^+-ATPases (7).

The mechanisms mediating NH_3/NH_4^+ transport across cell membranes into urine have only recently become uncovered. Members of the Rhesus protein family have been identified as pathways for NH_3/NH_4^+ transport in yeast, plants, fish, and mammals (2, 5, 8). In the kidney CD, RhCG and RhBG are expressed (9, 10). Mice lacking *Rhbg* show either no phenotype or only a very mild reduction in urinary ammonium excretion (11, 12). In contrast, cell-specific or complete *Rhcg* deficiency

* This work was supported in part by Grants 3100A0-122217 and 31003A_138143 from the Swiss National Science Foundation (to C. A. W.), the 7th European Union Framework Project EUNEFRON (to P. H., E. I. C., O. D., and C. A. W.), the Danish Medical Research Council, The Novo Nordisk Foundation (to E. I. C.), and the Swiss National Centre of Competence in Research (to O. D. and C. A. W.).
[1] Supported by Erasmus Mundus External Cooperation Window Lot 15, India.
[2] To whom correspondence should be addressed: Institute of Physiology, University of Zurich, Winterthurerstrasse 190, CH-8057 Zurich, Switzerland. Tel.: 41-44-63-55023; Fax: 41-44-63-56814; E-mail: Wagnerca@access.uzh.ch.

[3] The abbreviations used are: dRTA, distal renal tubular acidosis; CD, collecting duct; CCD, cortical CD; BCECF, 2′,7′-bis(2-carboxyl)-5-(and-6)-carboxyfluorescein; PEPCK, phosphoenolpyruvate carboxykinase; PDG, phosphate-dependent glutaminase; NMDG, *N*-methyl-D-glutamine; OMCD, outer medullary collecting duct; IMCD, inner medullary collecting duct.

causes a massive reduction in urinary ammonium excretion in three different mouse models (13–15). Microperfusion experiments using CDs from *Rhcg*-deficient mice demonstrated that RhCG is critical for the apical exit of NH_3 into urine (13). Thus far, a phenotype of dRTA has only been reported in $Rhcg^{-/-}$ mice, whereas potential changes caused by haploinsufficiency in Rhcg have not been investigated. This issue is relevant because heterozygous abnormalities in RhCG might be more frequent and may affect the renal capacity to cope with an acid load leading to incomplete dRTA. Furthermore, $Rhcg^{+/-}$ mice may also serve as a model to examine the consequences of reduced RhCG expression that may occur during kidney disease. Finally, RhCG localization has been controversial for years. RhCG has been localized by some groups only at the apical side of CD cells, whereas others have found RhCG on both the apical and basolateral membranes (9, 10, 16, 17). The functionality of basolateral RhCG protein remains unknown.

Here, we used a novel *Rhcg* mouse model to provide the first evidence that haploinsufficiency in *Rhcg* impairs the handling of a chronic acid load in $Rhcg^{+/-}$ mice, which develop an incomplete metabolic acidosis. Microperfusion studies provide the functional basis of the defect and show that RhCG is absolutely required for apical and partially for basolateral NH_3 transport. Moreover, loss of Rhcg is associated with a profound down-regulation of NKCC2 and reduced medullary accumulation of ammonium impairing the gradient necessary for the final excretory step. These data provide new insights into the complex role of RhCG and suggest that congenital or acquired defects in *RhCG* protein expression may be associated with incomplete dRTA.

EXPERIMENTAL PROCEDURES

Animals—$Rhcg^{+/-}$ mice were purchased from the Texas Institute of Genomic Medicine (Houston TX). Mice were generated by replacing exon 1 by a vector carrying a LacZ/Neo cassette (Fig. 1*A*). Mice were genotyped by PCR directly on a 3-μl 25 mM NaOH tail digestion product. Genomic DNA was amplified using primer pairs specific for exon 1 forward (AGACCCCACAATGGAAAGCTATAA), wild type reverse (CAACCAGAACTCCCCAGTGTCAGA), and knock-out reverse (ATGGGCTGACCGCTTCCTCGTGCTTTAC). The products were separated by electrophoresis in 1% agarose gel (mutant product, 522 bp; wild type product, 376 bp). Mice were generated by mating $Rhcg^{+/-}$ mice, and mice were bred in the Êntres Vivants Exempts d'Organismes Pathogènes Spécifiques Animal Facility. For acid-loading experiments, mice in metabolic cages were given 0.2 M HCl added to powdered standard food. All experiments were performed according to Swiss Animal Welfare laws and approved by the local veterinary authority (Veterinäramt Zürich).

In Vivo Experiments—All experiments were performed using age- and sex-matched *Rhcg* wild type ($Rhcg^{+/+}$), *Rhcg* knock-out ($Rhcg^{-/-}$), and *Rhcg* heterozygote ($Rhcg^{+/-}$) littermate mice (3–4 month-old) that were housed in metabolic cages (Techniplast, Switzerland). Mice were given deionized water *ad libitum* and were fed with a standard powdered laboratory chow (Kliba, Augst, Switzerland). Mice were allowed to adapt to metabolic cages for 3 days, and a first retro-orbital blood sample was taken for blood gas analysis under base line. Then two 24-h urine samples were collected under light mineral oil in the urine collector to determine daily urinary parameters. Mice were then allowed to recover for 2 weeks before giving an HCl-containing diet (0.2 M HCl added to powdered standard food) in normal cages. Food, water intake, and urine excretion were monitored following the same procedures as under base-line conditions. Urine collections were performed on the 1st and 2nd day of acid loading and then on the 6th and 7th day. Retro-orbital blood samples were taken on the 2nd and 7th days of HCl diet.

Analytic Procedures—Blood pH, pCO_2, and electrolytes were measured with a pH/blood-gas analyzer (ABL 77 Radiometer). Urinary Na^+ and K^+ concentrations were measured by flame photometry (IL943, Instruments Laboratory); titratable acids were measured using a DL 50 titrator (Mettler Toledo) (18, 19) and creatinine by a modified kinetic Jaffé colorimetric method (20). Urinary pH and bicarbonate were measured with a pH/blood-gas analyzer (ABL 725, Radiometer). Urinary NH_4^+ was measured with the Berthelot protocol (21).

Immunoblotting—Crude membrane proteins or cytosolic fractions were obtained from kidneys homogenized in 250 mM sucrose, 10 mM Tris-HCl, pH 7.5, and in the presence of protease inhibitors.

Forty micrograms of crude membrane proteins or cytosolic proteins were solubilized in loading buffer containing DTT and separated on 8–10% polyacrylamide gels. For immunoblotting, the proteins were transferred electrophoretically to polyvinylidene fluoride membranes (Immobilon-P, Millipore Corp., Bedford, MA). After blocking with 5% milk powder in Tris-buffered saline, 0.1% Tween 20 for 60 min, the blots were incubated with primary antibodies overnight at 4 °C as follows: phosphate-dependent glutaminase (PDG), which recognizes both the rat (KGA) and human (GAC) kidney-type isoforms of PDG forming the mature PDG protein (66 and 68 kDa; a kind gift from N. Curthoys, Colorado State University; diluted 1:5000) (22); rabbit polyclonal anti-PEPCK (Cayman Chemical, Ann Arbor, MI; diluted 1:5000); rabbit polyclonal anti-NKCC2 (kind gift from Johannes Loffing, Institute of Anatomy, University of Zurich; diluted 1:5000); rabbit polyclonal anti-NHE3 (StressMarq Biosciences Inc., Victoria, British Columbia, Canada); rabbit polyclonal anti-pendrin (Pineda Antibody Service, Berlin, Germany, diluted 1:5000) (23); and mouse monoclonal anti-β-actin antibody (Sigma; diluted 1:5000). After washing and blocking with 5% milk powder for 60 min, membranes were then incubated for 2 h at room temperature with secondary goat anti-rabbit or donkey anti-mouse antibodies (diluted 1:5000) linked to alkaline phosphatase (Promega, Madison, WI). The protein signal was detected with the appropriate substrate (Millipore Corp, Bedford, MA) using the las-4000 image analyzer system (Fujifilm Life Science). All images were analyzed using the software Advanced Image Data Analyzer AIDA (Raytest, Straubenhardt, Germany) to calculate the protein of interest/β-actin ratio.

Immunostaining and Immunogold—Immunohistochemistry and immunogold staining were performed on frozen sections, and specificity was demonstrated on $Rhcg^{-/-}$ tissues. Mouse kidneys were fixed by perfusion retrograde through the aorta

with 3% paraformaldehyde in 0.1 M sodium cacodylate buffer, pH 7.2. The tissue was either trimmed into small blocks, further fixed by immersion in 1% paraformaldehyde, infiltrated with 2.3 M sucrose for 30 min, and frozen in liquid nitrogen or prepared for routine paraffin embedding.

For electron microscopy, 70–90-nm cryosections were obtained at −100 °C with an FCS Reichert Ultracut S cryoultramicrotome as described previously (24), and 2-μm paraffin sections were obtained with a Leica RM2165 microtome. For LM immunolabeling, the sections were incubated with a rabbit polyclonal antibody against RhCG (a kind gift from Dr. Yves Colin, INSERM, Paris, France (16, 25)) at room temperature for 1 h after preincubation in PBS containing 0.05 M glycine and 1% bovine serum albumin. The sections were subsequently incubated with peroxidase-conjugated secondary antibody (Dako); the peroxidase was visualized with diaminobenzidine, and the sections were counter-stained with Maier's stain for 2 min. The sections were examined in a Leica DMR microscope equipped with a Leica DFC320 camera. Images were transferred by a Leica TFC Twain 6.1.0 program and processed using Adobe Photoshop 8.0. For EM immunolabeling, the sections were incubated with the primary antibody at 4 °C overnight followed by incubation at room temperature for 1 h with 10-nm gold particles coupled to anti-rabbit IgG (BioCell, Cardiff, UK). The cryosections were embedded in methylcellulose containing 0.3% uranyl acetate and studied under a Philips CM100 electron microscope. For controls, sections were incubated with secondary antibodies alone or with nonspecific IgG.

RNA Extraction and Reverse Transcription—Snap-frozen kidneys (five kidneys for each condition) were homogenized in RLT-Buffer (Qiagen, Basel, Switzerland) supplemented with β-mercaptoethanol to a final concentration of 1%. Total RNA was extracted from 200-μl aliquots of each homogenized sample using the RNeasy mini kit (Qiagen, Basel, Switzerland) according to the manufacturer's instructions. Quality and concentration of the isolated RNA preparations were analyzed on the ND-1000 spectrophotometer (Nano-Drop Technologies). Total RNA samples were stored at −80 °C. Each RNA sample was diluted to 100 ng/μl, and 3 μl was used as a template for reverse transcription using the TaqMan reverse transcription kit (Applied Biosystems, Foster City, CA). For reverse transcription, 300 ng of RNA template were diluted in a 40-μl reaction mix that contained (final concentrations) RT buffer (1×), $MgCl_2$ (5.5 mM), random hexamers (2.5 μM), RNase inhibitor (0.4 unites/μl), the multiscribe reverse transcriptase enzyme (1.25 units/μl), dNTP mix (500 μM each), and RNase-free water.

Real Time Quantitative PCR—Quantitative real time quantitative RT-PCR was performed on the ABI PRISM 7700 sequence detection system (Applied Biosystems, Foster City, CA). Primers were chosen using the BLAST tool of Ensemble to result in amplicons no longer than 150 bp spanning intron-exon boundaries to exclude genomic DNA contamination. The specificity of all primers was first tested on mRNA derived from kidney and always resulted in a single product of the expected size (data not shown). Probes were labeled with the reporter dye 6-carboxyfluorescein at the 5′ end and the quencher dye 5-(and 6-)-carboxytetramethylrhodamine at the 3′ end (Microsynth, Balgach, Switzerland). The primers were designed to target the deleted sequence in *Rhcg*$^{-/-}$ animals (accession number NM_019799) with 5′-ATGCAGGGATGGTTCCATTA-3′ (238–258 bp) as the left primer located within exon 1 and 5′-TGGAAGAAGGTCATAATGAGCAG-3′ (373–392 bp) as the right primer located within exon 2, and 5′-TTACTATCGCTACCCGAGCTTCCAG-3′ as the probe (292–317 bp). Real time PCRs were performed using TaqMan Universal PCR master mix (Applied Biosystems, Foster City, CA). Briefly, 3 μl of cDNA, 0.8 μl of each primer (25 μM), 0.4 μl of labeled probe (5 μM), 5 μl of RNase-free water, and 10 μl of TaqMan Universal PCR master mix reached 20 μl of final reaction volume. Reaction conditions were denaturation at 95 °C for 10 min followed by 40 cycles of denaturation at 95 °C for 15 s and annealing/elongation at 60 °C for 60 s with auto ramp time. All reactions were run in triplicate. For analyzing the data, the threshold was set to 0.2 as this value had been determined to be in the linear range of the amplification curves for all mRNAs in all experimental runs. The expression of the genes of interest was calculated in relation to hypoxanthine-guanine phosphoribosyltransferase (accession number NM_013556, forward primer, 5′-TTATCAGACTGAAGAGCTACTGTAAGATC-3′ (442–471), reverse primer, 5′-TTACCAGTGTCAATTATATCTTCAACAATC-3′ (539–568), and probe, 5′-TGAGAGATCATCTCCACCAATAACTTTTATGTCCC-3′ (481–515)). Relative expression ratios were calculated as $R = 2^{(Ct(\mathrm{HPRT}) - Ct(\mathrm{test\ gene})}$, where *Ct* represents the cycle number at the threshold 0.02; and HPRT is hypoxanthine-guanine phosphoribosyltransferase.

Measurement of Renal Ammonia Content—The renal tissue ammonia content was measured by an enzymatic technique (ammonia assay kit, Sigma) as described previously (26). Mice were anesthetized, and the kidneys were removed and immediately frozen in liquid nitrogen. They were then sliced frozen to yield a column of tissue, which extended from the cortex to the tip of the papilla. Sections were cut along the corticomedullary axis to yield three slices as follows: cortex, outer medulla, and inner medulla. Two kidneys from the same animal were pooled for each sample. Tissue slices were then homogenized in 300 μl of ice-cold 7% trichloroacetic acid, and the solution was centrifuged. The supernatant was drawn off, and the pH of a 250-μl sample was adjusted to near neutral by the addition of 12 μl of 10 mM Na_2HPO_4 in 9 N NaOH. A 200-μl sample of buffered supernatant was then analyzed for ammonium. The pellet was resuspended in 1 N NaOH, shaken overnight, and analyzed for total protein using the Bio-Rad protein assay.

Microperfusion Studies on Isolated Tubules—Mice were anesthetized with 50 mg/kg pentobarbital sodium or xylazine/ketamine intraperitoneally. Both kidneys were cooled *in situ* with control bath solution (see below) for 1 min and then removed and cut into thin coronal slices for tubule dissection. CCDs were dissected from the cortex at 10 °C in the control solution. *In vitro* microperfusion of single CCD segments, intracellular pH, and transepithelial NH_3 permeability measurements were performed as described previously (13).

Intracellular pH Measurement—The isolated tubule was transferred to the bath chamber on the stage of an inverted microscope (Axiovert 200, Carl Zeiss, Germany) in the control

solution containing (in mM) 138 NaCl, 1.5 $CaCl_2$, 1.2 $MgSO_4$, 2 K_2HPO_4, 10 HEPES, 5.5 glucose, 5 alanine, pH 7.40, and then was mounted on concentric pipettes and perfused *in vitro* with Na^+-free, ammonium-free solution, where *N*-methyl-D-glutamine$^+$ ($NMDG^+$) replaced Na^+. All solutions were equilibrated with 100% O_2 passed through a 3 N KOH CO_2 trap. Once the solutions were gassed and the pH checked, they were placed in a reservoir and were continuously bubbled with 100% O_2. The average tubule length exposed to bath fluid was limited to 300–350 μm to prevent motion of the tubule. CCDs or OMCDs were loaded with 5 μM of the fluorescent probe 2′,7′-bis(2-carboxyl)-5-(and-6)-carboxyfluorescein (BCECF Invitrogen) for ~20 min at 37 °C in the control bath solution. The loading solution was then washed out by initiation of bath flow, and the tubule was equilibrated with dye-free control bath solution for 5 min. Bath solution was delivered at a rate of 20 ml/min and warmed to 37 °C by a water jacket immediately upstream to the chamber. After this temperature equilibration in control solution, tubules were first transiently acidified by peritubular Na^+ removal (sodium-free, ammonium-free solution) (10 min duration), replaced by $NMDG^+$ to avoid exit of NH_4^+ by basolateral Na^+-coupled transport. This maneuver was done in the luminal absence of Na^+. During the fluorescence recording, perfusion solution was delivered to the perfusion pipette via a chamber under an inert gas (N_2) pressure (around 1 bar) connected through a manual six-way valve. With this system, opening of the valve instantaneously activates flow of solutions. The majority of the fluid delivery to the pipette exits the rear of the pipette system through a drain port at 4 ml/min. This method results in a smooth and complete exchange of the luminal or the peritubular solution in less than 3–4 s (27). After the fluorescence signal stabilization, luminal medium was instantly (at the rate of 4 ml/min in the draining) replaced by a Na^+-free solution containing 20 mM NH_4Cl (and 118 mM NMDG-Cl) that elicited a rapid intracellular alkalinization, followed by a sharp acidification. The rate of intracellular alkalinization has been associated with the entry of NH_3, whereas the subsequent phase of intracellular acidification in the continued presence of extracellular NH_4Cl reflects mostly NH_4^+ entry (28). Fluorescence monitoring and calibration were performed with a video imaging system (Visitron Systems, Germany) as described previously (11, 13). For peritubular ammonium pulse, peritubular solution was changed by a 6 mM NH_4Cl solution, pH 7.40. in the presence of 1 mM furosemide and 2.5 mM ouabain in the bath.

Intrinsic Buffering Capacity Determination—The intrinsic buffering capacity (βi) of CCD cells was determined, as reported previously (29), using a 40 mM NH_4Cl basolateral pulse to acidify the cells. To exclude HCO_3^-/CO_2 as a buffering component and block Na^+-dependent pH_i regulatory mechanisms, Na^+-free, HEPES-buffered solutions were used in the perfusate; the bath contained 1 mM amiloride (to inhibit Na^+/H^+ exchangers), and bath and perfusate also contained 100 μM Sch28080 (to block H^+/K^+-ATPases) and 200 nM concanamycin A (to block H^+-ATPases). Addition of 40 mM NH_4Cl to the bath induced an increase following by a decrease in pH_i. The pK_a of ammonia (9.03) was used to calculate the intracellular NH_4^+ concentration when cell acidification plateaued. βi was calculated as the ratio of the change in intracellular NH_4^+ concentration to the change in pH_i. Therefore, we determined the correlation between intracellular pH and β_i, which was −32.7–22.3·pH in wild types, −2.3–8.2·pH in heterozygotes, and 1,4–5.0· pH_i in *Rhcg*$^{-/-}$ mice. We measured cellular buffering power (β_i) in CCDs from all three genotypes of mice.

NH_3 Permeability Measurement—The basic approach used to determine NH_3 permeability involved construction of a transepithelial gradient of NH_3 and measurement of the resulting NH_3 flux from the basolateral to the luminal side as described previously (11, 13, 30). The isolated CCD was transferred to the bath chamber on the stage of an inverted microscope (Axiovision A1, Zeiss, Germany) and mounted on concentric glass pipettes for microperfusion. Bath solution was delivered at a rate of 20 ml/min and warmed to 37 °C by a water jacket immediately upstream of the chamber. The perfusion rate was adjusted by hydrostatic pressure to ~10 nl/min. The tubules were equilibrated for 20–30 min at 37 °C before the beginning of collections. To construct a transepithelial NH_3 gradient, the perfusion (lumen) solution contained (in mM) 139 NaCl, 1 NH_4Cl, 2.5 K_2HPO_4, 2 $NaHCO_3$, pH 6.4; the bath solution contained (in mM) 117 NaCl, 1 NH_4Cl, 2.5 K_2HPO_4, 23 $NaHCO_3$, pH 7.4, and in addition, both solutions contained (in mM) 5.5 glucose, 2 $CaCl_2$, 1.2 $MgSO_4$ and 10 HEPES. The osmolarity of the solution was 295 ± 5 mosmol/kg H_2O. All solutions were equilibrated with 95% O_2, 5% CO_2. Once the solutions were gassed and the pH checked, they were placed in a reservoir and continuously bubbled with 95% O_2, 5% CO_2. The actual pH of the solutions was monitored several times during the experiments, and the pH of solutions was checked at the end of the experiment to ensure that changes did not occur. Carbonic anhydrase (Sigma) was added to the perfusate solution (1 mg/10 ml of solution). The purpose of carbonic anhydrase was to prevent any pH disequilibrium that might arise from proton secretion or NH_3 transport. Total ammonium concentration was measured in 10–12-nl samples of peritubular, perfused, and collected fluids using an NH_3 diagnostic kit (Sigma) and the flow-through microfluorometer Nanoflow apparatus (World Precision Instruments, UK) (31).

Calculations of Transepithelial NH_3 Permeability—Assuming an absence of osmotic or hydrostatic pressure gradients across the epithelium and therefore an absence of net fluid transport, the passive transepithelial transport of total ammonium (Am) may be described by Equation 1,

$$J_{Am} = P_{NH3} \times A_S \times \Delta C_{NH3} \quad \text{(Eq. 1)}$$

where P_{NH3} is diffusive permeability of NH_3 (cm/s), A_S is tubule luminal surface area (cm^2), and ΔC_{NH3} is the transepithelial concentration difference for NH_3 (mM). To calculate the permeability to NH_3, Equation 1 is rearranged as Equation 2,

$$P_{NH3} = J_{Am}/(A_S \times \Delta C_{NH3}) \quad \text{(Eq. 2)}$$

The net rate of transport J_{Am} is calculated as shown in Equation 3,

$$J_{Am} = ([Am]_i - [Am]_o) \times V/L \quad \text{(Eq. 3)}$$

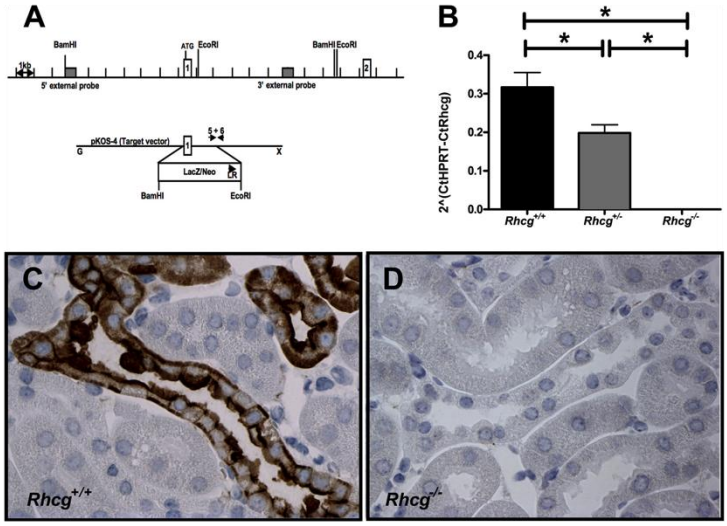

FIGURE 1. ***Rhcg* gene targeting and deletion.** *A*, *Rhcg* gene knock-out was achieved by replacement of exon 1 by a LacZ/neomycin cassette (Texas Institute of Genomic Medicine, Houston, TX). *B*, RT-quantitative PCR with primers placed in exon 1 of *Rhcg* demonstrated lower mRNA in kidneys from $Rhcg^{+/-}$ mice and absence of a detectable PCR product in kidneys from $Rhcg^{-/-}$ mice ($n = 5$ mice). *C* and *D*, *Rhcg* immunodetection in kidney sections from wild type (*C*) and $Rhcg^{-/-}$ (*D*) mice. * indicates significantly different $p < 0.05$.

where $[Am]_i$ is the concentration of total ammonium in the perfusate; $[Am]_o$ is the concentration of total ammonium in the collected fluid; V is the collection rate (nl/min), as measured in precalibrated constriction pipettes, and L is the perfused tubule length (mm). A_S may be calculated as $L\pi d$, where d (mm) is the inner tubule diameter. The total ammonium concentration ([Am]) is equal to the sum of the concentrations of the two species NH_3 and NH_4^+ and is the quantity actually measured by the microfluorimetric assay. The equilibrium between the two species is defined by the Henderson-Hasselbalch Equation 4,

$$pH = pK_a + \log([NH_3]/(NH_4^+)) \quad \text{(Eq. 4)}$$

The pK_a equals 9.03 at physiological pH and temperature. Knowing the values for pH and [Am], the values for $[NH_3]$ and $[NH_4^+]$ may be determined simultaneously.

Statistics—Data are expressed as means ± S.E. Statistical comparisons were tested by analysis of variance and Student's t test using the Graphpad Prism software (GraphPad). p values $<$ 0.05 were considered as statistically significant.

RESULTS

Deletion of Rhcg in Mice—Mice lacking *Rhcg* were generated using gene trap technology in a mixed genetic background (129SvEvBrd, C57/BL6) (Fig. 1*A*) and were purchased from the Texas Institute of Genomic Medicine (32). *Rhcg* mRNA was undetectable in renal tissue from Rhcg knock-out ($Rhcg^{-/-}$) mice and reduced by ~50% in heterozygous mice ($Rhcg^{+/-}$) mice (Fig. 1*B*). RhCG protein was completely absent from the kidney of $Rhcg^{-/-}$ mice as confirmed by immunohistochemistry (Fig. 1*C*).

Heterozygous Mice Develop Metabolic Acidosis While on Long Term Acid Load—We first assessed acid-base status under basal conditions and during an acid load in *Rhcg* littermates. Throughout the study, food intake was similar in all three genotypes. At base line, no difference in acid-base and electrolyte levels was observed (Tables 1 and 2).

The effects of both acute (2 days) and chronic (7 days) HCl load were tested (Tables 1–3 and Fig. 2). On the 2nd day of the HCl load, blood pH and HCO_3^- concentration were decreased in all genotypes, as compared with base line (Table 1, and Fig. 2, *D* and *E*). Blood pH and HCO_3^- concentrations were significantly lower in $Rhcg^{-/-}$ mice but similar in $Rhcg^{+/-}$ and $Rhcg^{+/+}$ mice. Urinary ammonium excretion rate increased significantly on the 1st day of acid loading in $Rhcg^{+/+}$ and $Rhcg^{+/-}$ mice but much less in $Rhcg^{-/-}$ mice (Tables 2 and 3 and Fig. 2*A*). Urinary pH decreased in $Rhcg^{+/+}$ and $Rhcg^{+/-}$ mice as compared with base-line values (Table 2 and Fig. 2*B*) but to a lesser extent in $Rhcg^{-/-}$ mice. Urinary titratable acid excretion was unaltered in all three genotypes during the acute acid load. Long term HCl loading resulted in the death of most $Rhcg^{-/-}$ mice, which poorly excreted ammonium and exhibited a very severe metabolic acidosis. These animals showed a higher loss of body weight after the acute HCl load presumably due to dehydration (Table 3).

In contrast to the $Rhcg^{+/+}$ mice, which adapted and nearly normalized their blood pH and HCO_3^- concentration, $Rhcg^{+/-}$ remained acidotic at day 7 of the HCl load, even though both genotypes maintained a high NH_4^+ excretion. At the end of the chronic acid load, $Rhcg^{+/-}$ mice showed less increase in their titratable acid excretion and had a more alkaline urine pH (Tables 1 and 2 and Fig. 2, *B* and *C*). Thus, both $Rhcg^{-/-}$ and $Rhcg^{+/-}$ exhibited renal acid handling defects.

Absence of RhCG Abolishes Medullary Ammonium Accumulation—To assess the cortico-papillary gradient of NH_3/NH_4^+ in kidneys from *Rhcg* mice, we measured ammonium content in

TABLE 1

Blood values in *Rhcg* littermates mice under normal diet and during an acid load

	Basal status			2 days HCl			7 days HCl		
	$Rhcg^{+/+}$ ($n = 10$)	$Rhcg^{+/-}$ ($n = 16$)	$Rhcg^{-/-}$ ($n = 9$)	$Rhcg^{+/+}$ ($n = 10$)	$Rhcg^{+/-}$ ($n = 10$)	$Rhcg^{-/-}$ ($n = 9$)	$Rhcg^{+/+}$ ($n = 12$)	$Rhcg^{+/-}$ ($n = 21$)	$Rhcg^{-/-}$ ($n = 2$)
pH	7.38 ± 0.02	7.38 ± 0.02	7.28 ± 0.04	7.17 ± 0.02[a]	7.17 ± 0.02[a]	7.07 ± 0.02[a,b]	7.24 ± 0.03[a]	7.17 ± 0.02[a,b]	6.88 ± 0.07
pCO_2 (mm Hg)	34.0 ± 1.3	37.2 ± 0.9	38.8 ± 1.4[b]	41.2 ± 2.0[a]	39.4 ± 0.7	37.8 ± 0.9	42.0 ± 1.4[a]	40.0 ± 0.8	44.6 ± 1.6
HCO_3 (mM)	19.0 ± 1.1	22.4 ± 1.0	18.3 ± 2.1	14.3 ± 0.6[a]	13.8 ± 0.5[a]	11.1 ± 0.6[a,b]	18.6 ± 1.3	13.9 ± 0.6[a,b]	7.9 ± 1.05
pO_2	74.7 ± 9.7	52.3 ± 3.4	63.6 ± 6.3	60.1 ± 2.3	59.4 ± 1.4	65.7 ± 4.1	57.1 ± 3.0	63.1 ± 3.4	82.3 ± 4.6
Na^+ (mM)	143.9 ± 1.5	145.4 ± 0.9	148.0 ± 0.4	150.1 ± 1.0	145.8 ± 0.8	150.4 ± 0.9	148.3 ± 0.6	149.1 ± 0.5	148.5 ± 1.5
Cl^- (mM)	117.5 ± 1.9	112.1 ± 1.7	111.7 ± 1.5	123.7 ± 1.0[a]	119.7 ± 1.0[a]	126.4 ± 0.9[a]	118.9 ± 0.9	122.6 ± 0.7[a,b]	134.0 ± 0.0
Ionized Ca^{2+} (mM)	1.23 ± 0.02	1.25 ± 0.01	1.29 ± 0.03	1.41 ± 0.03[a]	1.35 ± 0.01[a]	1.42 ± 0.02[a]	1.34 ± 0.01[a]	1.37 ± 0.01[a,b]	1.01 ± 1.9
Glucose (mM)	10.6 ± 0.7	10.9 ± 0.5	10.8 ± 0.8	7.8 ± 0.4[a]	9.0 ± 0.3[b]	6.5 ± 0.4[a,b]	9.6 ± 0.4	8.8 ± 0.3[a]	ND[c]
Hb (g/dl)	15.0 ± 1.1	15.7 ± 0.3	16.3 ± 0.5	16.3 ± 0.4	15.5 ± 0.3	17.5 ± 0.3[a,b]	15.2 ± 0.5	14.9 ± 0.4	17.4 ± 1.0

[a] $p < 0.05$ *versus* base-line period in same genotype is shown.
[b] $p < 0.05$ *versus* $Rhcg^{+/+}$ mice during the same period is shown.
[c] ND, not determined.

TABLE 2

Weight, food intake, and urinary values in *Rhcg* littermate mice under a normal diet and a 2-day HCl load

TA means titratable acid; NA means net acid; UNH_4 means urinary ammonium; UCr means urinary creatinine; UTa means urinary titratable acids; UP_i means urinary inorganic phosphate; Uurea means urinary urea; UNa means urinary Na^+; UCl means urinary Cl^-; and UK means urinary K^+.

	Basal status			2 days of HCl		
	$Rhcg^{+/+}$ ($n = 14$)	$Rhcg^{+/-}$ ($n = 13$)	$Rhcg^{-/-}$ ($n = 13$)	$Rhcg^{+/+}$ ($n = 14$)	$Rhcg^{+/-}$ ($n = 13$)	$Rhcg^{-/-}$ ($n = 13$)
Weight (g)	26.4 ± 0.6	28.7 ± 1.2	27.6 ± 1.0	24.9 ± 0.5	26.6 ± 0.8	25.0 ± 1.1
Weight lose in % of body weight under basal status	ND[a]	ND	ND	8,3 ± 0.4	11.4 ± 1.3	15.0 ± 1.0[b]
Food intake (g/24 h/body weight)	0.31 ± 0.06	0.26 ± 0.02	0.26 ± 0.02	0.24 ± 0.01	0.21 ± 0.01	0.21 ± 0.02
Urine values						
Volume (ml/24 h)	1.9 ± 0.2	2.0 ± 0.1	1.9 ± 0.1	2.5 ± 0.3	2.1 ± 0.2	2.1 ± 0.4[c]
Creatinine excretion (μmol/24 h)	7.6 ± 0.3	6.2 ± 0.6	7.8 ± 0.4	7.5 ± 0.7	5.6 ± 1.4	8.3 ± 2.3
Urinary pH	6.13 ± 0.04	6.18 ± 0.06	6.03 ± 0.06	5.47 ± 0.05[c]	5.44 ± 0.02[c]	5.68 ± 0.06[b,c]
UNH_4/UCr (mEq/mmol)	4.6 ± 1.0	5.1 ± 0.7	4.1 ± 1.0	37.8 ± 4.1[c]	43.8 ± 6.0[c]	11.1 ± 1.5[b,c]
UTA/UCr (mEq/mmol)	15.4 ± 1.2	14.4 ± 1.0	13.6 ± 1.1	20.9 ± 2.5	15.9 ± 3.2	14.5 ± 1.9
UP_i/UCr (mEq/mmol)	16.1 ± 1.7	20.3 ± 1.0	17.7 ± 1.4	9.3 ± 1.5	10.7 ± 1.7	8.2 ± 1.6
Uurea/UCr (mg/mmol)	266.3 ± 14.8	279.3 ± 14.8	280.8 ± 15.0	229.2 ± 17.1	255.1 ± 24.01	146.8 ± 15.7[b,c]
UNA/UCr (mEq/mmol)	20.0 ± 1.4	19.4 ± 0.8	17.7 ± 1.3	58.7 ± 4.9[c]	60.9 ± 9.0[c]	25.6 ± 2.9[b,c]
UNa/UCr (mEq/mmol)	16.8 ± 2.0	10.0 ± 2.0	15.5 ± 2.0	15.4 ± 1.6	15.8 ± 3.6	9.7 ± 1.7
UCl/UCr (mEq/mmol)	32.8 ± 2.0	30.6 ± 1.7	32.6 ± 2.3	133.0 ± 14.4[c]	132.3 ± 19.8[c]	40.5 ± 9.2[b,c]
UK/UCr (mEq/mmol)	60.1 ± 3.9	60.2 ± 4.6	63.1 ± 4..9	53.9 ± 4.3	56.3 ± 7.3	27.7 ± 3.2

[a] ND, not determined.
[b] $p < 0.05$ *versus* $Rhcg^{+/+}$ mice during the same period is shown.
[c] $p < 0.05$ *versus* base-line period in same genotype is shown.

TABLE 3

Weight, food intake, and urinary values in 3-month-old $Rhcg^{+/+}$ and $Rhcg^{+/-}$ littermates during 6 or 7 days of HCl load

TA means titratable acid; NA means net acid; UNH_4 means urinary ammonium; UCr means urinary creatinine; UTa means urinary titratable acids; UP_i means urinary inorganic phosphate; Uurea means urinary urea; UNa means urinary Na^+; UCl means urinary Cl^-; and UK means urinary K^+.

	6 days of HCl			7 days of HCl	
	$Rhcg^{+/+}$ ($n = 8$)	$Rhcg^{+/-}$ ($n = 10$)	$Rhcg^{-/-}$ ($n = 2$)	$Rhcg^{+/+}$ ($n = 8$)	$Rhcg^{+/-}$ ($n = 10$)
Weight (g)	ND[a]	ND	19.6–22.4	25.1 ± 1.2	23.3 ± 0.8[b]
Weight lose in % of body weight under basal status	ND	ND	ND	10.0 ± 1.1 ($n = 5$)	14.8 ± 2.1 ($n = 5$)
Food intake (g/24 h/body weight)	ND	ND	0.31–0.44	0.37 ± 0.03	0.39 ± 0.02
Urine values					
Volume (ml/24 h)	3.8 ± 0.8[b]	4.4 ± 0.8[b]	2.5–2.6	3.1 ± 0.2[b]	3.9 ± 0.1[b]
[a]Creatinine excretion (μmol/24 h)	8.5 ± 2.0	7.2 ± 1.8	3.8–4.3	6.6 ± 0.3	7.9 ± 1.4
[a]Urinary pH	5.39 ± 0.13[b]	5.59 ± 0.07[b]	5.20–5 .52	5.57 ± 0.02[b]	5.73 ± 0.05[b,c]
[a]UNH_4/UCr (mEq/mmol)	153.9 ± 31.1[b]	173.1 ± 20.6[b]	17.3–36.3	147.4 ± 26.3[b]	171.8 ± 22.3[b]
[a]UTA/UCr (mEq/mmol)	25.4 ± 2.6[b]	17.9 ± 2.5	28.6–36.2	26.3 ± 0.6[b]	16.6 ± 0.7[c]
[a]UP_i/UCr (mEq/mmol)	ND	ND	ND	9.8 ± 3.7	25.0 ± 8.8
[a]UNA/UCr (mEq/mmol)	131.2 ± 6.3[b]	128.5 ± 16.4[b]	68.9–53.4	126.8 ± 9.8	118.3 ± 15.0
[a]Uurea/UCr (mg/mmol)	205.2 ± 11.2[b]	220.3 ± 9.9[ab]	186.4–230.1	208.9 ± 6.3[b]	220.6 ± 5.5[b]
[a]UNa/UCr (mEq/mmol)	36.9 ± 3.8[b]	32.9 ± 2.8[b]	67.4–70.9	43.0 ± 3.0[b]	38.4 ± 4.0[b]
[a]UCl/UCr (mEq/mmol)	242.6 ± 11.2[b]	253.6 ± 11.4[b]	135.1–173.1	269.5 ± 12.0[b]	263.5 ± 14.9[b]
[a]UK/UCr (mEq/mmol)	77.6 ± 4.2	79.7 ± 4.1	19.6–22.4	92.2 ± 2.0	85.2 ± 9.9

[a] ND means not determined.
[b] $p < 0.05$ *versus* base-line period in the same genotype.
[c] $p < 0.05$ *versus* $Rhcg^{+/+}$ mice during the same period.

the cortex and outer and inner medulla after 4 days of HCl treatment. There was no difference between $Rhcg^{+/+}$ and $Rhcg^{+/-}$ mice. However, the inner medulla ammonium content was strongly reduced to 39% in $Rhcg^{-/-}$ mice (Fig. 3). Thus, the absence of *Rhcg* impairs the ability to concentrate ammonium in the interstitium of the inner medulla.

RhCG Is Located at the Apical and Basolateral Sides of Cells Along the Distal Nephron—RhCG has been localized to most cells of the CD, including type A intercalated cells as well as principal cells (9, 17). However, the subcellular localization of RhCG has remained controversial because some groups reported both apical and basolateral staining (10, 17), whereas

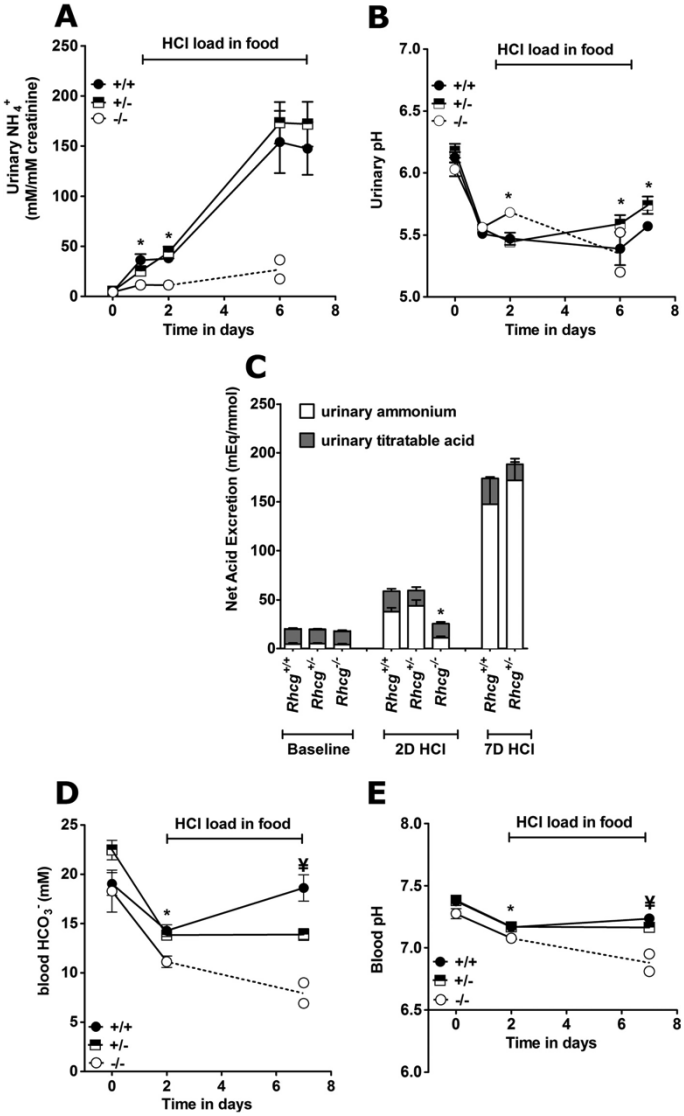

FIGURE 2. **Incomplete dRTA in *Rhcg*$^{+/-}$ and *Rhcg*$^{-/-}$ mice.** Mice were observed in metabolic cages under basal conditions and during an acid load for up to 7 days with HCl added to the diet (n = 5–10 per genotype). *Rhcg*$^{-/-}$ could only be observed for 6 days during the HCl-containing diet because most animals had to be terminated earlier. *A*, urinary ammonium excretion in 24-h urine collections normalized for urinary creatinine. *B*, urinary pH in 24-h urine collections. *C*, urinary net acid excretion (*total bars*) calculated from urinary ammonium (*open bars*) plus titratable acid (*gray bars*). Urinary bicarbonate levels were measured and negligible. *D*, blood bicarbonate concentrations. *E*, blood pH values. *, $p < 0.05$ for *Rhcg*$^{-/-}$ *versus Rhcg*$^{+/+}$. ¥, $p < 0.05$ for *Rhcg*$^{+/-}$ *versus Rhcg*$^{+/+}$.

others detected only apical staining for RhCG (9) based on different immunohistochemical methods. We confirmed a strong labeling of both apical and basolateral poles of CD cells in mouse kidneys (Fig. 4 and Table 4). This staining was absent from *Rhcg*$^{-/-}$ kidneys demonstrating its specificity. In the kidney cortex, RhCG was localized in the distal convoluted tubule, connecting tubule, and CCD (Fig. 4*A*). In the distal convoluted tubule cells, RhCG was mainly present at the apical side (Fig. 4*A*). In the connecting tubule, CCD and OMCD, both intercalated and principal cells, were stained. Principal cells and some intercalated cells exhibited RhCG staining at both the apical and basolateral sides (Fig. 4, *A–C*). However, in some cells

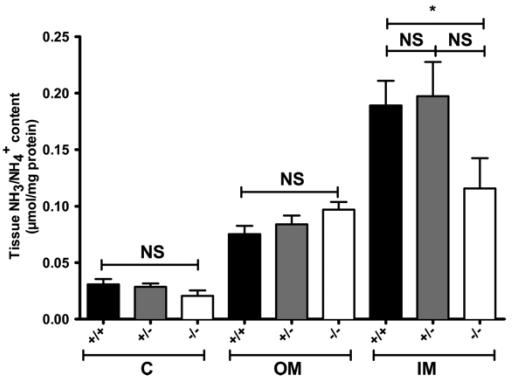

FIGURE 3. **Medullary ammonium accumulation is altered in *Rhcg*$^{-/-}$ mice.** Kidneys from all three genotypes were dissected after 4 days of HCl load. Cortex (*C*), outer medulla (*OM*), and inner medulla (*IM*) were separated, and tissue ammonium content was measured. In wild type and heterozygous mice, a gradient in renal tissue ammonia content from cortex to inner medulla was observed. In *Rhcg*$^{-/-}$ mice, the ammonia content increased from cortex to outer medulla, but ammonium content was lower in the inner medulla than in mice from the other two genotypes. (n = 5–8 mice/genotype), * statistically different from *Rhcg*$^{+/+}$ mice ($p < 0.05$). *NS*, not significant.

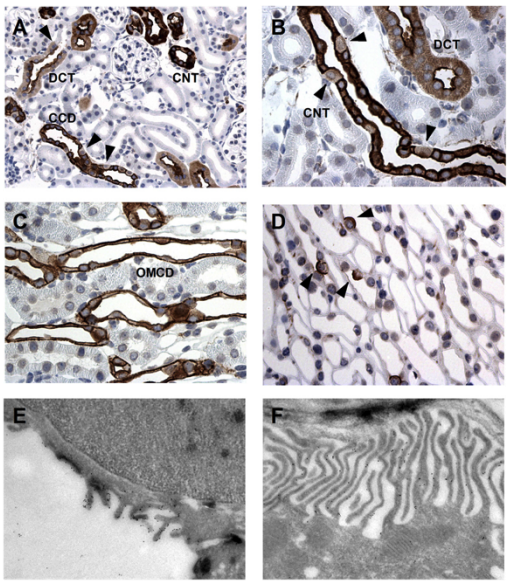

FIGURE 4. **Rhcg immunodetection in mouse kidney and immunogold electron microscopic localization of Rhcg in CCD.** *A* and *B*, Rhcg protein immunodetection in mouse kidney cortex. *Rhc*-related staining was detected in the distal convoluted tubule (*DCT*) starting immediately at the transition from the thick ascending limb (*TAL*) to the distal convoluted tubule (*arrowhead*), in the connecting tubule (*CNT*) and CCD. Most but not all cells are stained. Rhcg staining is observed in most cells at the apical and basolateral sides, but in some cells (*arrowheads*) only an apical signal is detected. *C*, Rhcg immunodetection in outer medulla. Rhcg is strictly expressed in collecting ducts at both sides of intercalated and segment-specific cells. *D*, in the inner medulla, Rhcg is expressed only in intercalated cells. *E* and *F*, Rhcg was detected both at the apical membrane (*E*) and at the invaginations of the basolateral membrane (*F*) of segment-specific cells in the cortical collecting duct by gold immunoelectron microscopy.

RhCG was strictly localized at the apical pole (see *arrowheads* in Fig. 4, *A*, *B*, and *D*). These cells have been previously identified as non-A/non-B type intercalated cells (33, 34). Finally, in the inner medulla, only strong apical and faint basolateral staining were found in intercalated cells (Fig. 4 and Table 4). Immunogold electron microscopy demonstrated RhCG associated with the apical membrane as well as the basolateral interdigitations of segment specific and intercalated cells (Fig. 4, *E* and *F*). No specific immunogold labeling was found in kidneys from *Rhcg*$^{-/-}$ mice (data not shown). Thus, RhCG protein is expressed on both apical and basolateral membranes in mouse segment-specific principal and intercalated CD cells.

Total and Apical Membrane Permeabilities for NH_3 Are Reduced in CDs from Rhcg$^{+/-}$ *Mice*—We assessed total transepithelial permeability for NH_3 in *in vitro* microperfused cortical CDs from *Rhcg* mice after a 2-day HCl diet, a condition causing a strong difference in urinary ammonium excretion between *Rhcg*$^{+/+}$ and *Rhcg*$^{-/-}$ mice. Imposing a bath-to-lumen NH_3 gradient in the nominal absence of an NH_4^+ gradient generated a measurable NH_3 secretory flux, which was significantly lower in CCDs from *Rhcg*$^{+/-}$ and *Rhcg*$^{-/-}$ mice *versus* *Rhcg*$^{+/+}$ mice. These differences were due to a decrease in transepithelial permeability to NH_3 by 54 and 83%, respectively (Table 5 and Fig. 5). Thus, one *Rhcg* allele was not sufficient to sustain normal transepithelial permeability to NH_3 in the mouse collecting duct.

Next, we tested whether the apical permeability to NH_3 was affected in CDs from *Rhcg*$^{+/-}$ mice. Therefore, we measured the effects of an inwardly directed gradient on pH_i on CCDs isolated from *Rhcg*$^{+/+}$ and *Rhcg*$^{+/-}$ mice (13). Fig. 6*A* depicts the typical time course of pH_i changes when NH_3/NH_4^+ was added to the lumen tubule. The initial rate of cellular alkalinization is proportional to the rate of apical NH_3 entry as described previously (13, 35, 36). To directly compare transport rates, we measured intracellular buffering power and calculated the amount of H^+ used to titrate NH_3 transported across the membrane. Fig. 6*B* depicts the calculated rate of NH_3 transported into CDs from *Rhcg*$^{+/+}$ and *Rhcg*$^{+/-}$ mice, which was drastically reduced in *Rhcg*$^{+/-}$ tissue.

Basolateral RhCG Accounts for Peritubular Membrane Permeability to NH_3—Because RhCG is expressed at both sides of at least a subset of CD cells (Fig. 4 and Table 4), we next tested the effect of *Rhcg* disruption on NH_3 transport across the basolateral membranes of CCD cells. Several transport pathways for NH_4^+ have been proposed at the basolateral side of CD cells, including the Na^+-K^+-$2Cl^-$ cotransporter NKCC1 and the Na/K-ATPase where NH_4^+ would substitute for K^+ (37, 38). Therefore, we performed experiments in the nominal absence of sodium to block the activity of both transport pathways.

Peritubular NH_3/NH_4^+ prepulses were performed on cortical CDs from *Rhcg*$^{+/+}$, *Rhcg*$^{+/-}$, and *Rhcg*$^{-/-}$ mice submitted to HCl loading for 2 days. As summarized in Fig. 7, when NH_3/NH_4^+ (6 mM) was applied to the basolateral side, the calculated rate of NH_3 transport into CD cells was unchanged in *Rhcg*$^{+/-}$ tissue but strongly reduced in *Rhcg*$^{-/-}$ tissue. Thus, RhCG sustains both apical and basolateral transport of NH3 in CD cells, in agreement

TABLE 4
Summary of RhCG localization along the mouse nephron
CNT is connecting tubule; DCT is distal convoluted tubule.

	Tubule type	Cell type	Localization	Staining intensity
Cortex	DCT		Apical	High
			Basolateral	Weak
	CNT	Principal cells	Plasma membrane	High
		Intercalated cells	Plasma membrane/apical	High
	CCD	Principal cells	Plasma membrane	High
		Intercalated cells	Plasma membrane/apical	High
Outer medulla	OMCD	Principal cells	Plasma membrane/apical	High
		Intercalated cells		
Inner medulla	IMCD	Principal cells	No staining	
		Intercalated cells	Plasma membrane/apical	Weak/high

TABLE 5
CCD *in vitro* microperfusion data from *Rhcg*$^{+/+}$, *Rhcg*$^{+/-}$, and *Rhcg*$^{-/-}$ mice
Values are mean ± S.E.; *n* means no. of mice.

	Rhcg$^{+/+}$ (*n* = 7)	*Rhcg*$^{+/-}$ (*n* = 9)	*Rhcg*$^{-/-}$ (*n* = 5)
Tubule length, mm	0.38 ± 0.04	0.36 ± 0.05	0.034 ± 0.08
Tubule diameter, μm	54.98 ± 4.55	47.92 ± 4.24	44.31 ± 8.88
Collection rate, nl·mm^{-1}·min^{-1}	4.61 ± 0.22	4.37 ± 0.29	3.96 ± 0.42
Perfusate pH	6.44 ± 0.04	6.37 ± 0.04	6.50 ± 0.04
Bath pH	7.42 ± 0.03	7.37 ± 0.03	7.38 ± 0.03
Total ammonia perfusate, mM	1.41 ± 0.08	1.40 ± 0.08	1.42 ± 0.13
[NH_3] perfusate, μM	3.74 ± 0.37	3.30 ± 0.32	4.16 ± 0.25
Total ammonia bath, mM	1.41 ± 0.08	1.40 ± 0.08	1.42 ± 0.13
[NH_3] bath, μM	34.38 ± 3.26	32.57 ± 3.72	31.39 ± 3.71
Total ammonia collected, mM	3.88 ± 0.42	2.47 ± 0.36	1.48 ± 0.35
[NH_3] collected, μM	10.37 ± 1.45	5.90 ± 1.24[a]	4.25 ± 0.93[a]
Total ammonia flux, pmol·mm^{-1}·min^{-1}	32.98 ± 3.32[a]	17.84 ± 4.56[a]	2.51 ± 3.51[a]
NH_3 permeability, mm/s	0.13 ± 0.02	0.08 ± 0.02[a]	0.02 ± 0.02[a]

[a] $p < 0.05$ *versus* control mice.

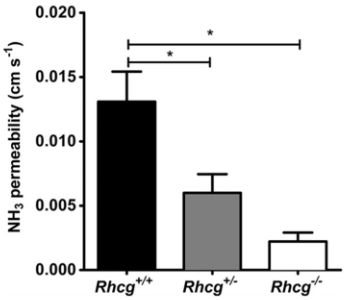

FIGURE 5. **Transepithelial NH_3 permeability is reduced in the cortical collecting duct from *Rhcg*$^{+/-}$ and *Rhcg*$^{-/-}$ mice.** Transepithelial permeability to NH_3 was assessed in *in vitro* isolated and microperfused cortical collecting ducts from mice kept for 2 days on an HCl diet by imposing a bath-to-lumen NH_3 gradient (see under "Experimental Procedures") (*, $p < 0.05$).

with structural data and reconstituted RhCG suggesting that the protein forms a NH_3-permeable channel (39, 40).

Compensatory Adaptations to the Loss of Rhcg—We finally examined whether *Rhcg* deletion affects mechanisms involved in renal ammoniagenesis and ammonium excretion. Surprisingly, immunoblots of whole kidney extracts from mice subjected to a 2-day HCl load revealed no differences in the expression of PEPCK expression (Fig. 8*A*). In contrast, the expression of the PDG, mediating the initial step of ammoniagenesis was decreased in *Rhcg*$^{+/-}$ kidneys as compared with both *Rhcg*$^{+/+}$ and *Rhcg*$^{-/-}$ kidneys (Fig. 8*B*). The abundance of the Na^+/H^+ exchanger NHE3, involved in NH_4^+ secretion into the proximal tubule lumen, was unchanged (Fig. 8*C*). Moreover, the expression of the Na^+-K^+-$2Cl^-$ cotransporter NKCC2, the main apical NH_4^+ transporter in the thick ascending limb, was highly down-regulated in kidneys from *Rhcg*$^{+/-}$ and *Rhcg*$^{-/-}$ mice (Fig. 8*D*).

DISCUSSION

Renal ammonium excretion is critical for acid-base homeostasis and is achieved by a complex process involving various nephron segments (2, 5, 6). A critical role for the Rhesus protein RhCG was demonstrated in tissue-specific and complete knock-out mouse models (13–15). However, metabolic effects of *Rhcg* haploinsufficiency, the role of RhCG in basolateral NH_3 transport in CD cells, and the response of other pathways critical for renal ammoniagenesis and ammonium transport have remained unknown. Based on a novel *Rhcg* mouse model, we show that *Rhcg* haploinsufficiency causes incomplete metabolic acidosis in mice. Next, RhCG contributes to peritubular NH_3 uptake giving functional evidence to the basolateral localization of RhCG in CD cells.

Rhcg$^{-/-}$ *Mice Develop a Severe Incomplete Renal Tubular Acidosis*—*Rhcg*$^{-/-}$ develop incomplete dRTA as evident from the inability to respond to an acute oral acid load. They showed severe hyperchloremic metabolic acidosis and did not increase urinary ammonium excretion resulting in low net acid excretion. Moreover, these animals had a drastic reduction in their blood HCO_3^- concentration and pH. *Rhcg*$^{-/-}$ mice developed severe dehydration as indicated by high blood hemoglobin and weight loss (Tables 2 and 4). These phenotypes are more pronounced than in mice with partial deletion of *Rhcg* (14, 15).

Rhcg Haploinsufficiency Leads to Metabolic Acidosis—Similarly, *Rhcg*$^{+/-}$ mice develop also an incomplete dRTA. However, these mice initially responded to the acid load by increasing urinary ammonium excretion to the same extent as

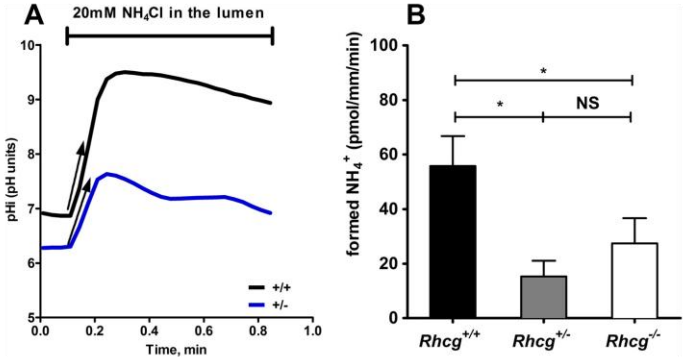

FIGURE 6. **RhCG is required for apical NH_3 permeability of cortical collecting duct cells.** Cortical collecting ducts were isolated from kidneys of $Rhcg^{+/+}$, $Rhcg^{+/-}$, and $Rhcg^{-/-}$ mice after 2 days of HCl loading, and intracellular pH was monitored with BCECF. 20 mM NH_4Cl was applied with the luminal perfusate. *A*, pH_i recording from CCD exposed to a luminal NH_4Cl pulse in $Rhcg^{+/+}$ and $Rhcg^{+/-}$ CCD. Exposure to NH_4Cl caused a rapid alkalinization corresponding to NH_3 entry into cells. The initial slopes ($\Delta pH_i/\Delta t$) of the alkalinization phase were measured, and the amount of NH_3 titrated into NH_4^+ was finally calculated based on intracellular buffering power. *B, bar graph* summarizing the amount of titrated NH_3 during luminal NH_4Cl pulses ($n = 8–12$ tubules/genotype). *, $p < 0.05$; *NS*, not significant.

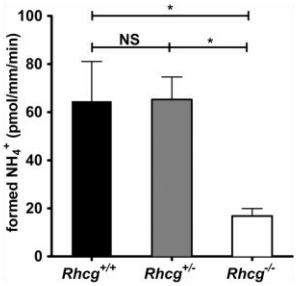

FIGURE 7. **Basolateral NH_3 permeability of cortical collecting duct cells.** Cortical collecting ducts were isolated from kidneys of $Rhcg^{+/+}$, $Rhcg^{+/-}$, and $Rhcg^{-/-}$ mice after 2 days of HCl loading, and intracellular pH was monitored with BCECF. After an equilibrium phase, 6 mM NH_4Cl was applied to the bath. Exposure to NH_4Cl caused a rapid alkalinization corresponding to NH_3 entry into cells. The initial slopes ($\Delta pH_i/\Delta t$) of the alkalinization phase were measured, and the amount of NH_3 titrated into NH_4^+ was finally calculated based on intracellular buffering power. The *bar graph* summarizes the amount of titrated NH_3 (alkalinization phase) during basolateral NH_4Cl pulses ($n = 5–7$ tubules/genotype). *, $p < 0.05$; *NS*, not significant.

$Rhcg^{+/+}$ mice. Later, they did not fully adapt to chronic acid loading and remained acidotic after 7 days of HCl loading, being unable to correct blood HCO_3^- concentration and excreting more alkaline urine, whereas total net acid excretion was comparable with $Rhcg^{+/+}$ animals. The incomplete chronic metabolic acidosis in $Rhcg^{+/-}$ mice is at least in part due to the inability to maximally acidify urine and to excrete adequate amounts of acid in the form of titratable acidity. The metabolic phenotype of $Rhcg^{+/-}$ mice was further supported by functional studies on microperfused CCDs. Transepithelial permeability to NH_3 was reduced in CCDs from $Rhcg^{-/-}$ and $Rhcg^{+/-}$ mice. The reduction in NH_3 permeability in CCDs from $Rhcg^{+/-}$ mice was less than in $Rhcg^{-/-}$ mice, suggesting that a 50% reduction in net NH_3 permeability in CCDs is still sufficient to support high ammonium excretion but is not enough to correct metabolic acidosis. Of note, medullary accumulation of NH_3/NH_4^+ appeared to be intact. Together, these results represent the first evidence that loss of a single *Rhcg* allele can lead to chronic hyperchloremic metabolic acidosis.

Renal Adaptation to Rhcg Invalidation—We further examined compensatory mechanisms in $Rhcg^{+/-}$ and $Rhcg^{-/-}$ mice. The generation of the cortico-papillary gradient of ammonium is required for the subsequent uptake of NH_3 and NH_4^+ by intercalated cells and the secretion of NH_3 into urine. Surprisingly, $Rhcg^{-/-}$ mice had low tissue ammonium content in the inner medulla after 4 days of acid loading. This result suggests that the absence of RhCG affects the ability of the medulla to generate or maintain a high interstitium ammonium content. Because the key enzymes of proximal tubular ammoniagenesis, PEPCK and PDG, were normally expressed in $Rhcg^{-/-}$ kidney tissue, mice most likely form adequate amounts of ammonium. In $Rhcg^{-/-}$ mice, this ammonium might be either shunted back into systemic circulation or not be absorbed at the level of the thick ascending limb.

Expression of NKCC2 was decreased in both $Rhcg^{+/-}$ and $Rhcg^{-/-}$ kidney tissues. NKCC2 is crucial for thick ascending limb NH_4^+ absorption and concentration in the medulla. Thus, our results suggest that mechanisms contributing to create a high medullary ammonium concentration are altered in *Rhcg*-deficient mice. Other mechanisms such as increased removal of ammonium from the interstitium with venous blood might contribute also to the low medullary ammonium content. Metabolic acidosis alters concentrations of various vasoactive substances in the kidney, including higher levels of endothelin and prostaglandins and lower concentrations of NO (41, 42), which may alter medullary blood flow and the ability of the kidneys to maintain the cortico-papillary ammonium gradient.

RhCG Mediates NH_3 Transport Also at the Basolateral Side of CD Cells—Subcellular RhCG localization has remained controversial for many years (9, 10, 17). Here, we confirmed a strong labeling of both apical and basolateral poles of CD cells in mouse kidneys. These data were corroborated by our functional study on *in vitro* microperfused CCDs. We measured a 60% reduction in the NH_3 permeability at the basolateral side of

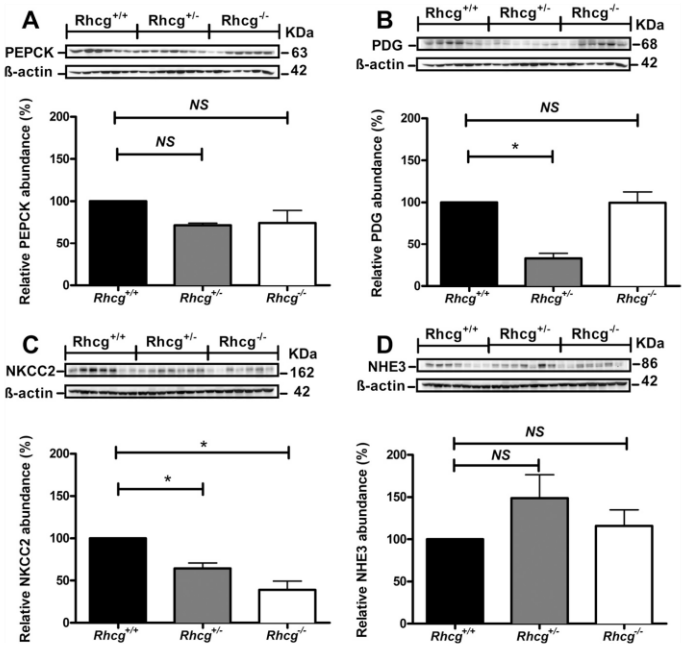

FIGURE 8. **Deletion of *Rhcg* affects the abundance of proteins involved in ammoniagenesis and ammonium transport.** Crude membrane and cytosolic fractions were prepared from total kidneys from $Rhcg^{+/+}$, $Rhcg^{+/-}$ and $Rhcg^{-/-}$ mice after 2 days of HCl loading, 40 μg loaded onto SDS-PAGE, and their abundance tested. *A*, PEPCK; *B*, PDG; *C*, the Na^+-K^+-$2Cl^-$ cotransporter isoform 2 (*NKCC2*); and *D*, Na^+/H^+ exchanger isoform 3 (*NHE3*). All membranes were stripped and reprobed for β-actin to control for loading. *Bar graphs* summarize results from densitometric analysis of proteins of interest normalized against β-actin. $n = 5$ mice/genotype. * statistically significant, $p < 0.05$ *versus* $Rhcg^{+/+}$ tissue. *NS*, not significant.

$Rhcg^{-/-}$ CCD cells. This is the first evidence that Rhcg is also functional at the basolateral side of CDs cells and participates in basolateral NH_3 uptake. Previously, it has been assumed that basolateral uptake occurs mostly if not exclusively in the form of NH_4^+ and that NH_3 plays no major role. Several pathways for NH_4^+ uptake have been delineated from pharmacological and functional experiments that demonstrated a role for the Na^+-K^+-$2Cl^-$ cotransporter NKCC1, the Na^+/K^+-ATPase, and possibly potassium channels where NH_4^+ always would replace potassium (37, 38, 43). We performed our experiments in the absence of sodium to reduce NKCC1 and Na^+/K^+-ATPase activity, respectively. Thus, our experiments do not allow conclusions regarding the relative importance and contribution of these different pathways to total NH_3/NH_4^+ uptake across the basolateral membrane, but they modify the current model of ammonium transport across the basolateral membrane. However it appears from the data on $Rhcg^{+/-}$ CCD that apical NH_3 flux critically depends on full RhCG expression, whereas basolateral NH_3 flux is sustained with reduced RhCG expression suggesting that transport of the NH_3 form is most important at the apical side. Finally, our findings could also explain the complete lack or only mild phenotype observed in *Rhbg* knock-out mice (11, 44), where RhCG may have compensated for the lack of *RhBG*.

In summary, reduced expression or complete loss of expression of RhCG affects the ability of the kidneys to excrete acidic urine and appropriately regulate acid/base homeostasis. We provide the first functional evidence for basolateral RhCG activity and show that RhCG is expressed and functional on apical and basolateral membranes of most cells lining the renal collecting duct. Thus, *Rhcg* haploinsufficiency or *Rhcg* deletion may contribute to orphan forms of inherited distal renal tubular acidosis in humans as well as to acquired forms of dRTA.

Acknowledgments—We thank Yves Colin and Isabelle Mourot-Chanteloup for fruitful discussions. We also thank Hanne Siedelmann for skillful technical assistance. The use of the Zurich Integrative Rodent Physiology Core Facility is gratefully acknowledged.

REFERENCES

1. Hamm, L. L., Alpern, R. J., and Preisig, P. A. (2008) in *Seldin and Giebisch's The Kidney. Physiology and Pathophysiology* (Alpern, R. J., and Hebert, S. C., eds) pp. 1539–1585, Academic Press, New York
2. Weiner, I. D., and Verlander, J. W. (2011) Role of NH_3 and NH_4^+ transporters in renal acid-base transport. *Am. J. Physiol. Renal Physiol.* **300,** F11–F23
3. Batlle, D. C., and Kurtzman, N. A. (1985) in *Renal Tubular Disorders* (Gonick, H. C., and Buckalew, V. M., eds) pp. 281–305, Marcel Dekker, Inc., New York
4. Good, D. W. (1994) Ammonium transport by the thick ascending limb of Henle's loop. *Annu. Rev. Physiol.* **56,** 623–647
5. Wagner, C. A., Devuyst, O., Belge, H., Bourgeois, S., and Houillier, P.

(2011) The rhesus protein RhCG. A new perspective in ammonium transport and distal urinary acidification. *Kidney Int.* **79,** 154–161
6. Wagner, C. A., Devuyst, O., Bourgeois, S., and Mohebbi, N. (2009) Regulated acid-base transport in the collecting duct. *Pflugers Arch.* **458,** 137–156
7. Wagner, C. A., Finberg, K. E., Breton, S., Marshansky, V., Brown, D., and Geibel, J. P. (2004) Renal vacuolar H^+-ATPase. *Physiol. Rev.* **84,** 1263–1314
8. DuBose, T. D., Jr., Good, D. W., Hamm, L. L., and Wall, S. M. (1991) Ammonium transport in the kidney: new physiological concepts and their clinical implications. *J. Am. Soc. Nephrol.* **1,** 1193–1203
9. Quentin, F., Eladari, D., Cheval, L., Lopez, C., Goossens, D., Colin, Y., Cartron, J. P., Paillard, M., and Chambrey, R. (2003) RhBG and RhCG, the putative ammonia transporters, are expressed in the same cells in the distal nephron. *J. Am. Soc. Nephrol.* **14,** 545–554
10. Brown, A. C., Hallouane, D., Mawby, W. J., Karet, F. E., Saleem, M. A., Howie, A. J., and Toye, A. M. (2009) RhCG is the major putative ammonia transporter expressed in the human kidney, and RhBG is not expressed at detectable levels. *Am. J. Physiol. Renal Physiol.* **296,** F1279–F1290
11. Chambrey, R., Goossens, D., Bourgeois, S., Picard, N., Bloch-Faure, M., Leviel, F., Geoffroy, V., Cambillau, M., Colin, Y., Paillard, M., Houillier, P., Cartron, J. P., and Eladari, D. (2005) Genetic ablation of Rhbg in the mouse does not impair renal ammonium excretion. *Am. J. Physiol. Renal Physiol.* **289,** F1281–F1290
12. Bishop, J. M., Verlander, J. W., Lee, H. W., Nelson, R. D., Weiner, A. J., Handlogten, M. E., and Weiner, I. D. (2010) *Am. J. Physiol. Renal Physiol.* **299,** F1065–F1077
13. Biver, S., Belge, H., Bourgeois, S., Van Vooren, P., Nowik, M., Scohy, S., Houillier, P., Szpirer, J., Szpirer, C., Wagner, C. A., Devuyst, O., and Marini, A. M. (2008) A role for rhesus factor Rhcg in renal ammonium excretion and male fertility. *Nature* **456,** 339–343
14. Lee, H. W., Verlander, J. W., Bishop, J. M., Igarashi, P., Handlogten, M. E., and Weiner, I. D. (2009) Collecting duct-specific Rh C glycoprotein deletion alters basal and acidosis-stimulated renal ammonia excretion. *Am. J. Physiol. Renal Physiol.* **296,** F1364–F1375
15. Han, K. H., Lee, S. Y., Kim, W. Y., Shin, J. A., Kim, J., and Weiner, I. D. (2010) Expression of ammonia transporter family members, Rh B glycoprotein and Rh C glycoprotein, in the developing rat kidney. *Am. J. Physiol. Renal Physiol.* **299,** F187–F198
16. Eladari, D., Cheval, L., Quentin, F., Bertrand, O., Mouro, I., Cherif-Zahar, B., Cartron, J. P., Paillard, M., Doucet, A., and Chambrey, R. (2002) Expression of RhCG, a new putative NH_3/NH_4^+ transporter, along the rat nephron. *J. Am. Soc. Nephrol.* **13,** 1999–2008
17. Kim, H. Y., Verlander, J. W., Bishop, J. M., Cain, B. D., Han, K. H., Igarashi, P., Lee, H. W., Handlogten, M. E., and Weiner, I. D. (2009) Basolateral expression of the ammonia transporter family member Rh C glycoprotein in the mouse kidney. *Am. J. Physiol. Renal Physiol.* **296,** F543–F555
18. Jorgensen, K. (1957) Titrimetric determination of the net excretion of acid/base in urine. *Scand. J. Clin. Lab. Invest.* **9,** 287–291
19. Nutbourne, D. M. (1961) The effect of dilution on the titratable acid in urine and acidified phosphate buffer solutions, and the correction for this effect in the determination of the rate of elimination of hydrogen ions from the body by the renal tubules. *Clin. Sci.* **20,** 263–278
20. Seaton, B., and Ali, A. (1984) Simplified manual high performance clinical chemistry methods for developing countries. *Med. Lab. Sci.* **41,** 327–336
21. Berthelot, M. (1859) Violet d'aniline. *Rep. Chim. App.* **1,** 284
22. Curthoys, N. P., Kuhlenschmidt, T., Godfrey, S. S., and Weiss, R. F. (1976) Phosphate-dependent glutaminase from rat kidney. Cause of increased activity in response to acidosis and identity with glutaminase from other tissues. *Arch. Biochem. Biophys.* **172,** 162–167
23. Hafner, P., Grimaldi, R., Capuano, P., Capasso, G., and Wagner, C. A. (2008) Pendrin in the mouse kidney is primarily regulated by Cl^- excretion but also by systemic metabolic acidosis. *Am. J. Physiol. Cell Physiol.* **295,** C1658–C1667
24. Christensen, E. I., Nielsen, S., Moestrup, S. K., Borre, C., Maunsbach, A. B., de Heer, E., Ronco, P., Hammond, T. G., and Verroust, P. (1995) Segmental distribution of the endocytosis receptor gp330 in renal proximal tubules. *Eur. J. Cell Biol.* **66,** 349–364
25. Marini, A. M., Matassi, G., Raynal, V., André, B., Cartron, J. P., and Chérif-Zahar, B. (2000) The human Rhesus-associated RhAG protein and a kidney homologue promote ammonium transport in yeast. *Nat. Genet.* **26,** 341–344
26. Packer, R. K., Desai, S. S., Hornbuckle, K., and Knepper, M. A. (1991) Role of countercurrent multiplication in renal ammonium handling. Regulation of medullary ammonium accumulation. *J. Am. Soc. Nephrol.* **2,** 77–83
27. Watts, B. A., 3rd, and Good, D. W. (1994) Apical membrane Na^+/H^+ exchange in rat medullary thick ascending limb. pH dependence and inhibition by hyperosmolality. *J. Biol. Chem.* **269,** 20250–20255
28. Roos, A., and Boron, W. F. (1981) Intracellular pH. *Physiol. Rev.* **61,** 296–434
29. Milton, A. E., and Weiner, I. D. (1998) Regulation of B-type intercalated cell apical anion exchange activity by CO_2/HCO_3^-. *Am. J. Physiol.* **274,** F1086–F1094
30. Flessner, M. F., Wall, S. M., and Knepper, M. A. (1992) Ammonium and bicarbonate transport in rat outer medullary collecting ducts. *Am. J. Physiol.* **262,** F1–F7
31. Zhelyaskov, V. R., Liu, S., and Broderick, M. P. (2000) Analysis of nanoliter samples of electrolytes using a flow-through microfluorometer. *Kidney Int.* **57,** 1764–1769
32. Hansen, G. M., Markesich, D. C., Burnett, M. B., Zhu, Q., Dionne, K. M., Richter, L. J., Finnell, R. H., Sands, A. T., Zambrowicz, B. P., and Abuin, A. (2008) Large-scale gene trapping in C57BL/6N mouse embryonic stem cells. *Genome Res.* **18,** 1670–1679
33. Verlander, J. W., Miller, R. T., Frank, A. E., Royaux, I. E., Kim, Y. H., and Weiner, I. D. (2003) Localization of the ammonium transporter proteins RhBG and RhCG in mouse kidney. *Am. J. Physiol. Renal Physiol.* **284,** F323–F337
34. Kim, H. Y., Verlander, J. W., Bishop, J. M., Cain, B. D., Han, K. H., Igarashi, P., Lee, H. W., Handlogten, M. E., and Weiner, I. D. (2009) *Am. J. Physiol. Renal Physiol.* **296,** F1364–F1375
35. Kikeri, D., Sun, A., Zeidel, M. L., and Hebert, S. C. (1989) Cell membranes impermeable to NH_3. *Nature* **339,** 478–480
36. Bleich, M., Köttgen, M., Schlatter, E., and Greger, R. (1995) Effect of NH_4^+/NH_3 on cytosolic pH and the K^+ channels of freshly isolated cells from the thick ascending limb of Henle's loop. *Pflugers Arch.* **429,** 345–354
37. Wall, S. M., and Koger, L. M. (1994) NH_4^+ transport mediated by Na^+-K^+-ATPase in rat inner medullary collecting duct. *Am. J. Physiol.* **267,** F660–F670
38. Wall, S. M., and Fischer, M. P. (2002) Contribution of the Na^+-K^+-$2Cl^-$ cotransporter (NKCC1) to transepithelial transport of H^+, NH_4^+, K^+, and Na^+ in rat outer medullary collecting duct. *J. Am. Soc. Nephrol.* **13,** 827–835
39. Gruswitz, F., Chaudhary, S., Ho, J. D., Schlessinger, A., Pezeshki, B., Ho, C. M., Sali, A., Westhoff, C. M., and Stroud, R. M. (2010) Function of human Rh based on structure of RhCG at 2.1 A. *Proc. Natl. Acad. Sci. U.S.A.* **107,** 9638–9643
40. Mouro-Chanteloup, I., Cochet, S., Chami, M., Genetet, S., Zidi-Yahiaoui, N., Engel, A., Colin, Y., Bertrand, O., and Ripoche, P. (2010) Functional reconstitution into liposomes of purified human RhCG ammonia channel. *PLoS ONE* **5,** e8921
41. Jones, E. R., Beck, T. R., Kapoor, S., Shay, R., and Narins, R. G. (1984) Prostaglandins inhibit renal ammoniagenesis in the rat. *J. Clin. Invest.* **74,** 992–1002
42. Prabhakar, S. S. (2004) Regulatory and functional interaction of vasoactive factors in the kidney and extracellular pH. *Kidney Int.* **66,** 1742–1754
43. Wall, S. M., Fischer, M. P., Kim, G. H., Nguyen, B. M., and Hassell, K. A. (2002) In rat inner medullary collecting duct, NH uptake by the Na,K-ATPase is increased during hypokalemia. *Am. J. Physiol. Renal Physiol.* **282,** F91–F102
44. Bishop, J. M., Verlander, J. W., Lee, H. W., Nelson, R. D., Weiner, A. J., Handlogten, M. E., and Weiner, I. D. (2010) Role of the Rhesus glycoprotein, Rh B glycoprotein, in renal ammonia excretion. *Am. J. Physiol. Renal Physiol.* **299,** F1065–F1077

III The role of the renal ammonia transporter in metabolic responses to dietary protein

Own contribution to the publication:

For the metabolic studies of *Rhcg*$^{+/+}$, $^{+/-}$ and $^{-/-}$ mice performed in**Figure 1** and **Supplementary Figure 1**, blood pH (**Figure 1A**, **Supplementary Figure 1A**) and blood bicarbonate (**Figure 1B and Supplementary Figure 1B**) were measured as well as urinary pH (**Figure 1C and Supplementary Figure 1C**) and NH_4^+ concentration (**Figure 1E and Supplementary Figure 1C**).

The mRNA and protein expression assessment realised in **Figure 2 and Supplementary Figure 2** in *Rhcg*$^{+/+}$, $^{+/-}$ and $^{-/-}$ mice were all carried out.

Western blotting analysis as well as kidney tissue NH_4^+ concentration measurement appearing in **Figure 3, Figure 4** and **Supplementary Figure 3**, **Supplementary Figure 4** were also all completed. Urinary volume evaluation was performed together with the metabolic studies presented in Figure 1.

All parameters presented in **Figure 5**were measured: ionized blood Ca^{2+} and osteocalcin levels as well as urinary Ca^{2+} and deoxypyrydinoline (Dpd) in *Rhcg*$^{+/+}$ and $^{-/-}$ mice.

In **Table 1** and **Supplementary Table 2** showing the metabolic parameters of *Rhcg*$^{+/+}$, $^{+/-}$ and $^{-/-}$ mice receiving respectively High Casein diet and High Soy diet, **body weight, food intake, water intake, urine volume, urine pH, urinary creatinine, urinary NH_4^+,** and **urinary Dpd** were achieved as well as all blood values appearing in **Supplementary table 1 and Supplementary table 4**.

Journal of the American Society of NEPHROLOGY

JASN

The role of the renal ammonia transporter Rhcg in metabolic responses to dietary protein

Journal:	*Journal of the American Society of Nephrology*
Manuscript ID:	JASN-2013-05-0466.R1
Manuscript Type:	Original Article - Basic Research
Date Submitted by the Author:	n/a
Complete List of Authors:	Bounoure, Lisa; University of Zurich, Institute of Physiology Ruffoni, Davide; ETH Zurich, Institute for Biomechanics Muller, Ralph; Institute for Biomechanics, ETH Zurich Kuhn, Gisela; ETH Zurich, Institute for Biomechanics Bourgeois, Soline; University of Zurich, Institute of Physiology Devuyst, Olivier; University of Zurich, Institute of Physiology Wagner, Carsten; University of Zurich, Institute of Physiology;
Keywords:	acidosis., Cell & Transport Physiology, collecting ducts, chronic kidney disease, bone, proximal tubule

The role of the renal ammonia transporter Rhcg in metabolic responses to dietary protein

Lisa Bounoure[*], Davide Ruffoni[‡], Ralph Müller[‡], Gisela Anna Kuhn[‡], Soline Bourgeois[*], Olivier Devuyst[*], Carsten A. Wagner[*]

[*]Institute of Physiology and Zurich Center for Integrative Human Physiology (ZIHP), University of Zurich, Zurich, Switzerland, [‡]Institute for Biomechanics, ETH Zurich, Zurich, Switzerland

Correspondence

Carsten A. Wagner and Soline Bourgeois
Institute of Physiology
University of Zurich
Winterthurerstrasse 190
CH-8057 Zurich
Switzerland
+41(0)44 635 50 23
+41 (0)44 635 68 14
wagnerca@access.uzh.ch or soline.bourgeois@access.uzh.ch

ABSTRACT

High dietary protein imposes a metabolic acid load requiring excretion and buffering by the kidney. Impaired acid excretion in chronic kidney disease (CKD), with potential metabolic acidosis may contribute to the progression of CKD. Here we investigated the renal adaptive response of acid-excretory pathways to high protein diets containing normal or low amounts of acid-producing sulphur-amino acids (SAA). We also examined how this adaption requires the RhCG ammonia transporter. Diets rich in SAA stimulated expression of enzymes and transporters involved in mediating NH_4^+reabsorption in the thick ascending limb of the loop of Henle. The SAA-rich diet increased diuresis paralleled by down-regulation of AQP2 water channels. The absence of Rhcg transiently reduced NH_4^+ excretion, stimulated the ammoniagenic pathway more strongly, and further enhanced diuresis by increasing the down-regulation of the $Na^+/K^+/2Cl^-$- cotransporter NKCC2 and AQP2 with less phosphorylation of AQP2 at serine 256. The high protein acid-load affected bone turnover, as indicated by higher Ca^{2+} and deoxypyrydinoline (Dpd) excretion, and changed tissue mineral density (TMD) in newly formed bone layers. Phenomena exaggerated in the absence of Rhcg. In animals receiving a high protein diet with low SAA content, the kidney excreted alkaline urine, with low $NH_4^{+\cdot\cdot}$ and no change in bone metabolism. Thus, the acid-load associated with high protein diets causes a concerted response of various nephron segments to excrete acid, mostly in the form of NH_4^+ requiring Rhcg. Bone metabolism is altered by a high protein acidogenic diet, presumably to contribute to buffering the acid-load.

INTRODUCTION

The kidney is the central organ excreting acid and replenishing bicarbonate buffer used by metabolism [1-2]. The importance of the kidney in acid-base balance is demonstrated by inherited and acquired renal diseases reducing its ability to excrete acid, reabsorb and synthesize bicarbonate (HCO_3^-) [3-5]. Recent studies suggest that the progression of CKD is delayed by alkalinizing therapies aiming to reduce the metabolic acidosis occurring with the disease [6-10].

In Western diet, protein intake exceeds by up to 50% the recommended average daily consumption of 0.8g/kg/day of protein with most protein of animal sources which are rich in sulfur-containing acidogenic amino acids[11-12]. High animal protein diets have gained additional popularity in the context of obesity and its treatment [13-14]. Adverse effects of high protein intake on many organs have been described,and particularly the negative impact on bone and the function of healthy kidney has been discussed controversially [15-23]. In kidney disease, high animal protein may accelerate decay of renal function, thus, current protocols strongly suggest reducing animal protein intake in CKD patients [24-26].

Dietary protein intake and its metabolism can provide a major acid load, however, the metabolic acid load depends on the nature and composition of the protein. Proteins rich in sulphur-amino acids (SAA, i.e. cysteine and methionine) release protons (H^+) and sulfate (SO_4^{2-}) during metabolism and cause increased renal acid and NH_4^+ excretion paralleled by high urinary SO_4^{2-} and urea removal [27-28]. Plant proteins such as soy protein contain only small amounts of SAA and consequently cause a milder acid or even alkaline load [19, 29-30]. The acid content of high protein diet has been linked to the development of tubular-interstitial injury secondary to augmented intrinsic acid production provoked by endothelin-stimulated enhanced aldosterone activity [29, 31-32].

The renal ammonia (NH_3) transporter RhCG is critical to eliminate NH_4^+ and maintain systemic acid-base balance [33-36]. RhCG is localized in most cells

along the collecting duct and mediates basolateral uptake of NH_3 and final excretion into urine. Its expression is stimulated by acidosis in mice and Rhcg becomes rate-limiting for urinary NH_4^+excretion during strong acid-loads (NH_4Cl or HCl-loading) [33, 36-38].

Here we examined the effect of high protein diets containing either acidogenic SAA (casein diet) or being almost devoid of these amino acids (soy protein diet) on renal mechanisms mediating ammoniagenesis and excretion of the acid-load. Our data demonstrate a concerted response of various nephron segments to eliminate the metabolic acid load, the requirement of Rhcg mediated NH_4^+ excretion, and effects on bone, altogether providing a molecular explanation for the stimulation and requirement of renal acid excretion.

RESULTS

High casein protein diet induces a transient acid load that *Rhcg*$^{-/-}$ mice can excrete

Metabolic parameters and acid-base status were assessed in *Rhcg*$^{+/+}$, *Rhcg*$^{+/-}$, and *Rhcg*$^{-/-}$ mice receiving normal diet (basal status with 20 % protein), acid-loading High Casein (HC) protein diet or non-acid loading High Soy control protein diet (HS) containing either high or low sulfur amino acid (SAA), respectively. Fifty % of HC or HS diets were provided either as casein or soy protein but the diets were otherwise isocaloric and identical in their composition. HC but not HS diet was associated with slightly reduced food intake (Table 1 and supplementary Table 1). However, no difference was found in food and water intakes between the 3 different genotypes at all time points measured and under all 3 types of diet (normal, HC and HS) (Table 1 and supplementary Table 1). Baseline blood and urine parameters (Table1 and supplementary Tables 1-4) were similar between all 3 genotypes. A transient decrease in blood pH and HCO_3^- after 2 days HC diet (Figure 1, A and B) but not HS diet (supplementary Figure 1, A and B) was identically observed in *Rhcg*$^{+/+}$, *Rhcg* $^{+/-}$, and *Rhcg* $^{-/-}$, confirming the acid-loading effect of HC diet. HC diet did not alter urinary pH but stimulated excretion of titratable acidity, most likely in the form of phosphate (Table 1 and supplementary Table 2) to a comparable extent in all three genotypes (Figure 1, C and D). In contrast, HS did not alter blood pH and HCO_3^- but led to a profound alkalinisation of urine pH and a fall in the urinary excretion of titratable acids (supplementary Figure 1C, supplementary Table 1). Urinary NH_4^+ excretion was markedly increased in the HC groups whereas it decreased in the HS groups (Table 1 and supplementary Table 1, Figure 1E and supplementary Figure 1D). *Rhcg* deletion delayed the increase in urinary NH_4^+ excretion in response to the HC acid challenge (Figure 1E). At days 2 and 4 HC diet, respectively, *Rhcg*$^{-/-}$ exhibited a 38.5%+/- 0.1 and 41.4% +/- 0.1 decrease in excreted urinary NH_4^+ compared to *Rhcg*$^{+/+}$ mice (Table 1). At day 9, *Rhcg*$^{-/-}$ adapted to the HC diet acid load and excreted similar amounts of NH_4^+ like *Rhcg*$^{+/+}$ mice. HS diet did not induce any difference in urinary NH_4^+ excretion in all 3 genotypes (supplementary Figure 2D). Taken together,

these data confirm that a diet containing high amounts of SAA causes a metabolic acid load and demonstrate that its elimination depends partially on the presence of the ammonia transporter Rhcg.

High casein diet stimulates ammoniagenesis in theproximal tubule

To assess the proximal tubule response to HC diet we studied the regulation of key molecules involved in NH_4^+ production and excretion (Figure 2, A-D, Supplementary Figures 2 - 4). High Casein diet caused a transient increase in Rhcg mRNA, whereas Rhbg mRNA was not altered in *Rhcg*$^{+/+}$ and *Rhcg*$^{-/-}$ kidneys. Four days HC induced a transient increase in SNAT3 and PDG mRNA levels compared with normal diet (Figure 2, A and C). SNAT3 protein levels were also higher after 4 days HC diet while PDG showed a higher protein expression at day 9 HC diet (Figure 2, B and D). PEPCK and NHE3 protein abundance remained unchanged in *Rhcg*$^{+/+}$ during HC treatment (Supplementary Figure 3, A and B). To test if the delayed adaptation to HC diet acid load observed in *Rhcg*$^{-/-}$ mice could be partly explained by an adaptive enhanced NH_4^+ production, we compared SNAT3, NHE3, PDG, and PEPCK mRNA and protein abundances in all 3 groups of mice after 4 and/or 9 days HC diet. NHE3 and PEPCK mRNA and protein expression levels were comparable between all 3 genotypes (Supplementary Figure 3, C-H). However, at day 4 HC diet, both *Rhcg*$^{+/-}$ and *Rhcg*$^{-/-}$ increased mRNA and protein expression of SNAT3 compared to *Rhcg*$^{+/+}$ (Figure 2, A,B, E, and F). PDG mRNA and protein were higher in *Rhcg*$^{-/-}$ than *Rhcg* $^{+/+}$ (Figure 2, C, D, G and H). After 9 days HC diet, SNAT3 and PDG mRNA and protein were still higher in *Rhcg*$^{-/-}$ than in *Rhcg*$^{+/+}$ while in *Rhcg*$^{+/-}$ mice only PDG protein levels were elevated. Thus, *Rhcg* null mice increase expression of some proteins critical for proximal tubular ammoniagenesis.

***Rhcg*$^{+/-}$and $^{-/-}$ mice have abnormal accumulation of NH_4^+ in the medullary interstitium**

Next we assessed mechanisms involved in the generation of the cortico-papillary NH_4^+ gradient hypothesizing that *Rhcg*$^{-/-}$ mice could increase the NH_4^+ excretion by stimulating NH_4^+ reabsorption by the thick ascending limb NKCC2 cotransporter.NKCC2 protein expression in *Rhcg*$^{+/+}$, *Rhcg*$^{+/-}$, and

Rhcg $^{-/-}$ mice after 4 and 9 days HC diet revealed two opposite regulations of the protein during HC treatment. NKCC2 levels were higher in *Rhcg*$^{+/-}$ and *Rhcg* $^{-/-}$ after 4 days (Figure 3A) but lower in *Rhcg*$^{-/-}$after 9 days (Figure 3B). NH_4^+tissue content incortex, outer medulla, and inner medulla followed NKCC2 expression. At day 4 HC (Figure 3C and D), both *Rhcg*$^{+/-}$ and *Rhcg* $^{-/-}$ accumulated more NH_4^+than *Rhcg*$^{+/+}$ in the inner medulla (+25.2 ± 0.1% for *Rhcg*$^{+/-}$ and +29.9 ± 0.1% for *Rhcg*$^{-/-}$). In contrast, at day 9 HC (Figure 3D), *Rhcg*$^{-/-}$ had lower inner medullary NH_4^+ content than *Rhcg*$^{+/+}$ (-37.0 ± 0.1%). Thus, the adaption of Rhcg deficient mice to high SAA diet involves regulation of the NKCC2 cotransporter and affects accumulation of NH_4^+ in the medullary interstitium.

High casein diet stimulates diuresis and downregulates NKCC2 and AQP2

Besides its role in NH_4^+ reabsorption, NKCC2 functions in the counter-current mechanism establishing the cortico-papillary osmotic gradient required for water reabsorption along the collecting duct. HC diet induced diuresis in all three genotypes (Figure 4E, Table 1) whereas diuresis was lower in animals receiving the HS diet despite quantitatively similar urea excretion (compare table 1 and supplementary table 1). We measured NKCC2 and collecting duct AQP2 protein expression levels in *Rhcg*$^{+/+}$ (Figure 4, A and B) and *Rhcg* $^{-/-}$ animals (Figure 4, C and D) at 0, 4 and 9 days HC and HS diet. NKCC2 and AQP2 were down-regulated by HC diet in both genotypes with reduced NKCC2 expression in *Rhcg* wild-type after 4 and 9 days HC (Figure 4A) and after 9 days in *Rhcg* null mice (Figure 4C). Similarly, AQP2 levels were lower after 9 days HC in *Rhcg*$^{+/+}$ and*Rhcg*$^{-/-}$ mice (Figure 4, B and D). Since *Rhcg*$^{-/-}$ excreted more urine than their littermates(5.7 ± 0.5 vs. 4.5 ± 0.3 mL/24h after 9 days HC, p≤0.01) (Figure 4E) we tested if the active phosphorylated form of AQP2 (pSer256-AQP2) was altered in *Rhcg*$^{-/-}$ mouse kidneys. The total abundance of mature pSer256-AQP2 (35 KDa band) was reduced as well as the ratio of phosphorylated AQP2 over total AQP2 (Figure 4F). In animals receiving the HS diet, no regulation of NKCC2 and AQP2 was observed (supplementary Figure 4). In summary, high SAA diet stimulates diuresis by down-regulating NKCC2 and AQP2, an effect amplified in *Rhcg*$^{-/-}$ mice.

High casein diet stimulates bone resorption exaggerated by absence of Rhcg

Two days HC diet caused a transient increase in ionized blood Ca^{2+} levels in both*Rhcg*$^{+/+}$ and *Rhcg*$^{-/-}$ animals but significantly higher in *Rhcg*$^{-/-}$ mice. In contrast, Ca^{2+} levels remained higher in *Rhcg*$^{-/-}$ mice and returned to normal only on day 9 (Figure 5, A). Urinary Ca^{2+} excretion was also transiently increased in *both genotypes* at days 2 and 4 HC diet, with significantly higher urinary Ca^{2+} levels in *Rhcg*$^{-/-}$ at day 4 (Figure 5B). To investigate bone remodelling, we measured urinary deoxypyrydinoline (Dpd) excretion, a marker of bone resorption and plasma concentration of osteocalcin, a marker of bone formation (Figure 5C and D). Dpd levels were elevated after 4 days HC diet in *Rhcg*$^{+/+}$ and *Rhcg*$^{-/-}$and remained higher in *Rhcg*$^{-/-}$after 9 days HC. No significant difference in plasma osteocalcin levels was found during the treatment and between the 2 groups suggesting that bone resorption in *Rhcg*$^{+/+}$ and *Rhcg*$^{-/-}$ mice is not compensated by increased bone formation. To further evaluate the direct impact of acidogenic high protein diet on bones, we measured tissue mineral density (TMD) of the mid-cortical region of femurs collected after 9 days HC diet (Figure 6A and 6B). Micro-computed tomography (micro-CT) scans were analysed by comparing TMD of a deep bone layer mineralised before the HC diet period and therefore not influenced by the acidogenic protein load (layer 12) with TMD of a more superficial layer close to the periosteum which contained bone formed during the HC diet (layer 2) (Figure 6A). Surprisingly, TMD of layer 12 in *Rhcg*$^{-/-}$ mice (diet independent) was higher than the corresponding layer in femurs from *Rhcg*$^{+/+}$ mice (1267.5 mhHA/cm^3 vs. 1206.0 mhHA/cm^3, $p \leq 0.01$). TMD of layer 2 was lower in both *Rhcg*$^{+/+}$ and *Rhcg*$^{-/-}$. However, the difference between genotypes was not detected anymore in layer 2 (formed during HC diet), suggesting that a more pronounced reduction of mineral content occurred in *Rhcg*$^{-/-}$mice induced by HC diet (917.4 mhHA/cm^3 vs. 944.8, $p \geq 0.05$) (Figure 6B). HS diet did not affect cortical mineral content of HS treated animals (data not shown). Moreover, no difference was detected in the standard morphometric parameters suggesting that all bones had similar size, shape and internal microarchitecture (supplementary table 5).

DISCUSSION

In the current study we examined the effect of an acidogenic high protein diet on the renal adaption through acid excretion. We compared two different diets with high protein content (50 %) containing either normal levels of SAA (casein protein) or low levels of these amino acids (soy protein). Intake of these diets was similar in all groups as evident from total food intake and total urinary urea excretion [39]. The dietary content of SAA is reflected by the excretion of SO_4^{2-} in urine much higher in the animals ingesting the casein diet. Based on this animal model we find that the kidney adapts to the high SAA diet with a parallel response of various nephron segments: i) stimulated NH_4^+ excretion and increased expression of key molecules of the ammoniagenic pathway in the proximal tubule, ii) reduced expression of the NKCC2 cotransporter, iii) increased diuresis and down-regulation of the AQP2 water channel, iv) loss of bone TMD, and v) all processes being dependent on the ammonia transporter Rhcg as evident from reduced ammonium excretion, exaggerated induction of ammoniagenic molecules, enhanced diuresis and downregulation of NKCC2 and AQP2, and more severe effects on bone remodelling.

Intake of high protein in the form of casein caused an increased urinary NH_4^+ and titratable acid excretion and a transient fall in blood pH and HCO_3^- indicative for the metabolic acid load and the kidneys' ability to adapt. In contrast, high soy protein reduced the dietary acid load as urinary NH_4^+ and titratable acid excretion decreased and urinary pH became more alkaline. Interestingly, TA excretion increased strongly with the SAA diet and remained high. This is in contrast to humans and rodents provided with an acid load in the form of NH_4Cl or HCl, respectively, where most acid is excreted in the form of ammonium [36, 40-41]. These differences may be in part due to different types of acid-loading.

The increased acid excretion found in animals fed with high acidogenic protein diet, was paralleled on the molecular level by a stimulation of expression of the glutamine transporter SNAT3 and the phosphate dependent

glutaminase in the proximal tubule. The regulation of SNAT3 by high protein intake had been reported previously [42]. In contrast, PEPCK, fueling alpha-keto-glutarate from ammoniagenesis into gluconeogenesis was decreased during high casein diet in *Rhcg*$^{+/+}$ kidneys suggesting a decrease in renal gluconeogenesis. In rat liver, PEPCK is stimulated by high protein intake which might indicate that high casein intake induces specifically renal ammoniagenesis and favors hepatic over renal gluconeogenesis [43].

The response of the collecting duct system to high protein intake has been previously described, mostly based on functional experiments demonstrating increased H^+ and NH_4^+ secretion [31-32]. Consistently, mice receiving high casein diet excreted high amounts of NH_4^+ into urine. Rhcg mRNA abundance increased transiently (day 4) at the time where *Rhcg*$^{-/-}$ mice showed decreased urinary ammonium excretion suggesting that Rhcg may be directly regulated and mostly needed during the earlier phase of adaption. Similarly, during NH_4Cl induced acidosis, Rhcg protein abundance is increased and staining enhanced at the luminal and basolateral membrane suggesting that Rhcg is regulated at different levels [44-45]. Rhbg mRNA was not regulated consistent with previous data from NH_4Cl-loaded mice and a less important role of Rhbg in renal ammonium excretion [45-47]. This later process along the collecting duct requires the formation of a NH_4^+ gradient from medullary interstitium into urine which is generated at least in part by the reabsorption of NH_4^+ by the NKCC2 cotransporter in the thick ascending limb of the loop of Henle. This transporter is stimulated by acidosis induced by NH_4Cl-feeding [48-51]. In contrast, high casein diet progressively decreased expression of NKCC2 without disturbing medullary NH_4^+ accumulation.

The renal adaptation to high casein diet was impaired in the absence of Rhcg. *Rhcg*$^{-/-}$ mice had a delayed increase in urinary NH_4^+ excretion, required a stronger and more sustained increase in PDG and SNAT3 expression, all indicating highly stimulated ammoniagenesis. Furthermore, NKCC2 expression was even more decreased than in wild-type animals and medullary NH_4^+ accumulation was impaired in the inner medulla.

High protein diets, casein and soy, stimulated diuresis in animals, however, casein produced a stronger diuresis than soy diet. Increased excretion of urea from hepatic protein metabolism may be in part responsible for the diuresis causing an osmotic driving force. The acid content of the high casein diet, however, provides likely an additional stimulus since mice receiving the acidogenic casein diet had higher diuresis despite almost identical urea excretion. Indeed, feeding mice or rats with NH_4Cl causes a similar diuresis [52-53]. Here we found that diuresis was accompanied by a progressive reduction in AQP2 water channel expression. *Rhcg*$^{-/-}$mice excreted even higher urine volumes than *Rhcg*$^{+/+}$ animals. No regulation of NKCC2 and AQP2 was observed in mice receiving the HS diet demonstrating that high protein per se does not regulate these proteins. Moreover, phosphorylation of AQP2 at serine 256, critical for the regulated insertion and activity of the channel in the membrane, was reduced in knock-out mice suggesting that increased diuresis may be part of a compensatory mechanism. Thus, the more pronounced reduction in NKCC2 expression and reduced insertion of AQP2 at the plasma membrane would allow *Rhcg*$^{-/-}$ mice to excrete the NH_4^+ formed in the proximal tubule by shunting the medullary interstitium passage, diluting and excreting the NH_4^+ load in the thick ascending limb and collecting duct. The time course of achieving similar rates of urinary ammonium excretion and stronger downregulation of NKCC2, reduced medullary ammonium accumulation, and lower AQP2 expression is similar, possibly indicating a concerted compensatory mechanism. We speculate that several hormones might be involved in mediating the effect of HC diet on NKCC2 and AQP2. Among them, aldosterone, endothelin, prostaglandin E_2 (PGE_2) and atrial natriuretic peptide (ANP) have been shown to be increased by high protein diets [32, 54-55]. ANP and PGE2 reduce AQP2 expression and NKCC2 function [56-57]. Also endothelin and aldosterone may reduce NKCC2 expression and function via a NO, cGMP and PDE2 dependent mechanism.

The beneficial or detrimental effects of high protein diets on bone are controversial and the positive or negative impact may depend on the type of protein, the content of minerals, and the content of carbohydrates (e.g.

whether diets are ketogenic) [21-23]. Acidosis has significant adverse effects on bone, stimulating osteoclast activity, increasing demineralization, and finally leading to loss of bone mineral density and stability [58-59]. The high casein diet stimulated bone degradation in *Rhcg*$^{-/-}$ as evident from the increased urinary excretion of deoxypyrydinoline and reduction of bone tissue mineral density in a layer close to the bone surface and hence containing newly formed bone. In wild-type animals, Dpd levels increased only transiently, whereas in *Rhcg*$^{-/-}$ mice, Dpd remained elevated consistent with increased bone degradation possibly contributing to the compensation of reduced NH_4^+ excretion. Surprisingly, no evidence was found for higher osteoblast activity reflected by constant osteocalcin levels suggesting that the high casein diet would eventually cause a small net loss of bone. Indeed, elevated urinary Ca^{2+} was paralleled with Dpd levels indicating that this calcium load may at least in part originate from bone. However, effects of acidosis on calcium binding to albumin could also contribute to hypercalciuria and hypercalcemia as well as stimulation of intestinal calcium absorption during acidosis [60]. The acidogenic HC diet reduced bone tissue mineral density of *Rhcg*$^{-/-}$ animals to help kidneys to buffer blood acidity and compensate for HC diet acid-load. The higher TMD found in the deeper bone layer of *Rhcg*$^{-/-}$remains to be clarified but suggests that *Rhcg* deletion might influence bone development towards a higher density. Expression of Rhcg has not been reported for bone indicating that differences in TMD are rather the consequence of absent Rhcg function in other organs.

In summary, we demonstrate that the kidney responds to acidogenic high protein diets with increased ammoniagenesis and NH_4^+ excretion and decipher the transport pathways contributing to this adaptive response. The renal ammonium transporter Rhcg is critical for the adaption and its absence or reduced activity in inherited or acquired kidney disease may contribute to metabolic acidosis, bone degradation, and eventually may fed back on the kidney contributing to the progression of kidney disease.

CONCISE METHODS

Animals

Mice were genotyped by PCR directly on a 3 µl 25 mM NaOH ear biopsy digestion product. Genomic DNA was amplified using primer pairs specific for exon 1: forward (AGACCCCACAATGGAAAGCTATAA), *Rhcg*$^{+/+}$ reverse (CAACCAGAACTCCCCAGTGTCAGA) and *Rhcg*$^{-/-}$ reverse (ATGGGCTGACCGCTTCCTCGTGCTTTAC)[36]. The products were separated by electrophoresis on 1 % agarose gels (mutant product: 522 bp, wild type product: 376 bp). Heterozygous mice were mated to generate mice of all genotypes. All animal experiments were conducted according to Swiss Laws of Animal Welfare and approved by the local Zurich Veterinary Authority (Kantonales Veterinäramt Zürich).

Metabolic cage studies

All experiments were performed using age- matched male *Rhcg* wild type (*Rhcg*$^{+/+}$), *Rhcg* knockout (*Rhcg*$^{-/-}$) and *Rhcg* heterozygous (*Rhcg*$^{+/-}$) littermate mice (3-4 month-old), housed in standard or metabolic cages (Tecniplast, Buguggiate, Italy). Mice were given deionized water and were fed a standard powdered laboratory chow *ad libitum* (Kliba, Kaiseraugst, Switzerland). Mice were allowed to adapt to metabolic cages for 2 days, then one 24 hrs urine sample was collected under light mineral oil in urine collectors to determine daily urinary parameters. Mice were then allowed to recover for 2 days in standard cages and were given high protein diet (50 % casein or 50 % soy) (Sniff Spezialdiaeten GmbH, Soest, Germany) for 9 days. Four 24 hrs urine samples were collected during the 9 days of high protein diet. Water and food intake, and urine excretion were monitored at baseline and during 9 days of high protein treatment. Blood was collected from the retroorbital plexus under isofluran anesthesia and analyzed in a Radiometer ABL 505 blood gas analyzer (Radiometer, Copenhagen, Denmark). Urinary pH was measured directly after collection using a pH microelectrode (691 pH meter, Metronohm). Urinary electrolytes concentrations were measured by flame photometry (IL943, Instruments Laboratory), titratable acid were measured using a DL 50 titrator (Mettler Toledo [36]). Urinary NH_3/NH_4^+ and

creatinine were assessed using the Berthelot and Jaffe methods, respectively [61-62]. Urinary SO_4^{2-} was measured by ion exchange chromatography using a IonPac® AS 11 analytical column on a Dionex DX-600 HPLC system (Dionex, Olten, Switzerland). Urinary Deoxypyridinoline (DPD) was measured with a DPD Enzyme Immunoassay kit (Microvue DPD EIA, Quidel Corporation, San Diego CA, USA) and plasma Osteocalcin using a Mouse Osteocalcin Immunoradiometric Assay kit (Mouse Osteocalcin IRMA Kit, Immunotopics, San Clemente CA, USA). Mice were anesthetized with ketamine and xylazine and sacrified at different time points to collect blood, kidneys, and femurs. Kidneys were immediately flash-frozen in liquid nitrogen and placed at -80ºC until further processing. Femurs were collected and stored in 70% ethanol at room temperature.

RNA extraction and reverse transcription

Snap-frozen kidneys (8 or 5 half kidneys for each condition, 9 days of diet or 4 days of diet, respectively) were homogenized in RLT-Buffer (Qiagen, Basel, Switzerland) supplemented with β-mercaptoethanol to a final concentration of 1%. Total RNA was extracted from 200 µl aliquots of each homogenized sample using the RNeasy Mini Kit (Qiagen, Basel, Switzerland) according to the manufacturer's instructions. Quality and concentration of the isolated RNA preparations were analyzed on the NanoDrop ND-1000 spectrophotometer (Wilmington, DE, USA). Total RNA samples were stored at −80°C. Each RNA sample was diluted to a final concentration of 100 ng/µl, and cDNA was prepared using the TaqMan Reverse Transcriptase Reagent Kit containing 10X RT buffer, $MgCl_2$, random hexamers, dNTPs, RNase inhibitors and Multiscribe reverse transcription enzyme (Applied Biosystems/Roche; Forster City, CA, USA). Reverse transcription was performed with the Biometra TGradient thermocycler (Goettingen, Germany), with thermocycling conditions set at 25ºC for 10 min, 48ºC for 30 min, and 95ºC for 5 min.

Real-time semi-quantitative PCR

Relative mRNA expression was determined using semi-quantitative Real-Time RT-PCR using the Applied Biosystems 7500 Fast Real-Time PCR

system. Thermocycling conditions consisted of: denaturation (95°C ;10 min) followed by 40 cycles of denaturation at 95°C for 15s and annealing/elongation (60°C; 60s) with auto ramp time. All reactions were run in triplicate. Forward and reverse primer and probe concentrations were 25 µM and 5 µM, respectively. TaqMan Universal PCR master mix 2X (Applied Biosystems/Roche) was used as the Taq polymerase. Primers and probes for SNAT3, phosphate-dependent glutaminase (PDG), NHE3, cytosolic phosphoenolpyruvate carboxykinase (PEPCK), NKCC2, and Hypoxanthine-guaninephosphoribosyltransferase (HPRT) were generated using Primer Express software from Applied Biosystems and synthesized at Microsynth (Balgach, Switzerland) as described previously[36, 63]. Probes were generated with the reporter dye FAM at the 5' end and TAMRA at the 3' end.Reactions were run in triplicates including a negative control (without Multiscribe reverse transcription enzyme). The cycle threshold (Ct) values obtained were ultimately compared to Ct values of the endogenous gene HPRT. Relative mRNA expression ratios were calculated as: $R = 2^{[Ct(HPRT/Ct(gene\ of\ interest)]}$, where Ct represents the cycle number at threshold 0.02.

Immunoblotting

Crude total membrane proteins or cytosolic fractions were obtained from kidneys homogenized in 250 mM sucrose, 10 mM Tris-HCl, pH 7.5, and in the presence of protease inhibitors (complete ULRA tablets, Roche, Rotkreuz, Switzerland). Fourty micrograms of crude membrane proteins or cytosolic proteins were solubilized in loading buffer containing DTT (2 M) and separated on 5 to 10% polyacrylamide gels. For immunoblotting, proteins were transferred electrophoretically to polyvinylidene fluoride membranes (Immobilon-P, Millipore Corp., Bedford, MA, USA). After blocking with 5 % milk powder in Tris-buffered saline-0.1% Tween-20 for 60 min, membranes were incubated with rabbit polyclonal anti-SNAT3 (diluted 1:1000)[63], anti-PDG (diluted 1:5000, kindly provided by Dr. N. Curthoys, Univ. of Colorado), anti-PEPCK (diluted 1:5000, Cayman Chemical, Ann Arbor, MI, USA), rabbit polyclonal anti-NKCC2 and anti-AQP2 (diluted 1:5,000, kindly provided by J. Loffing, Institute of Anatomy, Univ. of Zurich), rabbit anti pSer256-AQP2 1:3000 (kindly provided by Dr. Soren Nielsen, University of Aarhus, Denmark),

rabbit polyclonal anti-NHE3 (StressMarq Biosciences Inc., Victoria, BC, Canada) and mouse monoclonal anti-β-actin antibody (Sigma, St. Louis, MO; 1:20,000) overnight at 4°C. After washing and blocking with 5 % milk powder for 60 min, membranes were then incubated for 2 h at room temperature with secondary goat anti-rabbit 1:5000 or donkey anti-mouse antibodies 1:10,000 linked to alkaline phosphatase (AP) (Promega, Madison, WI, USA) or horseradish peroxydase (HRP) (Promega, Madison, WI, USA), respectively. The protein signal was detected with the appropriate substrate (CDP-Star, Roche, Rotkreuz, Switzerland for AP, Millipore Corp, Bedford, MA, USA for HRP) using the Las-4000 image analyzer system (Fujifilm Life Science, USA). All images were analyzed with Advanced Image Data Analyzer AIDA (Raytest, Straubenhardt, Germany) to calculate the protein of interest/β-actin ratio.

Measurement of renal ammonium content

Renal tissue ammonium content was measured by an enzymatic technique (SIGMA, Ammonia Assay Kit) as previously described [36]. Mice were anesthetized, kidneys removed, and immediately frozen in liquid nitrogen. Kidneys were then sliced frozen to yield a column of tissue, which extended from the cortex to the tip of the papilla. Sections were cut along the cortico-medullary axis to yield 3 slices: cortex, outer medulla, and inner medulla. Two kidneys were pooled for each sample. Tissue slices were then homogenized in 300 µl of ice cold 7 % trichloroacetic acid, and the solution was centrifuged. The supernatant was drawn off and the pH of a 250 µl sample was adjusted to near neutral by the addition of 12 µl of 10 mM Na_2HPO_4 in 9 N NaOH. A 200 µl sample of buffered supernatant was then analyzed for ammonium concentration. The pellet was re-suspended in 1 N NaOH, shaken overnight, and analyzed for total protein concentration using the Biorad protein assay (Biorad Hercules, CA, USA).

Micro-CT imaging and quantitative analysis

Whole femurs of n = 5 *Rhcg*$^{+/+}$ and n = 5 *Rhcg*$^{-/-}$ were scanned with a desktop micro-CT (µCT40, Scanco Medical, Switzerland) operated at 55 kVp and 145 µA. The samples were scanned with the long axis perpendicular to

the beam direction and using an integration time of 300 ms and a frame averaging of 3, resulting in a total scanning time of approximately 5.1 hours per sample. Before image reconstruction, a voltage-specific third-order polynomial correction [52] provided by the manufacturer was applied to minimize the influence of beam hardening. The reconstructed scans had a nominal isotropic resolution of 10 µm. A three-dimensional Gaussian filter (sigma 0.8, support 1) was applied to reduce the noise present in the images and the grey levels of the scans were then transformed into tissue mineral density (TMD) by using the manufacturer calibration record based on a phantom of 1200 mg HA/cm^3 [64]. The micro-CT scanner was calibrated weekly for mineral equivalent value, and monthly for determining in-plane spatial resolution. All measurements and analyses were performed according to the guidelines for assessment of bone microstructure in rodents using micro-CT [65]. Standard three-dimensional morphometric parameters were computed for full, cortical and trabecular bone as described elsewhere [66]. TMD was evaluated in the cortical bone compartment having a size of 30% of the total femoral lengthby averaging the TMD values in different layers having the same distance to the bone surface, accordingly to a recently developed layer analysis [67]. Specifically, we analyzed the TMD in layer 2 (i.e., close to the bone periosteal surface and hence affected by diet) and in layer 12 (i.e. far from the bone surface and thus not affected by diet).

Statistics

Statistical comparisons were tested by ANOVA (1 way, Newman-Keuls multiple comparison test) and unpaired t-test using Graphpad Prism (GraphPad Software). P values < 0.05 were considered as statistically significant.

ACKNOWLEDGEMENTS

This study was supported by a grant from the Swiss National Science Foundation to C.A. Wagner (31003A_138143). The studies were further supported in part by the European Community's Seventh Framework

Programme (FP7/2007-2013) under grant agreement n° 305608 (EURenOmics) to OD and CAW; an Action de Recherche Concertée (ARC, Communauté Française de Belgique) to OD; the FNRS and FRSM; the Inter-University Attraction Pole (IUAP, Belgium Federal Government); and the NCCR Kidney.CH program (Swiss National Science Foundation) to OD. We thank Julien Weber and Sebastien Druart for their help in the biochemical profiling of the mouse models. The use of the Zurich Integrative Rodent Physiology (ZIRP) Core Facility is gratefully acknowledged.

DISCLOSURES

None.

FIGURE LEGENDS

Table 1

Body weight, food intake, and urinary values of *Rhcg*$^{+/+}$, *Rhcg*$^{+/-}$, and *Rhcg*$^{-/-}$ m**ice** during 9 days high casein (HC) protein loading (n = 8 mice for each group). ND not determined, # *P* ≤ 0.05 significantly different from same genotype under control conditions, * *P* ≤ 0.05 significantly different from *Rhcg*$^{+/+}$ mice under same treatment conditions, ** *P* ≤ 0.01 significantly different from *Rhcg*$^{+/+}$ mice under same treatment conditions

Figure 1. Acid-base parameters in *Rhcg*$^{+/+}$, $^{+/-}$ and $^{-/-}$ mice during 9 days high casein diet

Blood and urine data were collected in *Rhcg*$^{+/+}$, $^{+/-}$ and $^{-/-}$ mice treated for 9 days on high casein (HC) diet. All animals showed a transient decrease of blood pH (A) and bicarbonate (B). (C) Titratable acids increased on high casein diet. (D) All mice rapidly increased urinary NH_4^+ excretion, however, *Rhcg*$^{-/-}$ had lower NH_4^+ excretion than *Rhcg*$^{+/+}$ during days 2 and 4 of the high casein diet. Values are mean ± SEM (n= 8 mice) *p ≤ 0.05 (*Rhcg*$^{-/-}$vs *Rhcg*$^{+/+}$), # *P* ≤ 0.05 significantly different from same genotype under control conditions (day 0), * *P* ≤ 0.05 significantly different from *Rhcg*$^{+/+}$ mice under same treatment conditions and for the same time point.

Figure 2. High casein diet stimulated the ammonagenic pathway

Kidneys collected from all 3 groups of mice after 4 or 9 days HC diet were analyzed by RT-qPCR and immunoblotting. After 4 days HC diet *Rhcg*$^{+/+}$highly increased mRNA (A) and protein (B) expression of SNAT3.*Rhcg*$^{+/-}$ and $^{-/-}$ exhibited higher SNAT3 mRNA (A) and protein (E) levels than *Rhcg*$^{+/+}$. At day 9, only *Rhcg*$^{-/-}$kept an enhanced level of SNAT3 mRNA (A) and protein (F). 4 or 9 days HC diet augmented *Rhcg*$^{+/+}$ PDG mRNA (C) or protein (D) abundance. *Rhcg*$^{-/-}$ displayed higher mRNA (C) after 9 days HC and higher protein (H) expressions after both 4 and 9 days HC. Values are mean ± SEM (n= 4-8 mice) # *P* ≤ 0.05 significantly different from same genotype under control conditions (day 0), * *P* ≤ 0.05, ** *P* ≤ 0.01, *** *P*

≤ 0.001 significantly different from *Rhcg*$^{+/+}$ mice under same treatment conditions and for the same time point.

Figure 3. Altered medullary absorption and accumulation of ammonium in Rhcg deficient mice

After 4 or 9 days HC diet treatment, *Rhcg*$^{+/+}$, $^{+/-}$ and $^{-/-}$ mice kidneys were submitted to Western blot analysis and NH_4^+ concentration was measured in dissected cortex, inner and outer medulla. Expression of NKCC2 was higher in *Rhcg*$^{+/-}$ and $^{-/-}$ than *Rhcg*$^{+/+}$at day 4 HC diet (A) while at day 9, *Rhcg*$^{-/-}$ showed a reduced level (B). (C) NH_4^+ concentration was similarly increased in *Rhcg*$^{+/-}$ and $^{-/-}$mice kidney inner medulla at day 4 HC diet. (D) At day 9, *Rhcg*$^{-/-}$ had much lower inner medullaryNH_4^+ content. Values are mean ± SEM (n= 6-7 mice) # *P* ≤ 0.05 significantly different from same genotype under control conditions (day 0), * *P* ≤ 0.05, *** *P* ≤ 0.001 significantly different from *Rhcg*$^{+/+}$ mice under same treatment conditions and for the same time point.

Figure 4. High casein diet stimulates diuresis and regulates NKCC2 and AQP2 expression

Protein expression levels were examined using immunoblotting and urine production was measured at different time points of HC diet in *Rhcg*$^{+/+}$ and $^{-/-}$ mice. NKCC2 protein level were decreased after 4 and 9 days HC diet in *Rhcg*$^{+/+}$ (A) and only after 9 days in *Rhcg*$^{-/-}$ (C) while AQP2 expression was reduced in *Rhcg*$^{+/+}$ (B) and $^{-/-}$ (D) mice at day 9 HC diet. *Rhcg*$^{-/-}$ showed higher urinary excretion than *Rhcg*$^{+/+}$ (E). Mature pSer256-AQP2 showed decreased abundance at day 9 in *Rhcg*$^{-/-}$ and the ratio of pSer256-AQP2 over total AQP2 was reduced in *Rhcg*$^{-/-}$ (F). Values are mean ± SEM (n= 4-8 mice), # *P* ≤ 0.05 significantly different from same genotype under control conditions (day 0), * *P* ≤ 0.05, ** *P* ≤ 0.01 significantly different from *Rhcg*$^{+/+}$ mice under same treatment conditions and for the same time point.

Figure 5. Hypercalcemia, hypercalciuria, and increased deoxypyridynoline (Dpd) excretion in *Rhcg*$^{-/-}$ mice

(A) After 2 and 4 days of high casein diet, ionized Ca^{2+} concentration was higher in *Rhcg*$^{-/-}$ blood. (B) At day 4, urinary Ca^{2+} excretion was also increased in *Rhcg* $^{-/-}$. (C) The release of the bone degradation marker deoxypyridinoline (Dpd) was augmented in *Rhcg*$^{-/-}$ compared to *Rhcg*$^{+/+}$ following 4 and 9 days high casein diet whereas the plasma concentration of the bone formation maker osteocalcin was not affected by diet and genotype. Values are mean ± SEM (n= 5-8 mice), # $P \leq 0.05$ significantly different from same genotype under control conditions (day 0), * $P \leq 0.05$, ** $P \leq 0.01$ significantly different from *Rhcg*$^{+/+}$ mice under same treatment conditions and for the same time point.

Figure 6. High casein diet reduces bone mineral density in *Rhcg*$^{-/-}$ mice

(A) Micro-CT reconstruction of a femur with the mid-cortical region considered for tissue mineral density (TMD) evaluation. The inset shows the different grey values (top), which carry information on TMD and a cross-section (bottom) with layer 2 close to the periosteum (light grey) and layer 12 (dark grey). (B) TMD of *Rhcg*$^{-/-}$ was higher than *Rhcg*$^{+/+}$ in the diet independent layer 12 but not in layer 2 which was formed during the diet. Data are represented by boxplots, i.e. the inner box contains 50 % of all data, the whisker bars denote the full range and the black line represents the median value (over all animals). Statistical significance was obtained with 2way ANOVA with Bonferroni's multiple comparisons test, ** $P \leq 0.01$ significantly different from wild-type mice under same treatment conditions and for the same time point, NS = not significant.

REFERENCES

1. Hamm, LL, Alpern, RJ, Preisig, PA: Cellular mechanisms of renal tubular acidification. In: *Seldin and Giebisch's The Kidney Physiology and Pathophysiology.* 4th ed. edited by ALPERN, R. J., HEBERT, S. C., Academic Press, 2008, pp 1539-1585.
2. Curthoys, NP: Renal ammonium ion production and excretion. In: *Seldin and Giebisch's The Kidney Physiology and Pathophysiology.* 4th ed. edited by ALPERN, R. J., HEBERT, S. C., Elsevier, 2008, pp 1601-1619.
3. Fry, AC, Karet, FE: Inherited renal acidoses. *Physiology (Bethesda),* 22**:** 202-211, 2007.
4. Laing, CM, Toye, AM, Capasso, G, Unwin, RJ: Renal tubular acidosis: developments in our understanding of the molecular basis. *Int J Biochem Cell Biol,* 37**:** 1151-1161, 2005.
5. Kraut, JA, Kurtz, I: Metabolic acidosis of CKD: diagnosis, clinical characteristics, and treatment. *Am J Kidney Dis,* 45**:** 978-993, 2005.
6. de Brito-Ashurst, I, Varagunam, M, Raftery, MJ, Yaqoob, MM: Bicarbonate supplementation slows progression of CKD and improves nutritional status. *J Am Soc Nephrol,* 20**:** 2075-2084, 2009.
7. Mahajan, A, Simoni, J, Sheather, SJ, Broglio, KR, Rajab, MH, Wesson, DE: Daily oral sodium bicarbonate preserves glomerular filtration rate by slowing its decline in early hypertensive nephropathy. *Kidney Int,* 78**:** 303-309, 2010.
8. Phisitkul, S, Khanna, A, Simoni, J, Broglio, K, Sheather, S, Rajab, MH, Wesson, DE: Amelioration of metabolic acidosis in patients with low GFR reduced kidney endothelin production and kidney injury, and better preserved GFR. *Kidney Int,* 77**:** 617-623, 2010.
9. Wesson, DE, Simoni, J, Broglio, K, Sheather, S: Acid retention accompanies reduced GFR in humans and increases plasma levels of endothelin and aldosterone. *Am J Physiol Renal Physiol,* 300**:** F830-837, 2011.
10. Goraya, N, Simoni, J, Jo, C, Wesson, DE: Dietary acid reduction with fruits and vegetables or bicarbonate attenuates kidney injury in patients

with a moderately reduced glomerular filtration rate due to hypertensive nephropathy. *Kidney Int,* 81**:** 86-93, 2012.

11. Smit, E, Nieto, FJ, Crespo, CJ, Mitchell, P: Estimates of animal and plant protein intake in US adults: results from the Third National Health and Nutrition Examination Survey, 1988-1991. *J Am Diet Assoc,* 99**:** 813-820, 1999.
12. Agency, EFS: Scientific opinion on dietary reference values for protein. In: EFSA PANEL ON DIETETIC PRODUCTS, N. A. A. (Ed.) Parma, Italy, EFSA Journal, 2012 pp 2257.
13. Westerterp-Plantenga, MS, Lejeune, MP, Nijs, I, van Ooijen, M, Kovacs, EM: High protein intake sustains weight maintenance after body weight loss in humans. *Int J Obes Relat Metab Disord,* 28**:** 57-64, 2004.
14. Astrup, A, Meinert Larsen, T, Harper, A: Atkins and other low-carbohydrate diets: hoax or an effective tool for weight loss? *Lancet,* 364**:** 897-899, 2004.
15. Brandle, E, Sieberth, HG, Hautmann, RE: Effect of chronic dietary protein intake on the renal function in healthy subjects. *Eur J Clin Nutr,* 50**:** 734-740, 1996.
16. Brenner, BM, Meyer, TW, Hostetter, TH: Dietary protein intake and the progressive nature of kidney disease: the role of hemodynamically mediated glomerular injury in the pathogenesis of progressive glomerular sclerosis in aging, renal ablation, and intrinsic renal disease. *N Engl J Med,* 307**:** 652-659, 1982.
17. Friedman, AN: High-protein diets: potential effects on the kidney in renal health and disease. *Am J Kidney Dis,* 44**:** 950-962, 2004.
18. King, AJ, Levey, AS: Dietary protein and renal function. *J Am Soc Nephrol,* 3**:** 1723-1737, 1993.
19. Kontessis, P, Jones, S, Dodds, R, Trevisan, R, Nosadini, R, Fioretto, P, Borsato, M, Sacerdoti, D, Viberti, G: Renal, metabolic and hormonal responses to ingestion of animal and vegetable proteins. *Kidney Int,* 38**:** 136-144, 1990.
20. Knight, EL, Stampfer, MJ, Hankinson, SE, Spiegelman, D, Curhan, GC: The impact of protein intake on renal function decline in women with

normal renal function or mild renal insufficiency. *Ann Intern Med,* 138**:** 460-467, 2003.

21. Eisenstein, J, Roberts, SB, Dallal, G, Saltzman, E: High-protein weight-loss diets: are they safe and do they work? A review of the experimental and epidemiologic data. *Nutr Rev,* 60**:** 189-200, 2002.
22. Darling, AL, Millward, DJ, Torgerson, DJ, Hewitt, CE, Lanham-New, SA: Dietary protein and bone health: a systematic review and meta-analysis. *Am J Clin Nutr,* 90**:** 1674-1692, 2009.
23. Alexy, U, Remer, T, Manz, F, Neu, CM, Schoenau, E: Long-term protein intake and dietary potential renal acid load are associated with bone modeling and remodeling at the proximal radius in healthy children. *Am J Clin Nutr,* 82**:** 1107-1114, 2005.
24. Odermatt, A: The Western-style diet: a major risk factor for impaired kidney function and chronic kidney disease. *Am J Physiol Renal Physiol,* 301**:** F919-931, 2011.
25. Pedrini, MT, Levey, AS, Lau, J, Chalmers, TC, Wang, PH: The effect of dietary protein restriction on the progression of diabetic and nondiabetic renal diseases: a meta-analysis. *Ann Intern Med,* 124**:** 627-632, 1996.
26. KDOQI Clinical Practice Guideline for Diabetes and CKD: 2012 Update. *Am J Kidney Dis,* 60**:** 850-886, 2012.
27. Remer, T, Manz, F: Estimation of the renal net acid excretion by adults consuming diets containing variable amounts of protein. *Am J Clin Nutr,* 59**:** 1356-1361, 1994.
28. Remer, T: Influence of nutrition on acid-base balance--metabolic aspects. *Eur J Nutr,* 40**:** 214-220, 2001.
29. Wesson, DE, Nathan, T, Rose, T, Simoni, J, Tran, RM: Dietary protein induces endothelin-mediated kidney injury through enhanced intrinsic acid production. *Kidney Int,* 71**:** 210-217, 2007.
30. Wesson, DE, Simoni, J: Increased tissue acid mediates a progressive decline in the glomerular filtration rate of animals with reduced nephron mass. *Kidney Int,* 75**:** 929-935, 2009.

31. Khanna, A, Simoni, J, Hacker, C, Duran, MJ, Wesson, DE: Increased endothelin activity mediates augmented distal nephron acidification induced by dietary protein. *J Am Soc Nephrol,* 15**:** 2266-2275, 2004.
32. Khanna, A, Simoni, J, Wesson, DE: Endothelin-induced increased aldosterone activity mediates augmented distal nephron acidification as a result of dietary protein. *J Am Soc Nephrol*, 2005.
33. Biver, S, Belge, H, Bourgeois, S, Van Vooren, P, Nowik, M, Scohy, S, Houillier, P, Szpirer, J, Szpirer, C, Wagner, CA, Devuyst, O, Marini, AM: A role for Rhesus factor Rhcg in renal ammonium excretion and male fertility. *Nature,* 456**:** 339-343, 2008.
34. Wagner, CA, Devuyst, O, Belge, H, Bourgeois, S, Houillier, P: The rhesus protein RhCG: a new perspective in ammonium transport and distal urinary acidification. *Kidney Int,* 79**:** 154-161, 2011.
35. Weiner, ID, Hamm, LL: Molecular mechanisms of renal ammonia transport. *Annu Rev Physiol,* 69**:** 317-340, 2007.
36. Bourgeois, S, Bounoure, L, Christensen, EI, Ramakrishnan, SK, Houillier, P, Devuyst, O, Wagner, CA: Haploinsufficiency of the ammonia transporter Rhcg predisposes to chronic acidosis: Rhcg is critical for apical and basolateral ammonia transport in the mouse collecting duct. *J Biol Chem,* 288**:** 5518-5529, 2013.
37. Lee, HW, Verlander, JW, Bishop, JM, Igarashi, P, Handlogten, ME, Weiner, ID: Collecting duct-specific Rh C glycoprotein deletion alters basal and acidosis-stimulated renal ammonia excretion. *Am J Physiol Renal Physiol,* 296**:** F1364-1375, 2009.
38. Lee, HW, Verlander, JW, Bishop, JM, Nelson, RD, Handlogten, ME, Weiner, ID: Effect of intercalated cell-specific Rh C glycoprotein deletion on basal and metabolic acidosis-stimulated renal ammonia excretion. *Am J Physiol Renal Physiol,* 299**:** F369-379, 2010.
39. Morris, SM, Jr.: Regulation of enzymes of urea and arginine synthesis. *Annu Rev Nutr,* 12**:** 81-101, 1992.
40. Sicuro, A, Mahlbacher, K, Hulter, HN, Krapf, R: Effect of growth hormone on renal and systemic acid-base homeostasis in humans. *Am J Physiol,* 274**:** F650-657, 1998.

41. Wrong, O, Davies, HE: The excretion of acid in renal disease. *Q J Med,* 28**:** 259-313, 1959.

42. Busque, SM, Wagner, CA: Potassium restriction, high protein intake, and metabolic acidosis increase expression of the glutamine transporter SNAT3 (Slc38a3) in mouse kidney. *Am J Physiol Renal Physiol,* 297**:** F440-450, 2009.

43. Peret, J, Chanez, M: Influence of diet, cortisol and insulin on the activity of pyruvate carboxylase and phosphoenolpyruvate carboxykinase in the rat liver. *J Nutr,* 106**:** 103-110, 1976.

44. Seshadri, RM, Klein, JD, Smith, T, Sands, JM, Handlogten, ME, Verlander, JW, Weiner, ID: Changes in subcellular distribution of the ammonia transporter, Rhcg, in response to chronic metabolic acidosis. *Am J Physiol Renal Physiol,* 290**:** F1443-1452, 2006.

45. Seshadri, RM, Klein, JD, Kozlowski, S, Sands, JM, Kim, YH, Han, KH, Handlogten, ME, Verlander, JW, Weiner, ID: Renal expression of the ammonia transporters, Rhbg and Rhcg, in response to chronic metabolic acidosis. *Am J Physiol Renal Physiol,* 290**:** F397-408, 2006.

46. Chambrey, R, Goossens, D, Bourgeois, S, Picard, N, Bloch-Faure, M, Leviel, F, Geoffroy, V, Cambillau, M, Colin, Y, Paillard, M, Houillier, P, Cartron, JP, Eladari, D: Genetic ablation of Rhbg in the mouse does not impair renal ammonium excretion. *Am J Physiol Renal Physiol,* 289**:** F1281-1290, 2005.

47. Bishop, JM, Lee, HW, Handlogten, ME, Han, KH, Verlander, JW, Weiner, ID: Intercalated cell-specific Rh B glycoprotein deletion diminishes renal ammonia excretion response to hypokalemia. *Am J Physiol Renal Physiol,* 304**:** F422-431, 2013.

48. Karim, Z, Attmane-Elakeb, A, Sibella, V, Bichara, M: Acid pH increases the stability of BSC1/NKCC2 mRNA in the medullary thick ascending limb. *J Am Soc Nephrol,* 14**:** 2229-2236, 2003.

49. Szutkowska, M, Vernimmen, C, Debaix, H, Devuyst, O, Friedlander, G, Karim, Z: Zeta-crystallin mediates the acid pH-induced increase of BSC1 cotransporter mRNA stability. *Kidney Int,* 76**:** 730-738, 2009.

50. Attmane-Elakeb, A, Mount, D B, Sibella, V, Vernimmen, C, Hebert, S C, Bichara, M: Stimulation by in vivo and in vitro metabolic acidosis of

expression of rBSC-1, the Na^+-K^+(NH_4^+)-2Cl^- cotransporter of the rat medullary thick ascending limb. *J Biol Chem,* 273**:** 33681-33691, 1998.

51. Laghmani, K, Richer, C, Borensztein, P, Paillard, M, Froissart, M: Expression of rat thick limb Na/H exchangers in potassium depletion and chronic metabolic acidosis. *Kidney Int,* 60**:** 1386-1396, 2001.
52. Nowik, M, Kampik, NB, Mihailova, M, Eladari, D, Wagner, CA: Induction of metabolic acidosis with ammonium chloride (NH4Cl) in mice and rats--species differences and technical considerations. *Cell Physiol Biochem,* 26**:** 1059-1072, 2010.
53. Mouri, T, Inoue, T, Nonoguchi, H, Nakayama, Y, Miyazaki, H, Matsuzaki, T, Saito, H, Nakanishi, T, Kohda, Y, Tomita, K: Acute and chronic metabolic acidosis interferes with aquaporin-2 translocation in the rat kidney collecting ducts. *Hypertens Res,* 32**:** 358-363, 2009.
54. Rodriguez-Iturbe, B, Herrera, J, Gutkowska, J, Parra, G, Coello, J: Atrial natriuretic factor increases after a protein meal in man. *Clin Sci (Lond),* 75**:** 495-498, 1988.
55. Yanagisawa, H, Wada, O: Effects of dietary protein on eicosanoid production in rat renal tubules. *Nephron,* 78**:** 179-186, 1998.
56. Bailly, C: Effect of luminal atrial natriuretic peptide on chloride reabsorption in mouse cortical thick ascending limb: inhibition by endothelin. *J Am Soc Nephrol,* 11**:** 1791-1797, 2000.
57. Klokkers, J, Langehanenberg, P, Kemper, B, Kosmeier, S, von Bally, G, Riethmuller, C, Wunder, F, Sindic, A, Pavenstadt, H, Schlatter, E, Edemir, B: Atrial natriuretic peptide and nitric oxide signaling antagonizes vasopressin-mediated water permeability in inner medullary collecting duct cells. *Am J Physiol Renal Physiol,* 297**:** F693-703, 2009.
58. Bushinsky, DA, Smith, S B, Gavrilov, K L, Gavrilov, L F, Li, J, Levi-Setti, R: Chronic acidosis-induced alteration in bone bicarbonate and phosphate. *Am J Physiol Renal Physiol,* 285**:** F532-539, 2003.
59. Lemann, J, Jr, Bushinsky, D A, Hamm, L L: Bone buffering of acid and base in humans. *Am J Physiol Renal Physiol,* 285**:** F811-832, 2003.
60. Gafter, U, Kraut, J A, Lee, D B, Silis, V, Walling, M W, Kurokawa, K, Haussler, M R, Coburn, J W: Effect of metabolic acidosis in intestinal

absorption of calcium and phosphorus. *Am J Physiol,* 239**:** G480-484, 1980.

61. Slot, C: Plasma creatinine determination. A new and specific Jaffe reaction method. *Scand J Clin Lab Invest,* 17**:** 381-387, 1965.
62. Berthelot, M: Violet d'aniline. . *Rep Chim App,* 1**:** 284, 1859.
63. Moret, C, Dave, MH, Schulz, N, Jiang, JX, Verrey, F, Wagner, CA: Regulation of renal amino acid transporters during metabolic acidosis. *Am J Physiol Renal Physiol,* 292**:** F555-566, 2007.
64. Burghardt, AJ, Kazakia, GJ, Laib, A, Majumdar, S: Quantitative assessment of bone tissue mineralization with polychromatic micro-computed tomography. *Calcif Tissue Int,* 83**:** 129-138, 2008.
65. Bouxsein, ML, Boyd, SK, Christiansen, BA, Guldberg, RE, Jepsen, KJ, Muller, R: Guidelines for assessment of bone microstructure in rodents using micro-computed tomography. *J Bone Miner Res,* 25**:** 1468-1486, 2010.
66. Kohler, T, Stauber, M, Donahue, LR, Muller, R: Automated compartmental analysis for high-throughput skeletal phenotyping in femora of genetic mouse models. *Bone,* 41**:** 659-667, 2007.
67. Lukas, C, Ruffoni, D, Lambers, FL, Schulte, A, Kuhn, G, Kollmannsberger, P, R., W, Müller, R: Mineralization kinetics in murine trabecular bone quantified by time-lapsed in vivo micro-computed tomography. *Bone*, 2013 (in press).

Table 1. Body weight, food intake, and urinary values of *Rhcg*$^{+/+}$, *Rhcg*$^{+/-}$, and *Rhcg*$^{-/-}$mice during 9 days high casein (HC) protein loading

	Basal status			**2 days HC diet**			**4 days HC diet**			**9 days HC diet**		
	***Rhcg*$^{+/+}$ (n=8)**	***Rhcg*$^{+/-}$ (n=8)**	***Rhcg*$^{-/-}$ (n=8)**	***Rhcg*$^{+/+}$ (n=8)**	***Rhcg*$^{+/-}$ (n=8)**	***Rhcg*$^{-/-}$ (n=8)**	***Rhcg*$^{+/+}$ (n=8)**	***Rhcg*$^{+/-}$ (n=8)**	***Rhcg*$^{-/-}$ (n=8)**	***Rhcg*$^{+/+}$ (n=8)**	***Rhcg*$^{+/-}$ (n=8)**	***Rhcg*$^{-/-}$ (n=8)**
Body weight (g)	28.2 ± 0.6	29.7 ± 0.4	27.0 ± 0.8	28.0 ± 0.5	29.5 ± 0.7	26.0 ± 0.9	27.6 ± 0.6	29.0 ± 0.7	25.7 ± 0.9	27.8 ± 0.4	27.3 ± 0.9	25.9 ± 0.9
Food intake (g/24hrs/body weight)	0.14 ± 0.02	0.14 ± 0.03	0.15 ± 0.02	0.10 ± 0.02$^{\#}$	0.08 ± 0.04$^{\#}$	0.10 ± 0.04$^{\#}$	0.10 ± 0.02$^{\#}$	0.10 ± 0.03$^{\#}$	0.10 ± 0.02$^{\#}$	0.12 ± 0.02$^{\#}$	0.10 ± 0.05$^{\#}$	0.10 ± 0.02$^{\#}$
Water intake (g/24hrs/body weight)	0.16 ± 0.01	0.14 ± 0.01	0.15 ± 0.01	0.24 ± 0.03$^{\#}$	0.21 ± 0.02$^{\#}$	0.21 ± 0.02$^{\#}$	0.22 ± 0.03$^{\#}$	0.23 ± 0.02$^{\#}$	0.26 ± 0.03$^{\#}$	0.25 ± 0.03$^{\#}$	0.24 ± 0.03$^{\#}$	0.26 ± 0.03$^{\#}$
Urine values												
Volume (ml/24h)	1.89 ± 0.32	1.91 ± 0.18	1.74 ± 0.19	4.51 ± 0.44$^{\#}$	4.34 ± 0.29$^{\#}$	5.20 ± 0.37$^{\#}$	4.24 ± 0.50$^{\#}$	4.38 ± 0.38$^{\#}$	5.523± 0.55$^{\#}$	4.52 ± 0.17$^{\#}$	4.36 ± 0.24$^{\#}$	5.65 ± 0.30$^{**\#}$
Urinary pH	5.94 ± 0.08	5.97 ± 0.04	6.03 ± 0.06	6.0 ± 0.04	5.94 ± 0.03	5.87 ± 0.04	5.97± 0.04	6.03 ± 0.05	5.89 ± 0.04	5.91 ± 0.04	5.85 ± 0.04	5.86 ± 0.07
NH_4^+/Urine volume (mmol/24h)	0.028 ± 0.01	0.028 ± 0.01	0.027 ± 0.01	0.26 ± 0.08$^{\#}$	0.24.0 ± 0.07$^{\#}$	0.16 ± 0.04$^{*\#}$	0.29 ± 0.08$^{\#}$	0.24 ± 0.07$^{\#}$	0.17 ± 0.05$^{***\#}$	0.28 ± 0.08$^{\#}$	0.28 ± 0.05$^{\#}$	0.29 ± 0.08$^{\#}$
TA/ Urine volume (mmol/24h)	0.08 ± 0.06	0.09 ± 0.03	0.07 ± 0.03	0.22 ± 0.09$^{\#}$	0.25 ± 0.05$^{\#}$	0.22 ± 0.06$^{\#}$	0.20 ± 0.08$^{\#}$	0.23 ± 0.06$^{\#}$	0.23 ± 0.08$^{\#}$	0.24 ± 0.07$^{\#}$	0.28 ± 0.06$^{\#}$	0.27 ± 0.05$^{\#}$
Ca^{2+}/ Urine volume (µmol/24h)	1.5 ± 0.1	1.6 ± 0.1	1.2 ± 0.1	3.3 ± 0.1$^{\#}$	3.2 ± 0.7$^{\#}$	6.5 ± 0.2$^{**\#}$	5.4 ± 0.3$^{\#}$	5.5 ± 0.2$^{\#}$	10.2 ± 0.4$^{*\#}$	4.1 ± 0.4	6.8 ± 0.2$^{\#}$	8.1 ± 0.4$^{\#}$
Dpd/Urine volume (nmol/24h)	0.076 ± 0.04 n=6	ND	0.073 ± 0.02 n=6	ND	ND	ND	0.100 ± 0.07 n=6	ND	0.211 ± 0.01$^{*\#}$ n=6	0.093 ± 0.02 n=6	ND	0.149 ± 0.05$^{*\#}$ n=6

Figure 1

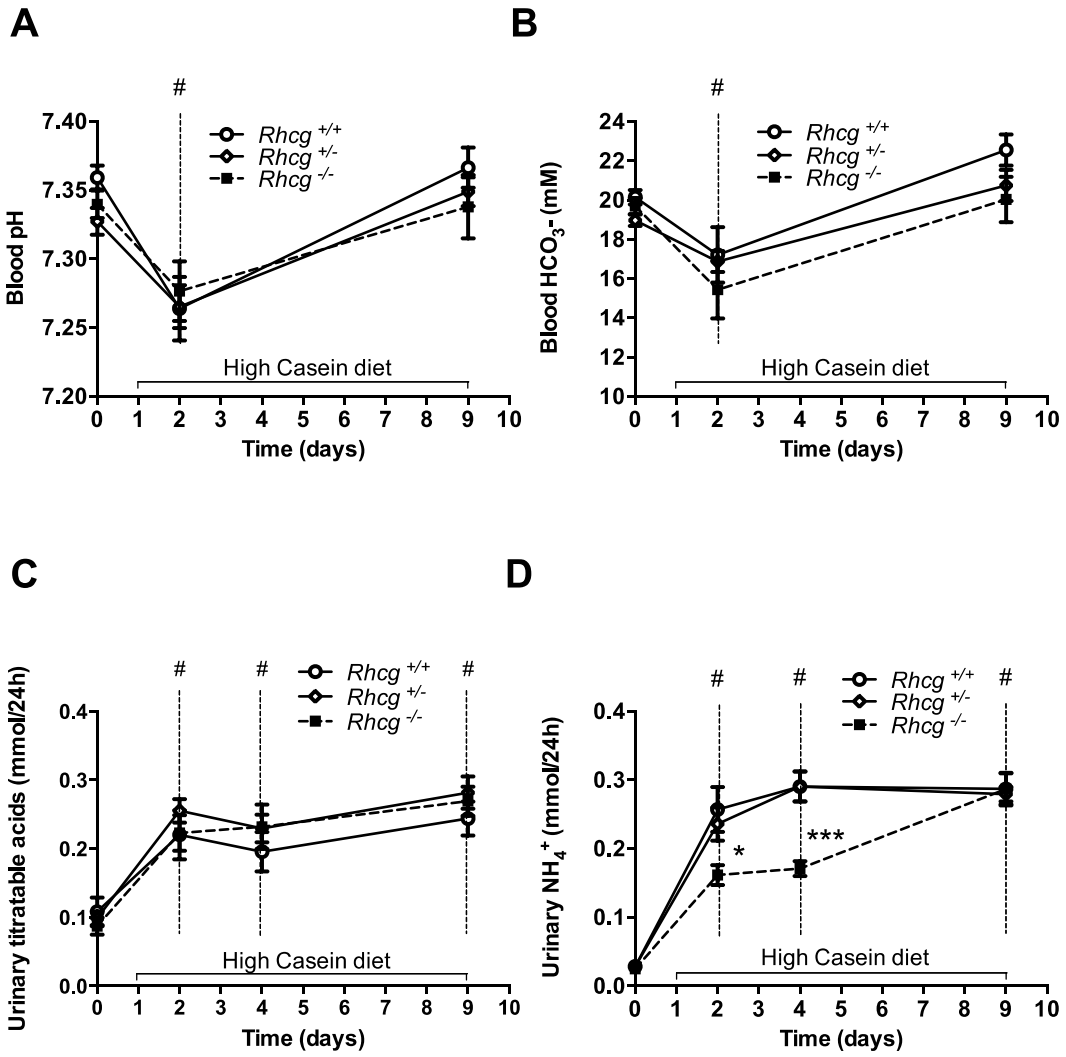
A
B
C
D
Blood pH
Blood HCO_3^- (mM)
Urinary titratable acids (mmol/24h)
Urinary NH_4^+ (mmol/24h)
Time (days)
High Casein diet
Rhcg +/+
Rhcg +/-
Rhcg -/-
#
*
***

Figure 2

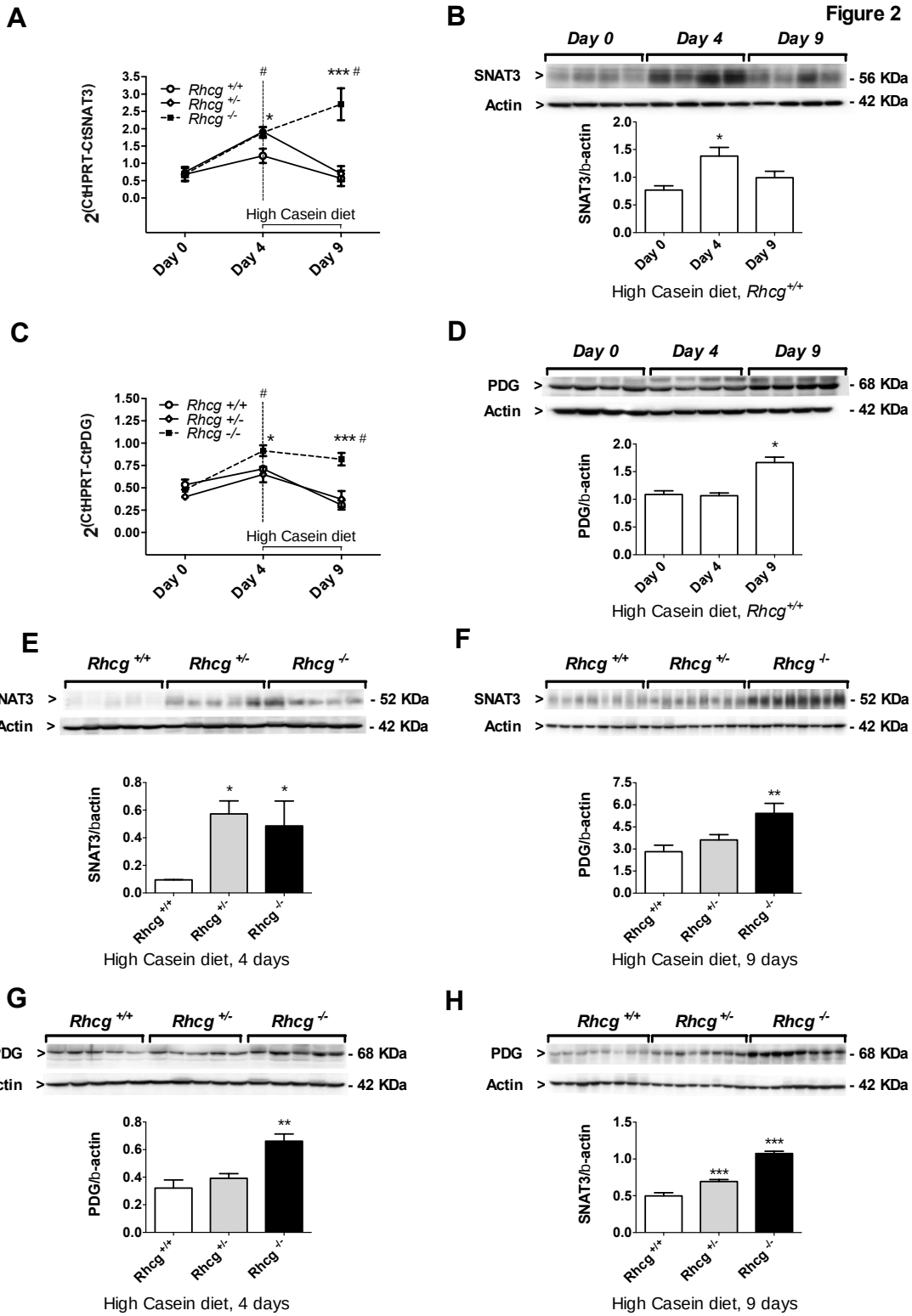
A
2(CtHPRT-CtSNAT3)
Rhcg +/+
Rhcg +/-
Rhcg -/-
High Casein diet
Day 0
Day 4
Day 9
B
Day 0
Day 4
Day 9
SNAT3
Actin
- 56 KDa
- 42 KDa
SNAT3/b-actin
High Casein diet, Rhcg+/+
C
2(CtHPRT-CtPDG)
High Casein diet
D
PDG
Actin
- 68 KDa
- 42 KDa
PDG/b-actin
High Casein diet, Rhcg+/+
E
Rhcg +/+
Rhcg +/-
Rhcg -/-
SNAT3
Actin
- 52 KDa
- 42 KDa
SNAT3/bactin
High Casein diet, 4 days
F
PDG/b-actin
High Casein diet, 9 days
G
PDG
Actin
- 68 KDa
- 42 KDa
PDG/b-actin
High Casein diet, 4 days
H
SNAT3/b-actin
High Casein diet, 9 days

Figure 3

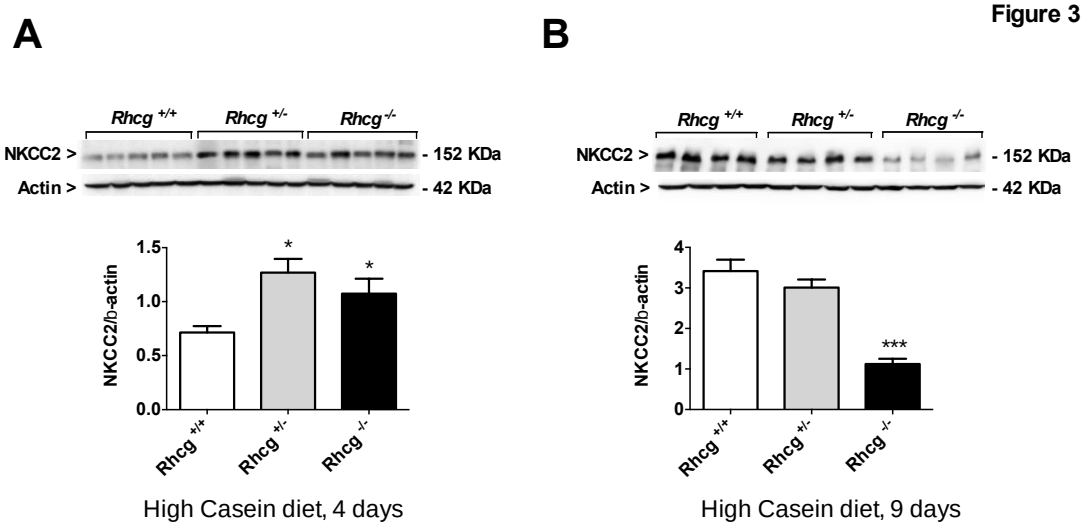

High Casein diet, 4 days

High Casein diet, 9 days

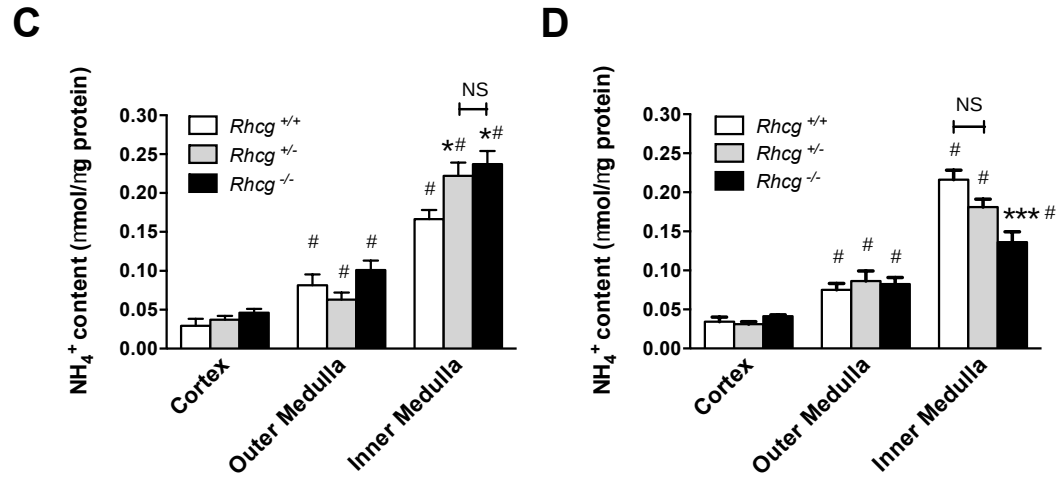

High Casein diet, 4 days

High Casein diet, 9 days

Figure 4

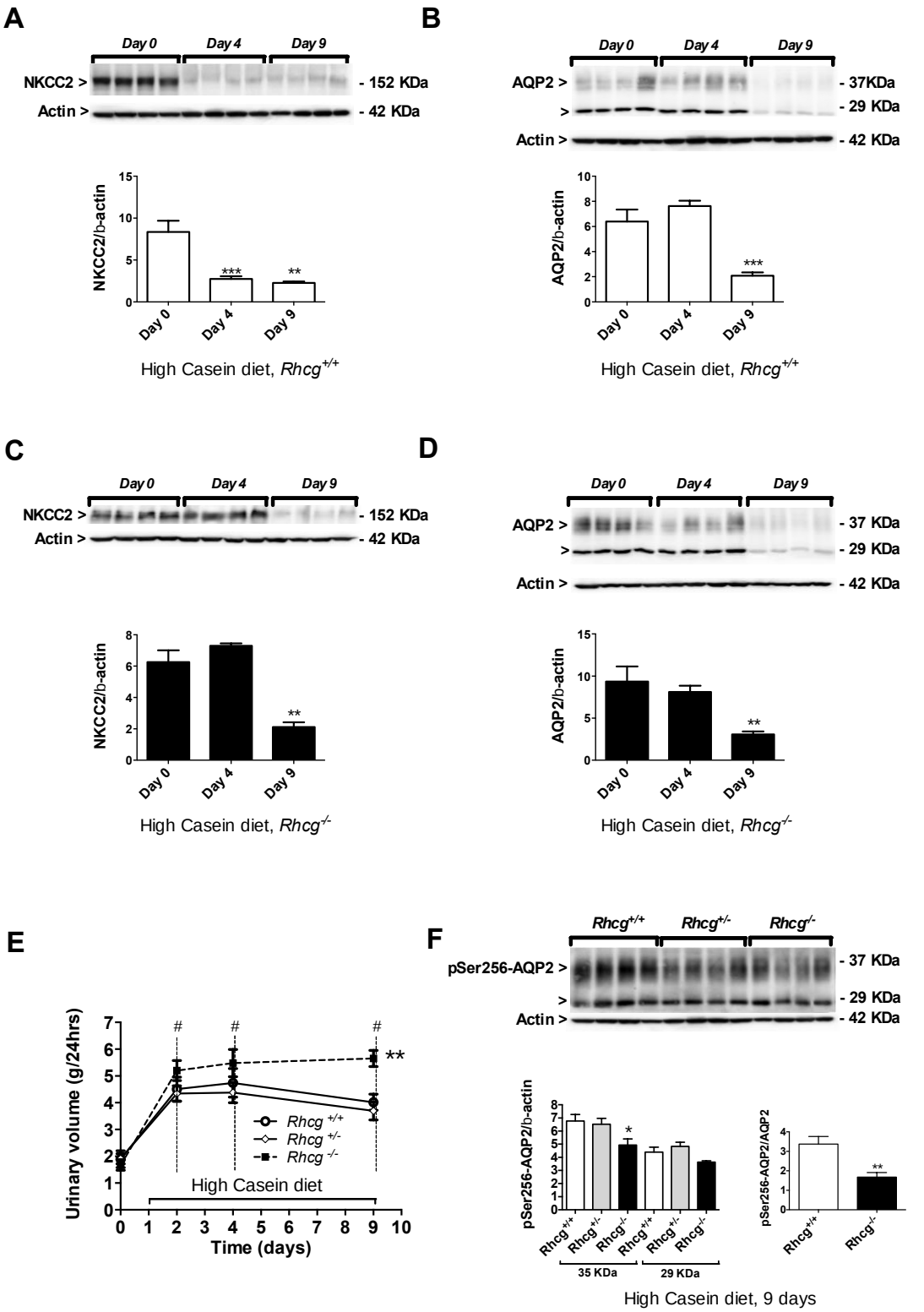
A
Day 0
Day 4
Day 9
NKCC2 >
- 152 KDa
Actin >
- 42 KDa
NKCC2/b-actin
***
**
High Casein diet, Rhcg+/+
B
AQP2 >
- 37KDa
- 29 KDa
Actin >
- 42 KDa
AQP2/b-actin
***
High Casein diet, Rhcg+/+
C
NKCC2 >
- 152 KDa
Actin >
- 42 KDa
NKCC2/b-actin
**
High Casein diet, Rhcg-/-
D
AQP2 >
- 37 KDa
- 29 KDa
Actin >
- 42 KDa
AQP2/b-actin
**
High Casein diet, Rhcg-/-
E
Urinary volume (g/24hrs)
Time (days)
Rhcg +/+
Rhcg +/-
Rhcg -/-
High Casein diet
#
**
F
Rhcg+/+
Rhcg+/-
Rhcg-/-
pSer256-AQP2 >
- 37 KDa
- 29 KDa
Actin >
- 42 KDa
pSer256-AQP2/b-actin
pSer256-AQP2/AQP2
35 KDa
29 KDa
High Casein diet, 9 days

Figure 5

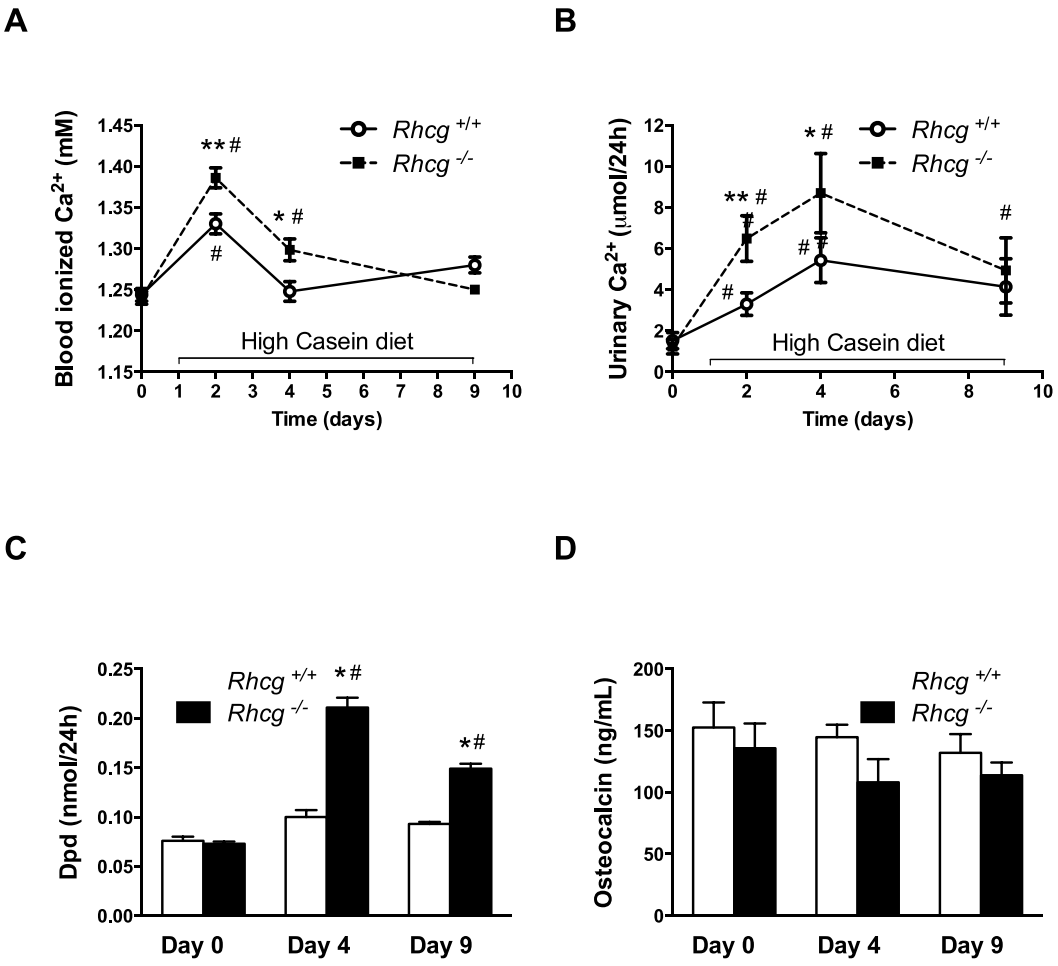
A
B
C
D
Blood ionized Ca2+ (mM)
Rhcg +/+
Rhcg -/-
High Casein diet
Time (days)
Urinary Ca2+ (µmol/24h)
Dpd (nmol/24h)
Osteocalcin (ng/mL)
Day 0
Day 4
Day 9

Figure 6

A


1 mm

B

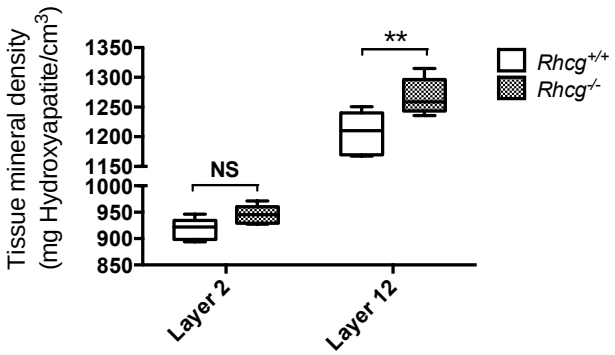
Tissue mineral density
(mg Hydroxyapatite/cm3)
1350
1300
1250
1200
1150
1000
950
900
850
NS
**
Layer 2
Layer 12
Rhcg+/+
Rhcg-/-

SUPPLEMENTARY DATA

for

The role of renal RhCG in metabolic responses to dietary protein

Lisa Bounoure*, Davide Ruffoni‡ , Ralph Müller‡ , Gisela Anna Kuhn‡, Olivier Devuyst*, Soline Bourgeois*, Carsten A. Wagner*

*Institute of Physiology and Zurich Center for Integrative Human Physiology (ZIHP), University of Zurich, Zurich, Switzerland, ‡Institute for Biomechanics, ETH Zurich, Zurich, Switzerland

Correspondence
Carsten A. Wagner
Institute of Physiology
University of Zurich
Winterthurerstrasse 190
CH-8057 Zurich
Switzerland
+41(0)44 635 50 23
+41 (0)44 635 68 14
wagnerca@access.uzh.ch

Supplementary table 1

Blood values of *Rhcg*$^{+/+}$, *Rhcg*$^{+/-}$, and *Rhcg*$^{-/-}$mice on normal diet and duringthe high casein (HC) protein loading (n = 8 mice for each group). ND notdetermined, # P ≤ 0.05 significantly different from same genotype undercontrol conditions, * P ≤ 0.05 significantly different from *Rhcg*$^{+/+}$ mice undersame treatment conditions, ** P ≤ 0.01 significantly different from *Rhcg*$^{+/+}$miceunder same treatment conditions

Supplementary table 2

Body weight, food intake and urinary values of *Rhcg*$^{+/+}$,*Rhcg*$^{+/-}$, and *Rhcg*$^{-/-}$mice during 9 days high soy (HS) protein loading (n = 6 mice for each group), # P ≤ 0.05 significantly different from same genotype under control conditions

Supplementary table 3

Urinary values of *Rhcg*$^{+/+}$,*Rhcg*$^{+/-}$, and *Rhcg*$^{-/-}$mice during 9 days high casein(HC) protein loading (n = 8 mice for each group). ND not determined, # P ≤0.05 significantly different from same genotype under control conditions, * P ≤0.05 significantly different from *Rhcg*$^{+/+}$mice under same treatment conditions,** P ≤ 0.01 significantly different from *Rhcg*$^{+/+}$mice under same treatmentconditions

Supplementary table 4

Blood values of *Rhcg*$^{+/+}$,*Rhcg*$^{+/-}$, and *Rhcg*$^{-/-}$mice on normal diet and duringthe high soy (HS) protein loading (n = 6 mice for each group). ND notdetermined, # P ≤ 0.05 significantly different from same genotype undercontrol conditions

Supplementary table 5

Standard morphometric bone parameters of *Rhcg*$^{+/+}$and *Rhcg*$^{-/-}$mice during 9days high casein (HC) protein loading (n = 5 mice for each group). Nosignificant differences were detected between genotypes.

Supplementary figure 1

Nine days high soy diet does not acid load *Rhcg*$^{+/+}$,*Rhcg*$^{+/-}$, and *Rhcg*$^{-/-}$ mice.

Blood and urine data were collected from *Rhcg*$^{+/+}$,*Rhcg*$^{+/-}$, and *Rhcg*$^{-/-}$mice treated for 9days with high soy (HS) diet. HS did not induce an acid load as indicated byblood pH (A) and bicarbonate (B), urinary titratable acidity (C) or NH_4^+excretion (D). Values are mean ± SEM (n = 6 mice) # P ≤ 0.05 significantlydifferent from same genotype under control conditions (day 0).

Supplementary figure 2

Rhcg mRNA expression is altered by HC diet while Rhbg mRNA level remainsunchanged.

Rhcg and Rhbg mRNA expression was measured by RT-qPCR in kidneysfrom *Rhcg*$^{+/+}$and *Rhcg*$^{-/-}$mice during 0, 4 and 9 days HC diet. Four days HCdiet induced a transient increase of Rhcg mRNA expression (A). mRNA levelsof RhBG remained unchanged in *Rhcg*$^{+/+}$and *Rhcg*$^{-/-}$during 0, 4 and 9 daysHC. Values are mean ± SEM (n= 6 mice), # P ≤ 0.05 significantly differentfrom same genotype under control conditions (day 0).

Supplementary figure 3

mRNA and protein expression of PEPCK and NHE3 proximal tubuleproteins areunchanged by HC diet.

Immunoblotting of *Rhcg*$^{+/+}$ kidney protein extracts collected during HC diet didnot show any changes in PEPCK (A) or NHE3 (B) expression in response tothe treatment. PEPCK (C) and NHE3 (D) mRNA levels assessed by RT-qPCRdid not display either differences comparing *Rhcg*$^{+/+}$,*Rhcg*$^{+/-}$, and *Rhcg*$^{-/-}$after 9 days HC.Similarly, PEPCK and NHE3 protein levels were identical comparing all 3groups of mice 4 or 9 days-HC diet fed. Values are mean ± SEM (n= 8 mice),p ≥ 0.05

Supplementary figure 4

High soy protein diet does not alter NKKC2 and AQP2 protein abundance in *Rhcg*$^{+/+}$mice.

The expression of NKCC2 (A) and AQP2 (B) was measured by immunoblotting in kidneys from *Rhcg*$^{+/+}$ mice and remained similar between days 0 and 9 of high soy diet. Values are mean ± SEM (n = 8 mice).

Suppplementary Table 1. Blood values of *Rhcg*$^{+/+}$, *Rhcg*$^{+/-}$, and *Rhcg*$^{-/-}$ mice on normal diet and during the high casein (HC) protein loading

	Basal status			**2 days HC diet**			**4 days HC diet**		**9 days HC diet**		
	***Rhcg*$^{+/+}$** (n=8)	***Rhcg*$^{+/-}$** (n=8)	***Rhcg*$^{-/-}$** (n=8)	***Rhcg*$^{+/+}$** (n=8)	***Rhcg*$^{+/-}$** (n=8)	***Rhcg*$^{-/-}$** (n=8)	***Rhcg*$^{+/+}$** (n=5)	***Rhcg*$^{-/-}$** (n=5)	***Rhcg*$^{+/+}$** (n=8)	***Rhcg*$^{+/-}$** (n=8)	***Rhcg*$^{-/-}$** (n=8)
pH	7.35 ± 0.01	7.33 ± 0.01	7.34 ± 0.01	7.26 ± 0.03$^{\#}$	7.27 ± 0.01$^{\#}$	7.28 ± 0.03$^{\#}$	7.36 ± 0.01	7.34 ± 0.01	7.37 ± 0.02	7.35 ± 0.01	7.34 ± 0.02
pCO_2 (mmHg)	37.4 ± 1.1	39.5 ± 1.0	37.5 ± 0.8	39.1 ± 1.4	38.4 ± 1.1	36.9 ± 1.1	37.1 ± 1.1	39.5 ± 1.8	40.2 ± 1.1	38.5 ± 1.2	38.9 ± 1.4
HCO_3^- (mM)	20.1 ± 0.4	19.0 ± 0.3	19.7 ± 0.4	17.2 ± 1.4$^{\#}$	16.9 ± 0.5$^{\#}$	15.5 ± 1.5$^{\#}$	22.2 ± 0.4	20.8 ± 0.9	22.5 ± 0.8	20.7 ± 0.7	20.1 ± 1.1
Hct (%)	49.9 ± 0.2	49.4 ± 0.6	50.2 ± 1.0	51.1 ± 0.7	50.7 ± 0.7	52.6 ± 0.7	49.6 ± 0.2	50.6 ± 0.6	53.5 ± 0.8$^{\#}$	52.2 ± 0.7$^{\#}$	55.8 ± 0.6$^{\#}$
Na^+ (mM)	146.5 ± 0.5	146.9 ± 0.4	145.5 ± 0.4	147.5 ± 0.4	148.7 ± 0.4	147.6 ± 0.7	144.8 ± 0.6	145.4 ± 0.5	147.8 ± 0.5	148.5 ± 0.5	146.5 ± 0.4
Cl^- (mM)	112.9 ± 0.4	114.1 ± 0.6	111.9 ± 0.5	117.7 ± 1.0$^{\#}$	118.3 ± 0.9$^{\#}$	121.4 ± 1.2$^{\#}$	110.4 ± 1.3	112.0 ± 0.8	116.8 ± 1.2$^{\#}$	116.3 ± 1.0$^{\#}$	119 ± 1.7$^{\#}$
Ionized Ca^{2+}(mM)	1.24 ± 0.006	1.26 ± 0.009	1.24 ± 0.002	1.33 ± 0.005$^{\#}$	1.30 ± 0.004$^{\#}$	1.39 ± 0.01$^{**\#}$	1.25± 0.008	1.30 ± 0.009$^{*\#}$	1.28 ± 0.009	1.29 ± 0.001	1.25 ± 0.006
K^+ (mM)	4.6 ± 1.2	4.4 ± 1.1	4.5 ± 1.1	4.8 ± 0.2	4.6 ± 0.2	4.1 ± 0.1	4.9 ± 0.2	4.7 ± 0.7	4.6 ± 0.1	4.6 ± 0.2	4.3 ± 0.2
Glucose (mM)	10.6 ± 0.6	10.7 ± 0.5	11.7 ± 0.5	8.0 ± 1.1$^{\#}$	8.9 ± 0.5$^{\#}$	9.4 ± 0.7$^{\#}$	11.9 ± 0.4	12.1 ± 0.5	10.0 ± 0.9	10.2 ± 0.6	12.2 ± 0.9
Lactate (mM)	3.6 ± 0.3	3.6 ± 0.2	3.9 ± 0.7	3.8 ± 0.4	3.3 ± 0.3	3.3 ± 0.3	3.5 ± 0.2	3.0 ± 0.4	2.4 ± 0.2$^{\#}$	2.6 ± 0.2$^{\#}$	2.9 ± 0.3$^{\#}$
Osteocalcin (ng/mL)	152.5 ± 20.4	ND	135.7 ± 20.0	ND	ND	ND	144.8 ± 10.0	108.1 ± 18.7	132.1 ± 15.1	ND	113.9 ± 10.4

Supplementary table 2. Body weight, food intake and urinary values of *Rhcg*$^{+/+}$, *Rhcg*$^{+/-}$, and *Rhcg*$^{-/-}$ mice during 9 days high soy (HS) protein loading.

	Basal status			2 days HS diet			4 days HS diet			9 days HS diet		
	Rhcg$^{+/+}$ (n=6)	*Rhcg*$^{+/-}$ (n=6)	*Rhcg*$^{-/-}$ (n=6)	*Rhcg*$^{+/+}$ (n=6)	*Rhcg*$^{+/-}$ (n=6)	*Rhcg*$^{-/-}$ (n=6)	*Rhcg*$^{+/+}$ (n=6)	*Rhcg*$^{+/-}$ (n=6)	*Rhcg*$^{-/-}$ (n=6)	*Rhcg*$^{+/+}$ (n=6)	*Rhcg*$^{+/-}$ (n=6)	*Rhcg*$^{-/-}$ (n=6)
Body weight (g)	28.5 ± 1.6	26.0 ± 1.1	27.2 ± 1.4	27.6 ± 1.5	25.2 ± 1.1	25.6 ± 1.3	26.8 ± 1.3	25.0 ± 1.1	25.6 ± 1.3	25.8 ± 0.9	25.0 ± 1.2	25.2 ± 1.1
Food intake (g/24hrs/body weight)	0.12 ± 0.01	0.12 ± 0.01	0.11 ± 0.02	0.12 ± 0.02	0.12 ± 0.01	0.13 ± 0.01	0.10 ± 0.01	0.12 ± 0.01	0.11 ± 0.01	0.14 ± 0.01	0.13 ± 0.01	0.13 ± 0.01
Water intake (g/24hrs/body weight)	0.15 ± 0.02	0.16 ± 0.01	0.16 ± 0.02	0.22 ± 0.03$^{\#}$	0.26 ± 0.02$^{\#}$	0.23 ± 0.02$^{\#}$	0.23 ± 0.01$^{\#}$	0.23 ± 0.02$^{\#}$	0.25 ± 0.03$^{\#}$	0.27 ± 0.03$^{\#}$	0.28 ± 0.02$^{\#}$	0.27 ± 0.03$^{\#}$
Urine values												
Volume (ml/24 h)	1.84 ± 0.22	1.83 ± 0.27	1.79 ± 0.20	2.95 ± 0.38$^{\#}$	2.87 ± 0.35$^{\#}$	3.37 ± 0.56$^{\#}$	2.58 ± 0.18$^{\#}$	2.03 ± 0.26$^{\#}$	2.50 ± 0.39$^{\#}$	3.24 ± 0.33$^{\#}$	2.53 ± 0.35$^{\#}$	3.36 ± 0.30$^{\#}$
Creatinine excretion (µmol/24h)	10.18± 0.53	11.52 ± 1.18	10.70± 1.57	7.92 ± 1.47$^{\#}$	7.15 ± 0.77$^{\#}$	7.51 ± 0.50$^{\#}$	5.98 ± 0.71$^{\#}$	4.76 ± 0.59$^{\#}$	5.34 ± 0.49$^{\#}$	6.92 ± 1.19$^{\#}$	5.71 ± 1.12$^{\#}$	7.11 ± 1.08$^{\#}$
Urinary pH	5.91 ± 0.08	5.63 ± 0.07	5.70 ± 0.11	6.83 ± 0.18$^{\#}$	7.06 ± 0.23$^{\#}$	6.95 ± 0.17$^{\#}$	7.09 ± 0.14$^{\#}$	7.26 ± 0.09$^{\#}$	7.29 ± 0.11$^{\#}$	7.11 ± 0.27$^{\#}$	7.15 ± 0.13$^{\#}$	6.99 ± 0.17$^{\#}$
NH_4^+/24h (µmol/24h)	46.9 ± 4.0	53.1 ± 4.3	46.2 ± 3.9	14.8 ± 1.5$^{\#}$	12.9 ± 1.2$^{\#}$	13.7 ± 2.0$^{\#}$	10.9 ± 2.9$^{\#}$	12.0 ± 1.6$^{\#}$	12.9 ± 1.2$^{\#}$	17.1 ± 1.8$^{\#}$	15.3 ± 1.7$^{\#}$	15.1 ± 1.9$^{\#}$
TA/24h (µmol/24h)	211.1 ± 11.5	182.8 ± 11.8	197.3 ± 12.1	19.1 ± 1.8$^{\#}$	20.7 ± 1.9$^{\#}$	23.3 ± 1.5$^{\#}$	27.1 ± 1.7$^{\#}$	23.22 ± 1.8$^{\#}$	24.1 ± 1.9$^{\#}$	23.3 ± 1.6$^{\#}$	28.4 ± 1.6$^{\#}$	25.2 ± 1.5$^{\#}$
PO_4^{2-}/Crea (mM/mM)	5.0 ± 0.8	6.0 ± 0.4	5.8 ± 0.6	2.8 ± 0.2$^{\#}$	2.1 ± 0.3$^{\#}$	1.9 ± 0.3$^{\#}$	2.8 ± 1.8$^{\#}$	2.8 ± 0.4$^{\#}$	2.6 ± 0.3$^{\#}$	3.0 ± 0.3$^{\#}$	3.8 ± 0.7$^{\#}$	3.7 ± 0.6$^{\#}$
Urea/24h (µmol/24h)	2.31 ± 0.52	2.64 ± 0.37	2.86 ± 0.78	6.90 ± 0.35$^{\#}$	7.33 ± 0.98$^{\#}$	7.02 ± 0.78$^{\#}$	6.18 ± 0.65$^{\#}$	7.51 ± 0.87$^{\#}$	6.97 ± 0.83$^{\#}$	8.21 ± 0.62$^{\#}$	7.69 ± 0.47$^{\#}$	8.02 ± 0.39$^{\#}$
Ca^{2+}/24h (µmol/24h)	2.16 ± 0.02	2.21 ± 0.03	2.33 ± 0.07	1.99 ± 0.05	2.09 ± 0.07	2.01 ± 0.02	2.14 ± 0.07	2.10 ± 0.03	2.16 ± 0.04	1.87 ± 0.06	1.98 ± 0.08	2.03 ± 0.07
Na^+/Crea (mM/mM)	17.5± 1.5	13.5± 2.9	11.6 ± 3.5	60.5 ± 13.2$^{\#}$	62.0 ± 7.0$^{\#}$	50.7 ± 8.3$^{\#}$	80.9 ± 9.8$^{\#}$	81.4 ± 9.3$^{\#}$	85.8 ± 9.7$^{\#}$	74.0 ± 9.0$^{\#}$	91.0 ± 7.0$^{\#}$	81.8 ± 11.3$^{\#}$
Cl^-/Crea (mM/mM)	41.6 ± 4.0	41.5 ± 1.9	33.0 ± 4.1	61.5 ± 17.2$^{\#}$	58.5 ± 5.7$^{\#}$	62.5 ± 2.5$^{\#}$	68.0 ± 8.7$^{\#}$	73.9 ± 5.3$^{\#}$	74.0 ± 8.9$^{\#}$	58.4 ± 7.5$^{\#}$	76.2 ± 10.1$^{\#}$	76.7 ± 9.0$^{\#}$
K^+/Crea (mM/mM)	58.2 ± 5.4	62.7± 90.6	50.9 ± 6.2	73.4 ± 19.4$^{\#}$	75.5 ± 6.3$^{\#}$	71.8 ± 5.3$^{\#}$	82.6 ± 10.2$^{\#}$	81.9 ± 6.8$^{\#}$	85.2 ± 6.9$^{\#}$	76.7 ± 10.9$^{\#}$	93.4 ± 11.0$^{\#}$	81.9 ± 11.9$^{\#}$
SO_4^2/24 h (µmol/24 h)	0.26± 0.4 n=6	0.21± 0.2 n=5	0.24.0 ± 0.7 n=6	ND	ND	ND	ND	ND	ND	0.30 ± 0.3 n=6	0.27 ± 0.6 n=5	0.28 ± 0.3 n=6

Supplementary table 3. Urinary values of *Rhcg*$^{+/+}$, *Rhcg*$^{+/-}$, and *Rhcg*$^{-/-}$ mice during 9 days high casein (HC) protein loading

	Basal status			2 days HC diet			4 days HC diet			9 days HC diet		
	***Rhcg*$^{+/+}$** (n=8)	***Rhcg*$^{+/-}$** (n=8)	***Rhcg*$^{-/-}$** (n=8)	***Rhcg*$^{+/+}$** (n=8)	***Rhcg*$^{+/-}$** (n=8)	***Rhcg*$^{-/-}$** (n=8)	***Rhcg*$^{+/+}$** (n=8)	***Rhcg*$^{+/-}$** (n=8)	***Rhcg*$^{-/-}$** (n=8)	***Rhcg*$^{+/+}$** (n=8)	***Rhcg*$^{+/-}$** (n=8)	***Rhcg*$^{-/-}$** (n=8)
Creatinine excretion (µmol/24h)	6.53 ± 0.38	6.81 ± 0.99	6.89 ± 0.85	6.45 ± 0.70	6.96 ± 0.73	6.59 ± 0.41	6.04 ± 0.60	6.56 ± 0.21	6.22 ± 0.81	6.57 ± 0.52	6.48 ± 0.33	6.85 ± 0.72
PO_4^{2-}/Crea (mM/mM)	8.0 ± 1.0	7.4 ± 1.1	6.2 ± 1.0	17.7 ± 1.6#	16.7 ± 0.9#	18.2 ± 3.1#	18.0 ± 1.8#	13.9 ± 0.9#	20.4 ± 1.3#	20.1 ± 1.9#	20.5 ± 0.9#	18.8 ± 3.3#
Urea/Urine volume (µmol/24h)	2.40 ± 0.17	2.60 ± 0.28	2.81 ± 0.26	7.79 ± 0.75#	7.81 ± 0.61#	7.89 ± 0.63#	6.37 ± 0.65#	8.27 ± 0.74#	8.12± 0.99#	6.89 ± 0.58#	9.48 ± 0.67#	10.84± 0.40*#
Na^+/Crea (mM/mM)	22.3 ± 3.7	28.0 ± 3.0	35.6 ± 8.4	35.2 ± 4.5	36.1± 49	42.5 ± 7.2	34.3 ± 4.0	25.9 ± 3.5	28.1 ± 2.1	35.2 ± 6.1	37.9 ± 3.2	29.8 ± 3.5
Cl^-/Crea (mM/mM)	54.7 ± 6.9	67.6 ± 6.7	63.6 ± 10.6	59.6 ± 6.1	61.0 ± 7.0	67.2 ± 10.9	58.5 ± 5.6	60.0 ± 3.2	50.4 ± 4.1	60.4 ± 7.7	68.5 ± 4.5	58.1 ± 6.4
K^+/Crea (mM/mM)	98.5 ± 7.3	92.3 ± 9.0	96.6 ± 14.2	106.9 ± 9.8	117.0 ± 10.6	133 ± 20.6	104.4 ± 8.9	89.7 ± 8.2	125.3 ± 14.4	113.5 ± 12.5	122.6 ± 6.4	123.2 ± 11.9
SO_4^{2-}/Urine volume (µmol/24h)	0.22 ± 0.9	0.18 ± 0.2	0.23 ± 0.4	0.43 ± 0.8#	0.49 ± 0.5#	0.53 ± 0.1#	0.51 ± 0.6#	0.53 ± 0.5#	0.47 ± 0.7#	0.52 ± 0.8#	0.58 ± 0.9#	0.56 ± 0.7#

Supplementary table 4. Blood values of *Rhcg*$^{+/+}$, *Rhcg*$^{+/-}$, and *Rhcg*$^{-/-}$ mice on normal diet and during the high soy (HS) protein loading.

	Basal status			2 days HS diet			9 days HS diet		
	***Rhcg*$^{+/+}$** (n=6)	***Rhcg*$^{+/-}$** (n=6)	***Rhcg*$^{-/-}$** (n=6)	***Rhcg*$^{+/+}$** (n=6)	***Rhcg*$^{+/-}$** (n=6)	***Rhcg*$^{-/-}$** (n=6)	***Rhcg*$^{+/+}$** (n=6)	***Rhcg*$^{+/-}$** (n=6)	***Rhcg*$^{-/-}$** (n=6)
pH	7.36 ± 0.004	7.37 ± 0.004	7.36 ± 0.003	7.37 ± 0.02	7.39 ± 0.02	7.37 ± 0.01	7.37 ± 0.02	7.38 ± 0.02	7.35 ± 0.01
pCO_2 (mmHg)	38.8 ± 0.8	38.9 ± 0.2	38.2 ± 0.5	38.1 ± 1.1	39.2 ± 0.8	39.5 ± 1.9	39.1± 1.7	39.7 ± 1.5	39.9 ± 1.3
HCO_3^- (mM)	21.1 ± 0.9	21.9 ± 0.2	21.5 ± 0.2	23.1 ± 1.4	24 ± 0.8	23.1 ± 0.9	22.6 ± 0.8	23.8 ± 0.3	23.2 ± 0.3
Hct (%)	49.4 ± 0.2	49.4 ± 0.4	49.0 ± 0.5	49.2 ± 0.7	49.5 ± 0.8	48.8 ± 1.1	49.3 ± 0.6	49.2 ± 0.8	49.1 ± 0.9
Na^+ (mM)	147.5 ± 0.5	149.3 ± 0.8	149.8 ± 0.4	148 ± 0.4	148.4 ± 0.5	148.7 ± 0.9	147.5 ± 0.5	147.2 ± 0.5	148.3 ± 0.6
Cl^- (mM)	115.0 ± 0.1	114.3 ± 0.4	115.1 ± 0.6	114.0± 0.9	113.6 ± 0.4	113.8 ± 2.0	111.1 ± 0.1$^{\#}$	112.0 ± 0.5$^{\#}$	111.5 ± 0.9$^{\#}$
Ionized Ca^{2+}(mM)	1.30 ± 0.005	1.27 ± 0.008	1.30 ± 0.005	1.29 ± 0.001	1.26 ± 0.001	1.25 ± 0.002	1.27 ± 0.04	1.28 ± 0.01	1.23 ± 0.01$^{\#}$
K^+ (mM)	5.2 ± 0.3	5.0 ± 0.2	5.2 ± 0.1	5.1 ± 0.5	5.1 ± 0.2	5.3 ± 0.3	5.3 ± 0.2	5.2 ± 0.3	5.2 ± 0.2
Glucose (mM)	12.1 ± 0.2	12.3 ± 0.4	12.0 ± 0.3	11.8 ± 0.4	11.2 ± 1.0	12.7 ± 1.2	12.0 ± 0.9	11.9 ± 1.0	11.8 ± 1.5
Lactate (mM)	4.7 ± 0.1	4.3 ± 0.3	4.4 ± 0.5	3.5 ± 1.3	3.7 ± 0.3	4.1 ± 0.7	3.4 ± 0.6	3.5 ± 0.2	3.3 ± 0.7

Supplementary table 5. Standard morphometric parameters from *Rhcg*$^{+/+}$ and *Rhcg* during 9 days high casein protein loading

	***Rhcg*$^{+/+}$**	***Rhcg*$^{-/-}$**
	(n=5)	*(n=5)*
Trabecular compartment		
Bone volume fraction (%)	16.32 ± 1.56	15.27 ± 0.78
Trabecular number (1/mm)	3.79 ± 0.47	3.38 ± 0.31
Trabecular thickness (mm)	0.060 ± 0.003	0.062 ± 0.003
Trabecular separation (mm)	0.277 ± 0.098	0.306 ± 0.037
Cortical compartment		
Total cross-sectional area inside the periosteal envelope (mm^2)	1.000 ± 0.046	1.076 ± 0.046
Cortical bone area (mm^2)	0.954 ± 0.045	1.029 ± 0.045
Cortical area fraction (mm^3)	0.954 ± 0.001	0.956 ± 0.001
Average cortical thickness (mm)	0.237 ± 0.007	0.241 ± 0.008
Full bone		
Apparent volume density (%)	57.44 ± 0.96	57.66 ± 0.99

Supplementary figure 1

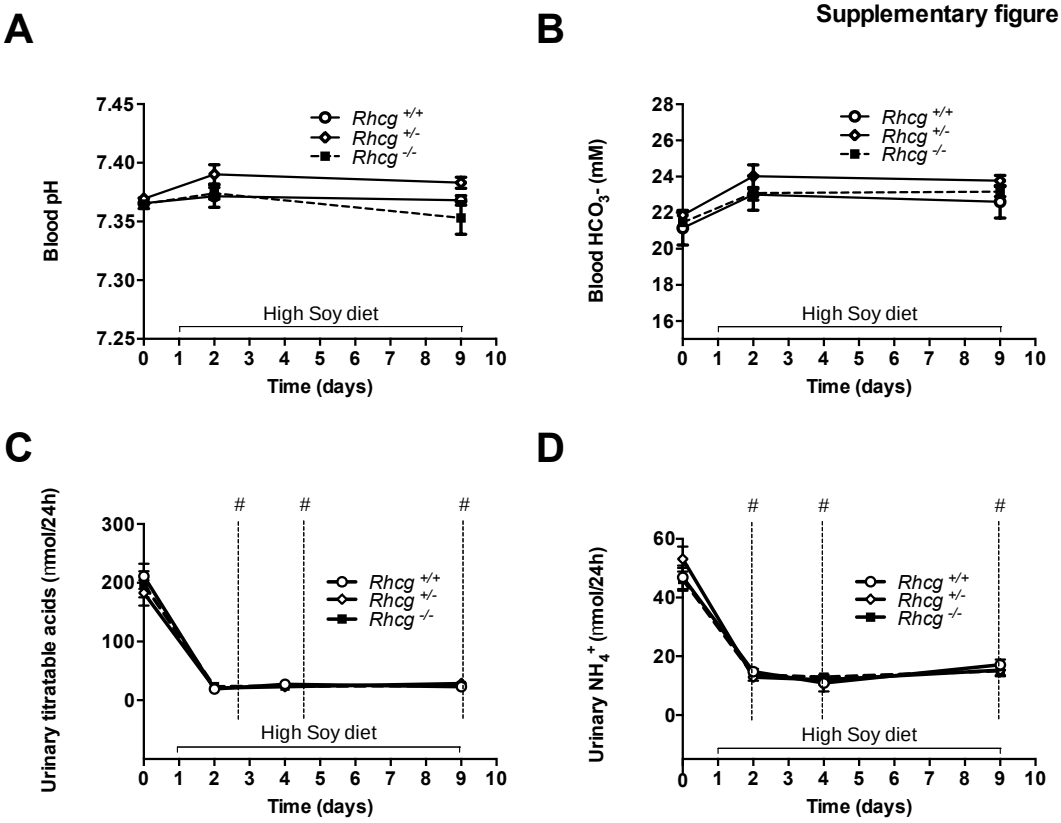

Supplementary figure 2

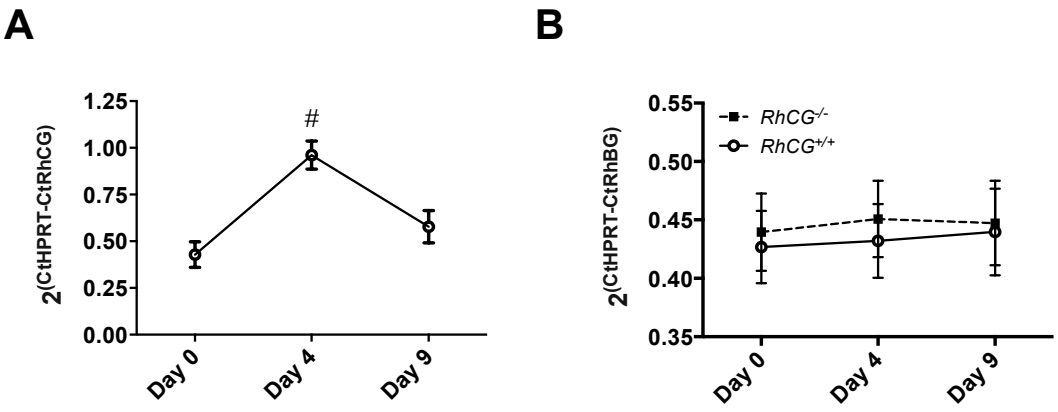

Supplementary figure 3

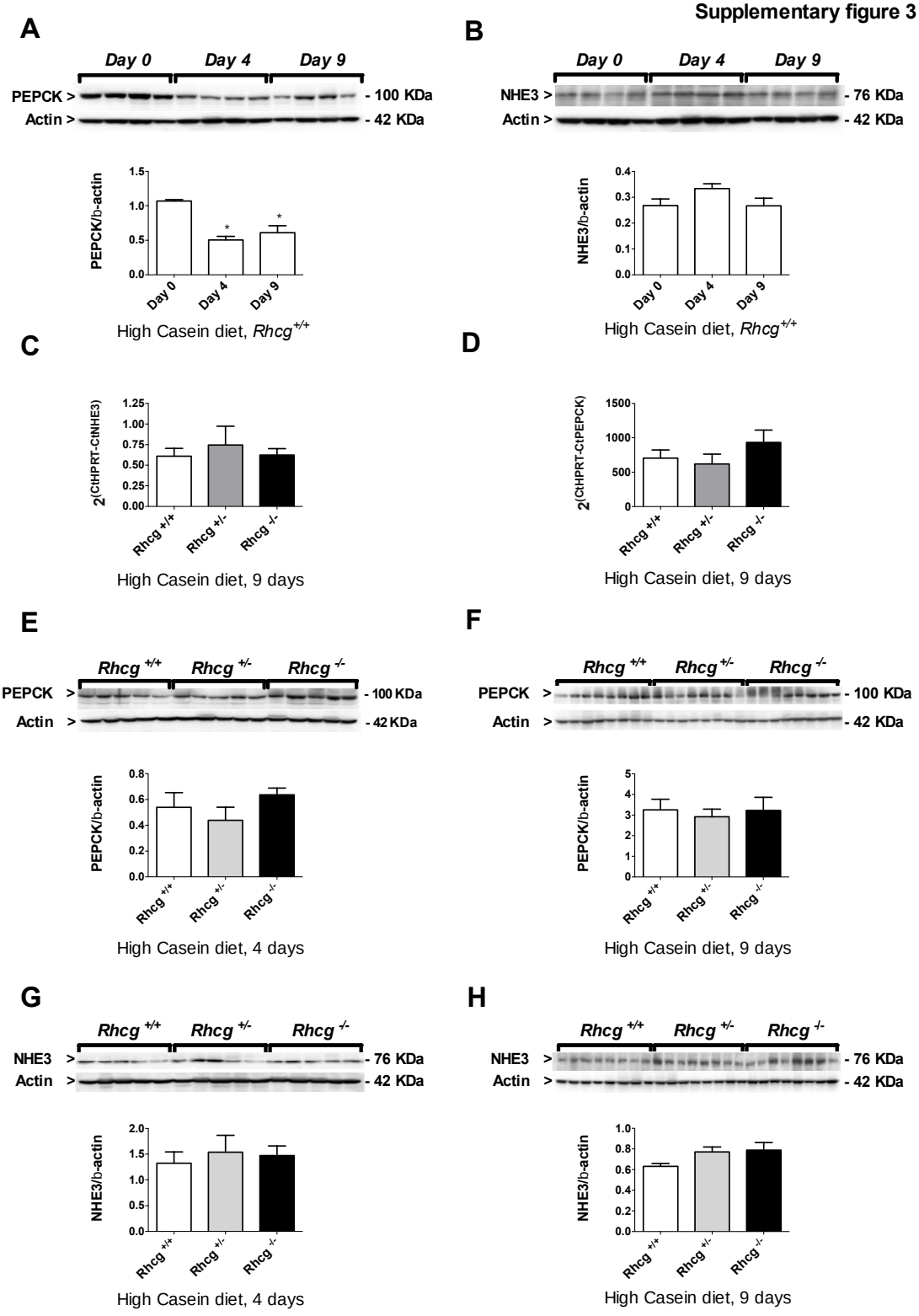

Supplementary figure 4

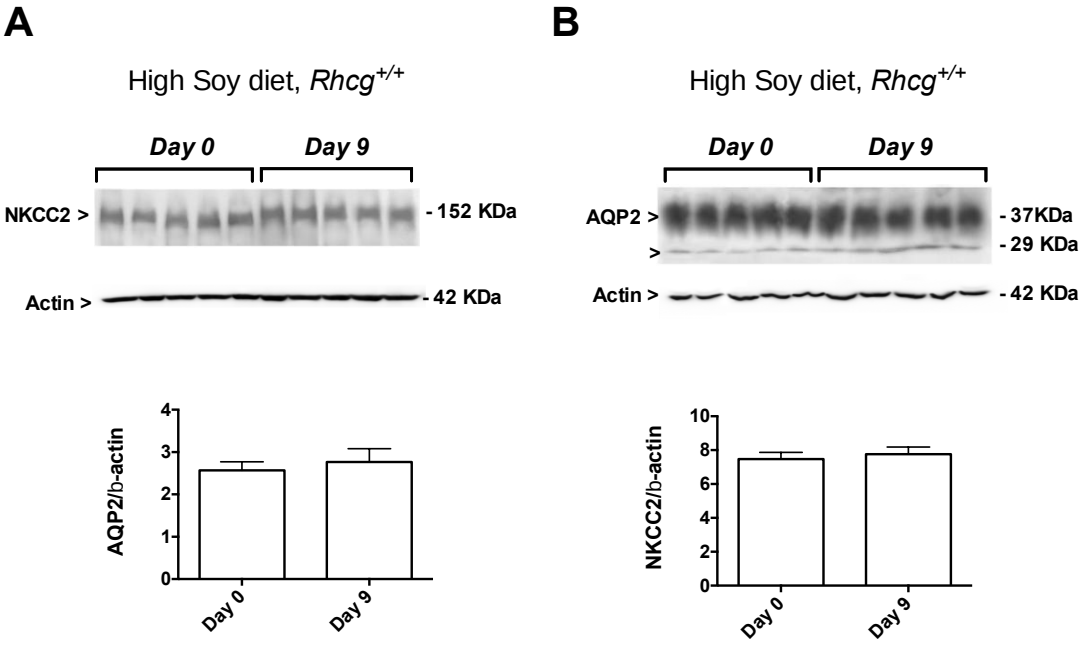

IV The ammonia transporter RhCG modulates vacuolar H^+-ATPase function in renal intercalated cells

Own contribution to the publication:

All mRNA analysis performed on *Rhcg*$^{+/+}$ and $^{-/-}$ mice receiving 2d HCl diet acid-load presented in **Figure 2** were carried out.

In **Figure 3**, all protein expression levels measured on *Rhcg*$^{+/+}$ and $^{-/-}$ mice were realized.

Similarly, the intracellular pH measurements on HEK-RhCG and HEK-WT cells represented in **Figure 5A** were performed and from this experiment, the H^+ fluxes in HEK-RhCG and HEK-WT displayedin **Figure 5B** were calculated.

Finally, mRNA expression levels of all genes measured in HEK-RhCG and HEK-WT were assessed and are showed in **Figure 6**.

Correspondence of modified urinary proton excretion activity in an ammonia transport-deficient mouse model

*The ammonia transporter RhCG modulates vacuolar H^+-ATPase function in renal intercalated cells**

Lisa Bounoure[1], Soline Bourgeois**[1], Isabelle Mouro-Chanteloup[2], Helmut Wieczorek[3], Yves Colin[2], Dennis Brown[4], and Carsten A. Wagner[1]**

[1]Institute of Physiology, University of Zurich, Zurich, Switzerland,[2]INSERM UMR665 and University Paris Diderot, Paris, France,[3]Department of Animal Physiology, University of Osnabrück, Germany,[4]Center for Systems Biology, Program in Membrane Biology, Department of Medicine, Massachusetts General Hospital and Harvard Medical School, Boston, United States

** L. Bounoure and S. Bourgeois contributed equally to this manuscript and therefore share firstauthorship

*Running title: Rhcg ammonia transporter modulates H^+-ATPase proton secretion

To whom correspondence should be addressed: Carsten A. Wagner, Institute of Physiology, University of Zurich, Winterthurerstrasse 190, 8057 Zurich, Switzerland, Tel: +41(0)44 635 50 23, Fax: +41 (0)44 635 68 14, Email: wagnerca@access.uzh.ch

Keywords: Urinary ammonium, vacuolar H^+-ATPase, ammonia transporter, collecting duct

Background: Urinary ammonium excretion is chiefly achieved by the ammonia transporter RhCG and vacuolar H^+-ATPases, both expressed in the renal collecting duct. Rhcg knockout mice have more alkaline urine than wildtype control.

Results: The activity of vacuolar H^+-ATPases is decreased in kidney intercalated cells of Rhcg knockout mice with similar subcellular localization and altered abundance of some isoforms. Overexpression of Rhcg stimulates H^+-ATPase activity in vitro. Genetic impairment of vacuolar H^+-ATPases does not modify NH_3 transport in intercalated cells of kidney.

Conclusion: Rhcg may modify the activity of vacuolar H^+-ATPases in intercalated cells of kidneys.

Significance: Delineating the precise molecular mechanisms of urinary ammonium excretion and acidification by intercalated cells of the collecting duct in kidney.

ABSTRACT

Ammonium (NH_4^+) is excreted into urine along the collecting duct (CDs) of kidneys representing the predominant mechanism of removing acid into urine. This process is dependent on the concomitant secretion of ammonia (NH_3) by the NH_3 transporter RhCG and protons(H^+) by vacuolar-type H^+-ATPases. Mice lacking Rhcg excrete more alkaline urine despite the lack of the NH_3/NH_4^+ buffer indicating impaired urinary acidification. Here, we demonstrated in microperfused cortical collecting ducts (CCD) from *Rhcg*$^{-/-}$mice that H^+-ATPase activity is reduced by 89%. Electron microscopy with immuno-gold detection of the H^+-ATPase A subunit demonstrated similar localization and density of staining. Moreover, expression ofthe a1, a4, and E2 H^+-ATPase subunits was similar in the renal medulla of *Rhcg*$^{+/+}$ and *Rhcg*$^{-/-}$ mice whereas the B1 isoform was enhanced and the B2 isoform reduced. Inversely, overexpression of RhCG in HEK293 cells resulted in higher H^+ secretion and increased B1 subunit mRNA (*ATP6V1B1*) expression. To further examine the functional interaction between RhCG and H^+-ATPases, we employed the H^+-ATPase inhibitor concanamycin A which reduced H^+-ATPase activity and RhCG mediated NH_3 transport in intercalated cells, suggesting that concanamycin A either acts on RhCG or that H^+-ATPase function is required for RhCG transport activity. Mice lacking the B1 H^+-ATPase isoform had reduced H^+-ATPase function without altering RhCG mediated NH_3 transport in microperfused collecting ducts. Thus, RhCG may modulate H^+-ATPase function, whereasH^+-ATPase activity does not directly affect RhCG mediated NH_3 transport.

INTRODUCTION

The renal collecting duct excretes acid into urine by parallel secretion of protons (H^+) and ammonia (NH_3) by V-type H^+-ATPases and the ammonia transporter RhCG, respectively(1-3). Renal acid excretion is critical for maintaining normal acid-base homeostasis and is increased during acidosis or following an acid-load (2).

Highly conserved through-out evolution from bacteria to humans, RhCG belongs to the Rhesus glycoprotein family and has been characterized by *in vitro* and *ex vivo* studies as a transporter selectively permeable to NH_3 but not to ammonium (NH_4^+) (4-6). In the kidney, RhCG expression specifically spreads from the late distal convoluted tubule (DCT) to the inner medullary collecting duct (IMCD), on both basolateral and apical poles of epithelial cells (7-11). We recently showed that RhCG is responsible for a major part of NH_3 transported through apical and basolateral membranes of the collecting duct resulting in a drastic reduction of transepithelial NH_3 transport in collecting ducts from total*Rhcg*$^{-/-}$ mice (11-12). Similarly, mice with partial deletion of Rhcg in different subtypes of cells causes a reduction in urinary ammonium excretion (13-14). As a consequence of this defect, chronically acid-loaded *Rhcg*$^{-/-}$ mice cannot eliminate NH_4^+ into urine and develop a severe distal renal tubular acidosis (dRTA) with low blood pH and HCO_3^- concentration (11-12).

While RhCG is responsible for luminal NH_3 secretion, the renal vacuolar H^+-ATPase (H^+-ATPase) in intercalated cells of the collecting duct is critical to actively secrete H^+ into urine (15-16). H^+-ATPases are ubiquitous multi-subunits proteins composed of a cytosolic V_1 catalytic domain, responsible for ATP hydrolysis and a membrane-associated V_0 domain responsible for H^+ translocation (16-17). In the collecting duct, vacuolar H^+-ATPases are localized at the luminal side of type-A intercalated cells and basolateral side of non-type Aintercalated cells. The V_1 domain contains 8 subunits A-H including the tissue-specific subunit isoforms B1 and B2. The B1 isoform is highly enriched in intercalated cells of kidney and its genetic mutation or deletion cause a form of distal renal tubular acidosis (18-19). The V_0 domain contains 6 different subunits, a, d, c, c', c'', and e including also the a1, a2, a3 and a4 isoforms. Also, the a4 isoform is highly expressed in kidney (20-21) and mutations in human and its deletion in mice are associated with renal tubular acidosis (22-24).

Secretion of NH_3 and protons by RhCG and vacuolar H^+-ATPases may be coordinated since protonation of NH_3 and subsequent trapping of NH_4^+ are critical for the efficient excretion of NH_4^+. The partial overlap of expression in type-A intercalated cells may allow even for a direct functional coupling or interaction. We have recently shown in two differently generated mouse models lacking Rhcg that urinary pH is more alkaline during stimulation of urinary acidification and NH_4^+ excretion. Since *Rhcg*$^{-/-}$ mice have highly reduced NH_3 secretion, the lack of NH_3 buffering capacity would be expected to result in a rather more acidic urinary pH, as shown in another mouse model with intact Rhcg-mediated NH_3 secretion but reduced medullary NH_4^+ accumulation (25). Thus, we hypothesized that the absence of Rhcg may reduce proton secretion by H^+-ATPases.

Here we demonstrate that the lack of Rhcg reduces H^+-ATPAse activity in microperfused collecting ducts. The absence of Rhcg did not alter H^+-ATPase localization. Overexpression of Rhcg in HEK293 cells stimulated H^+-ATPAse activity and increased expression of the B1 subunit. The H^+-ATPase inhibitor concanamycin reduced both H^+-ATPase activity and Rhcg-mediated NH_3 secretion. However, in mice lacking the B1 subunit (*Atp6v1b1*$^{-/-}$) H^+-ATPase activity was reduced without changing NH_3 permeability, suggesting that H^+-ATPase function does not directly affect Rhcg activity.

EXPERIMENTAL PROCEDURES

Animals - *Rhcg*$^{+/+}$ and $^{-/-}$mice were bred as described before (26). Also, *Atp6v1b1*$^{+/+}$ and $^{-/-}$ mice were bred as described before (27-28). Mice were genotyped by PCR directly on a 3 µl 25 mM NaOH tail digestion product.

Genomic DNA was amplified using primer pairs specific for *Rhcg* exon 1: forward (AGACCCCACAATGGAAAGCTATAA)and wildtype reverse (CAACCAGAACTCCCCAGTGTCAGA) and knock-out reverse(ATGGGCTGACCGCTTCCTCGTGC TTTAC) and *Atp6v1b1* primer pairs specific for the *Neo* cassette: forward (CACGACGAGATCCTCGCCGTC) and

reverse (GCGCAGCTAGTGCTCGACGTTG) and an *Atp6v1b1* 3′ flanking sequence not included within the targeting vector: forward (CTGGCACTGACCACGGCTGAG) and reverse (CCAGCCTGTGACTGAGCCCTG). The products were separated by electrophoresis in 1% agarose gel (*Rhcg* mutant product: 522 bp, wildtype product: 376 bp, *Atp6v1b1* mutant product: 300 bp, wildtype product: 200bp).
All animal experiments were performed in acid-loading conditions for which mice were given 0.2 M HCl added to powdered standard food for 2 days. All experiments were performed according to Swiss Animal Welfare laws and were approved by the local veterinary authority (Veterinäramt Zürich).

In vivo experiments - All experiments were performed using age- and sex-matched *Atp6v1b1* wildtype(*Atp6v1b1*$^{+/+}$) and *Atp6v1b1* knockout (*Atp6v1b1*$^{-/-}$) littermate mice (3-4 month-old), housed in metabolic cages (Techniplast, Switzerland). Mice were given deionized water ad libitum and were fed with a standard powdered laboratory chow (Kliba, Augst, Switzerland). Some mice were placed in metabolic cages and were allowed to adapt to metabolic cages for 3 days.A first retro-orbital blood sample was taken for blood gas analysis at baseline. Then two 24 hrs urine samples were collected under light mineral oil in the urine collector to determine daily urinary parameters. Mice were then allowed to recover for 2 weeks before given a HCl-containing diet (0.2 M HCl added to powdered standard food) in normal cages. Food, water intake, and urine excretion was monitored following the same procedures as under baseline conditions. Urine collections were performed on the first, second and fourth day of acid-loading. Retro-orbital blood samples were taken on the second and fourth day of the HCl diet.

Analytic procedures - Blood pH, pCO_2, and electrolytes were measured with a pH/blood-gas analyzer (ABL 77 Radiometer). Urinary pH was measured with a pH-meter (Metrohm AG, Canada) and creatinine by a modified kinetic Jaffé colorimetric method (29). Urinary NH_4^+ was measured with the Berthelot protocol (30).Urine Pi concentration was determined by the phosphomolybdate method (29).

Electron microscopy and immunogold labeling Mice were anesthetized with 2.5 % Isoflurane/pressurized air and perfused through the left ventricle with PBS (0.9% NaCl in 10 mM phosphate buffer, pH 7.4) followed by paraformaldehyde-lysine-periodate fixative (PLP: 4% paraformaldehyde, 75 mM lysine HCl, 10 mM sodium periodate, and 0.15 M sucrose in 37.5 mM sodium phosphate)(31). After 5 minutes the kidneys were removed and postfixed for an additional hour on ice in the same fixative solution. Following fixation, the kidneys were stored at 4°C in PBS.
For immunogold staining, small pieces of *Rhcg*$^{+/+}$ and $^{-/-}$ kidneys were dehydrated through a graded series of ethanol to 100% ethanol and then embedded in LR White resin (Electron Microscopy Sciences, Fort Washington, PA, USA). Thin sections were incubated on drops of primary anti-V-ATPase (A-subunit, 1:200) antibody for 2 h. After rinsing with PBS, the grids were incubated on drops of goat anti-rabbit IgG coupled to 15nm gold particles (Ted Pella, Redding, CA, USA) for 1 h. Following several rinses with distilled water, the grids were stained with 2% uranyl acetate for 10 min, rinsed in distilled water, and dried. Sections were examined in a JEM-1011 transmission electron microscope (JEOL Ltd, Tokyo, Japan).

Immunoblotting - Crude total membranes were obtained from *Rhcg*$^{+/+}$ and $^{-/-}$ mouse renal medulla homogenized in 250 mM sucrose, 10 mM Tris-HCl, pH 7.5, and in the presence of protease inhibitors. Fourty micrograms of crude membrane proteins were solubilized in loading buffer containing 10% DTT and separated on 8 to 10% polyacrylamide gels. For immunoblotting, proteins were transferred electrophoretically to polyvinylidene fluoride membranes (Immobilon-P, Millipore Corp., Bedford, MA, USA). After blocking with 5 % milk powder in Tris-buffered saline/0.1% Tween-20 for 60 min, blots were incubated with primary antibodies: rabbit anti-mouse ATP6V1B1 (B1) (raised against the sequence CAQQDPASDTAL, Pineda Berlin, 1 :5,000), rabbit anti-ATP6V1B2 (B2) (raised against thesequence EFYPRDSAKH, Pineda Berlin, 1 :5,000), rabbit anti-ATP6V0a4 (32), 1 :5000, rabbit anti-ATP6V0a1 (a kind gift of Dr Xie, Dallas, TX, USA) (33), 1 :5000, and mouse anti-ATP6V1E2 (a kind gift of Dr. S. L Gluck, University of California, San Francisco, CA,

USA), 1 :5000, and mouse monoclonal anti-β-actin antibody (Sigma, St. Louis, MO; 1:10,000) overnight at 4°C. After washing and blocking with 5 % milk powder for 60 min, membranes were incubated for 2 h at room temperature with secondary goat anti-rabbit or donkey anti-mouse antibodies 1:5,000 linked to alkaline phosphatase (Promega, Madison, WI, USA). The protein signal was detected with the appropriate substrate (Millipore Corp, Bedford, MA, USA) using the las-4000 image analyzer system (Fujifilm Life Science USA). All images were analyzed using Advanced Image Data Analyzer AIDA (Raytest, Straubenhardt, Germany) to calculate the protein of interest/β-actin ratio.

Cell culture - HEK293 (human embryonic kidney) non transfected (HEK-WT) or stably transfected with human RhCG (HEK-RhCG) cell lines had beenpreviously generated (6) and grown at 37°C, 5% CO_2 in DMEM (Dulbecco's modified Eagle's medium)/Glutamax I (Invitrogen)supplemented with 10% (v/v) fetal bovine serum. Selection of HEK-RhCG cells was performed in culture medium supplemented with 0.3 mg/ml hygromycin (Invitrogen). Forall pH experiments, cells were passaged, disseminated onto coverslips and grown to sub-confluency for 48 hours. The final medium exchange was performed 24 hours before the experiments were started. Medium pH was maintained at pH 7.4.

RNA extraction and reversetranscription - Snap-frozen kidneys (five kidneys for each condition) or HEK-WT and HEK-RhCG cells (3 petri dishes of $5x10^6$ cells for each condition) were homogenized in RLT-Buffer (Qiagen, Basel, Switzerland) supplemented with β-mercaptoethanol to a final concentration of 1%. Total RNA was extracted from 200 µl aliquots of each homogenized sample using the RNeasy Mini Kit (Qiagen,Basel, Switzerland) according to the manufacturer's instructions. Quality and concentration of the isolated RNA preparations were analyzed on the ND-1000 spectrophotometer (Nano-Drop Technologies). Total RNA samples were stored at −80°C. Each RNA sample was diluted to 100 ng/µl and 3 µl used as a template for reverse transcription using the TaqMan Reverse Transcription Kit (Applied Biosystems, Forster City, CA, USA). For reverse transcription, 300 ng of RNA template were diluted in a 40-µl reaction mix that contained (final concentrations) RT buffer (1×), $MgCl_2$ (5.5 mM), random hexamers (2.5 µM), RNase inhibitor (0.4U/µl), the multiscribe reverse transcriptase enzyme (1.25U/µl), dNTP mix (500 µM each), and RNase-free water.

Reverse Transcription and semiquantitative real-time PCR -Semiquantitative real-time RT-qPCR was performed on the ABI PRISM 7700 Sequence Detection System (Applied Biosystems, Forster City,CA). Primers and probes were chosen using BLAST tool: Ensemble(http://www.ensembl.org/index.html) to result in amplicons no longer than 150 bp spanning intron-exon boundaries to exclude genomic DNA contamination. The specificity of all primers was first tested on mRNA derived from kidney and always resulted in a single product of the expected size (data not shown). Probes were labeled with the reporter dye FAM at the 5' end and the quencher dye TAMRA at the 3' end (Microsynth, Balgach, Switzerland). Primers and probes sequences are summarized in supplementary table 1.

Real-Time PCR reactions were performed using TaqMan Universal PCR Master Mix (Applied Biosystems, Forster City,CA). Briefly, 3 µl cDNA, 0.8 µl of each primer (25 µM), 0.4 µl labeled probe (5 µM), 5 µl RNAse-free water, and 10 µl TaqMan Universal PCR Master Mix reached 20 µl of final reaction volume. Reaction conditions were denaturation at 95°C for 10 min followed by 40 cycles of denaturation at 95°C for 15s and annealing/elongation at 60°C for 60s with auto ramp time. All reactions were run in triplicate. For analyzing the data, the threshold was set to 0.2 as this value had been determined to be in the linear range of the amplification curves for all mRNAs in all experimental runs. The expression of the genes of interest was calculated in relation to hypoxanthine guanine phosphoribosyl transferase (mouse HPRT or human HPRT). Relative expression ratios were calculated as $R = 2^{(Ct(HPRT) - Ct(test\ gene)}$, where Ct represents the cycle number at the threshold 0.02.

Intracellular pH (pH_i) measurements on HEK293 cells - For pH_i measurements, individual slides seeded with HEK-WT or HEK-RhCG cells were transferred into a

perfusion chamber (~ 3-5 ml/min flow rate) and mounted on an inverted microscope (Zeiss Axiovert 200, Carl Zeiss, Feldbach, Switzerland) equipped with a video imaging system (Visitron, Munich, Germany) for the duration of the experiment. The temperature of the chamber was maintained at 37°C by an electronic feedback circuit. The control bath solution was initially a HEPES-buffered Ringer solution (125 mM NaCl/ 5 mM KCl/ 1 mM $CaCl_2$/ 1.2 mM $MgSO_4$/ 2 mM NaH_2PO_4/ 32.2 mM HEPES/ 5 mM Glucose). Cells were loaded with the acetoxymethyl ester of the pH sensitive dye BCECF (10 µM, Invitrogen) for 15 min and washed to remove all non-deesterified dye. pH_i was measured by microfluorometry by exciting the BCECF dye with a spot of light alternately at 490 and 440 nm while monitoring the emission at 532 nm with a video-imaging system (34). H^+-ATPase activity was measured after induction of anintracellular acidification using the NH_4Cl (20 mM) prepulse technique (34). Bicarbonate-free solutions were used and Na^+ was replaced by N-methyl-D-glucamine (NMDG). Each experiment was calibrated for pH_i using the nigericin/high K^+ method (35) and the obtained ratios were converted to pH_i. Na^+-independent pH_i recovery rates in response to an acid load were calculated in HEK293 wildtype and HEK293 RhCG stably transfected cells. Data are shown as changes in pH_i (ΔpH_i) per minute.

Microperfusion of isolated cortical collecting ducts - Male *Rhcg*$^{+/+}$, *Rhcg*$^{-/-}$, *Atp6v1b1*$^{+/+}$, and *Atp6v1b1*$^{-/-}$ mice were given a HCl-containing diet (0.2 M HCl added to powdered standard food) in normal cages for 2 days. Mice were anesthetized with Xylazin/Ketamin i.p. Both kidneys were cooled *in situ* with control bath solution (see below) for 1 min and then removed and cut into thin coronal slices for tubule dissection. Cortical CDs (CCDs) were dissected from the cortex at 10°C in the control solution.

Intracellular pH_i measurement in microperfused cortical collecting ducts - The isolated tubule was transferred to the bath chamber on the stage of an inverted spinning-disc microscope (IX81, Olympus, Japan) in the control solution containing (in mM) 138 NaCl, 1.5 $CaCl_2$, 1.2 $MgSO_4$, 2 K_2HPO_4, 10 HEPES, 5.5 glucose, 5 alanine, pH 7.40) and then, was mounted on concentric pipettes and perfused *in vitro* with Na^+-free, ammonium-free solution where N-methyl-D-Glutamine$^+$ ($NMDG^+$) replaced Na^+. The average tubule length exposed to bath fluid was limited to 300 – 350 µm in order to prevent motion of the tubule. CCDs were loaded with 5 µM of the fluorescent probe BCECF (2',7'-bis(2-carboxyl)-5-(and-6)-carboxyfluorescein (Invitrogen, Switzerland) for ~20 min at 37°C in the control bath solution. The loading solution was then washed out by initiation of bath flow and the tubule was equilibrated with dye-free control bath solution for 5 min. Bath solution was delivered at a rate of 20 ml/min and warmed to 37°C by water jacket immediately upstream to the chamber. After this temperature equilibration in control solution, tubules were first transiently acidified by peritubular Na^+ removal (Na-free, ammonium-free solution) (10 min duration), replaced by $NMDG^+$ to avoid exit of NH_4^+ by basolateralNa^+-coupled transport. This maneuver was performed in the luminal absence of Na^+. During the fluorescence recording, perfusion solution was delivered to the perfusion pipette via a chamber under an inert gas (N_2) pressure (around 1 bar) connected through a manual 6-way valve. With this system, opening of the valve instantaneously activates flow of solutions. The majority of the fluid delivery to the pipette exits the rear of the pipette system through a drain port at 4 ml/min. This method results in a smooth and complete exchange of the luminal or the peritubular solution in less than 3 to 4 s (36). After the fluorescence signal stabilization, luminal medium was instantly (at the rate of 4 ml/min in the draining) replaced by a Na^+-free solution containing 20 mM NH_4Cl (and 118 mM NMDG-Cl) that elicited a rapid intracellular alkalinization, followed by a sharp acidification. The initial rate of intracellular alkalinization has been associated with the entry of NH_3 whereas the subsequent phase of intracellular acidification in the continued presence of extracellular NH_4Cl reflects mostly NH_4^+ entry (37). After the acidification reached a plateau, NH_4Cl was removed from the lumen causing a further acidification of cells and initiating H^+-excretion with a maximum rate. The measured light intensities were digitized with the CellM&CellR Imaging hardware system (Olympus, Japan) for further analysis as

previously described (11-12,38). For peritubular ammonium pulses, peritubular the peritubular solution was changed to a 6 mM NH_4Cl solution, pH 7.40 in the absence of sodium in bath and lumen.

Intrinsic buffering capacity determination - The intrinsic buffering capacity (ßi) of CCD cells was determined for the *Rhcg* strain, as previously reported (11,26,39), using a 40 mM NH_4Cl basolateral pulse to acidify the cells. To exclude HCO_3^-/CO_2 as a buffering component and block Na^+-dependent pH_i regulatory mechanisms, Na^+-free, HEPES-buffered solutions were used in perfusate and bath containing 1 mM amiloride and bath and perfusate also contained 100 µM Sch28080 and 200 nM Concanamycin A. Addition of 40 mM NH_4Cl to the bath induced an increase followed by a decrease in pH_i. Cellular buffering power (β_i) was measured in CCDs from *Rhcg*$^{+/+}$ and *Rhcg*$^{-/-}$ mice.

Statistics - Statistical comparisons were tested by unpaired t-test using Graphpad Prism (GraphPad Software). P values < 0.05 were considered as statistically significant.

RESULTS

Rhcg$^{-/-}$ *mice show a reduced capacity to excrete* H^+ *from kidney CCD cells* - We recently showed in *in vitro* microperfusion experiments that collecting duct cells from *Rhcg*$^{-/-}$ mice exhibited a reduced NH_3 transepithelial flux due to reduced apical and basolateral NH_3 transport (11-12). Here, using the same approach, we assessed H^+ transport activity in microperfused CCD from *Rhcg*$^{+/+}$ and *Rhcg*$^{-/-}$ mice challenged for 2 days with an HCl load in the food to maximize transport activities. Luminal NH_3/NH_4^+ prepulses were performed and H^+ transport activity was assessed from the pH_i recovery rates after maximal intracellular acidification after the removal of NH_4Cl from the lumen (32,40). The initial rate of alkalinisation reflects H^+ extrusion, mostly by H^+-ATPases (32) (Figure 1A). However, as the initial pH_i values were different in CCDs from *Rhcg*$^{-/-}$ and *Rhcg*$^{+/+}$ mice, we also measured intracellular buffering power and calculated H^+ fluxes (JH^+) across the membrane to directly compare transport rates. JH^+ was greatly reduced in CCDs from *Rhcg*$^{-/-}$ by 89% (32.6 ± 12.8 pmol/mm/min vs. 3.6 ± 0.6 pmol/mm/min, $p \leq 0.0001$) (Figure 1B). Thus, the more alkaline urine observed in *Rhcg*$^{-/-}$ during acid-loading results from impaired proton secretion along the collecting duct.

The absence of RhCG alters B1 and B2 H^+*-ATPase subunit expression* - Next, we investigated whether the reduced H^+ flux observed in microperfused CCDs from *Rhcg*$^{-/-}$ mice could be linked to altered expression of H^+-ATPase subunits. We measured mRNA and protein expression levels of various subunits of the H^+-ATPase. At the level of mRNA, we could not detect any variation of the intercalated cell-enriched B1 H^+-ATPase isoform (Figure 2A), and more ubiquitous B2 (Figure 2B) and a4 (Figure 2C) H^+-ATPase isoforms between *Rhcg*$^{+/+}$ and $^{-/-}$ mice. For protein detection, we isolatedmembrane fractions from medullary kidney tissue to enrich the fraction of H^+-ATPases originating from intercalated cells. The protein abundance of the ubiquitous E2 (Figure 3C) and a1 isoforms (Figure 3D) as well as the kidney-enriched a4 (Figure 3E) subunits of the H^+-ATPase was not different between the 2 genotypes. However, the amount of the intercalated cell-enriched B1 isoform (Figure 3A) was increased whereas the ubiquitious B2 isoform (Figure 3B) was decreased in membrane fractions from medullary kidney tissue of *Rhcg*$^{-/-}$ mice ($p \leq 0.01$).

The localization of H^+*-ATPases is not different in Rhcg*$^{-/-}$ *intercalated cells* - Reduced H^+-ATPase activity may result from altered subcellular localization of H^+-ATPases. Kidneys from *Rhcg*$^{+/+}$ and *Rhcg*$^{-/-}$ acid-loaded for 2 days were examined by electron microscopy and immunogold staining for the ubiquitious A subunit (Figure 4). The absence of Rhcg did not affect the immunoreactivity for the A subunit in type A intercalated cells of *Rhcg*$^{-/-}$ mice. H^+-ATPase staining was detected mostly in intercalated cells and was associated with the luminal membrane as well as with intracellular vesicles as described previously (16). Thus, absence of Rhcg is not associated with an obvious redistribution of H^+-ATPases in type A intercalated cells.

The overexpression of RhCG in HEK293 cells increases H^+ *excretion rates* - To test if the expression of RhCG was correlated with stimulation of H^+-ATPase activity, we used

HEK293 cells, which express H^+-ATPases and exhibit H^+-ATPase-mediated proton secretion across the membrane (41). Untransfected HEK293 cells and HEK293 cells stably transfected with human RhCG were used to measure H^+-ATPase activity. qRT-PCR confirmed high expression levels of RhCG in RhCG-transfected HEK293 cells as reported previously (Figure 5A) (5).

Following NH_4Cl prepulse acidification in a HCO_3^- and Na^+ free solution, we measured intracellullar pH recovery rates, similar to experiments in microperfused CCDs (Figure 5A). We have previously demonstrated that this pH_i recovery is mediated solely by H^+-ATPases and sensitive to the H^+-ATPase blocker bafilomycin (41). The initial intracellular pH of both groups of cells measured was in the same range (pH 7.16 ± 0.001 for untransfected HEK293 cells and 7.18 ± 0.002 for RhCG expressing RhCG cells), which allowed us to compare directly $\Delta pHi/\Delta t$.In HEK-RhCG cells, the rate of pH_i-recovery observed after NH_4Cl removal was 52 % higher than the one observed in wildtype HEK 0.020 ± 0.003 pH units/min vs. 0.042 ± 0.003 pH units/min ($p \leq 0.01$). This result suggests that the presence of RhCG can stimulate H^+ secretion and is in agreement with our data showing that H^+ secretion is impaired in collecting ducts from *Rhcg*$^{-/-}$ mice. Finally, we compared the expression levels of genes encoding different subunits of the vacuolar H^+-ATPase, *ATP6V1B1* (Figure 6A), *ATP6V1B2* (Figure 6B) and *ATP6V0A1* (Figure 6C), and found an exclusive increase in mRNA expression of *ATP6V1B1* in HEK-RhCG compared to HEK-WT cells (Figure 6A).

Concanamycin A inhibits H^+-ATPases activity and apical NH_3 permeability - To further examine the functional interaction between RhCG and H^+-ATPases, we used the H^+-ATPase inhibitor concanamycin (200 nM) in microperfused CCDs from wildtype mice receiving a NH_4Cl acid-load for 2 days. Concanamycin reduced pH_i recovery rates from 0.13 ± 0.02 pH units/min to 0.06 ± 0.01 pH units/min indicating that H^+-ATPases contribute to pH_i recovery as reported previously (28,32,42) (Figure 7A, control = 10, concanamycin n = 5). Concanamycin A also reduced apical NH_3 permeability from 2.48 ± 0.35 pH units/min to 0.41 ± 0.11 pHunits/min as measured from initial alkalinization rates (Figure 7B, control n = 10, concanamycin n= 5).

Lack of the Atp6v1b1 H^+-ATPase subunit reduces H^+-ATPase activity without effect on NH_3 permeability - The results from the concanamycin A experiment offered at least two different interpretations: inhibition of H^+-ATPase activity reduces Rhcg-mediated NH_3 permeability or concanamycin A acts independently on H^+-ATPase and Rhcg activities. In order to distinguish between these two possibilities, we used a genetic animal model with reduced H^+-ATPase activity, mice lacking the Atp6v1b1 (B1) subunit (19,28,43).As a consequence of their genetic impairment, *Atp6v1b11*$^{-/-}$mice receiving HCl acid-loading diet showed a more alkaline urinary pH compared to *Atp6v1b1*$^{+/+}$ mice (Figure 8A and Supplementary table 1) as described previously (19). Urinary NH_4^+ excretion was comparable between both genotypes before and during acute HCl treatment. However, after 4 days of the diet, *Atp6v1b1*$^{-/-}$ presented a 23% reduction of NH_4^+ excretion (Figure 8B). To assess whether collecting ducts from *Atp6v1b11*$^{-/-}$mice had altered NH_3 permeability, we performed microperfusion studies on isolated CCDs from *Atp6v1b1*$^{+/+}$ and$^{-/-}$mice receiving 2 days of HCl diet. We confirmed the expected reduction in H^+ secretion in *Atp6v1b1*$^{-/-}$mice when NH_4Cl was applied from the tubular lumen (Figure 8C) but were not able to detect any differences in NH_3 membrane permeability across the apical (Figure 8D) or basolateral (Figure 8E) membranes. Thus, in a genetic model, reduced H^+-ATPase activity is not paralleled by reduced apical or basolateral NH_3 permeability.

DISCUSSION

Intercalated cells in the renal collecting duct secrete $NH_3$and protons. NH_3 secretion occurs also from neighbouring segment-specific cells of the distal convoluted tubule and connecting tubule expressing the water channel AQP2, the epithelial channel ENaC, and Rhcg (7,9,11). Parallel NH_3 and proton secretion are intricately linked: high luminal proton concentrations are required to protonate NH_3 trapping NH_4^+ in urine, whereas buffering of protons by titratable acids such as phosphate or creatinine together with protonation of NH_3 ensures that urinary pH

does not become too acidic, generating an unfavorable pH gradient for further H^+-ATPase activity.

Mice with a total deficiency of Rhcg excrete more alkaline urine during acid-loading (11-12). This observation suggested a defect in urinary acidification since reduced secretion of ammonia due to the deletion of Rhcg should result in rather more acidic urine. Our results demonstrate that Rhcg stimulates H^+-ATPase function and that in its absence H^+-ATPase activity is reduced explaining the more alkaline urine and possibly contributing to the more pronounced metabolic acidosis in *Rhcg* deficient mice. Here we demonstrate that i) in microperfused collecting ducts from *Rhcg*$^{-/-}$ mice, H^+-ATPase activity is greatly reduced, ii) the deletion of Rhcg does not alter mRNA abundance of major H^+-ATPase subunits, iii) loss of Rhcg does not affect the apparent subcellular localization of H^+-ATPases in intercalated cells, iv) absence of Rhcg alters the relative abundance of the B1 and B2 H^+-ATPase isoforms with B1 being upregulated, v) overexpression of Rhcg in renal HEK293 cells is sufficient to stimulate H^+-ATPase activity paralleled by increased B1 mRNA abundance, vi) pharmacological inhibition of H^+-ATPases with concanamycin blocks H^+-ATPase and Rhcg transport activity, and vii) that genetic reduction of H^+-ATPase activity in mice lacking the B1 H^+-ATPase subunit reduces only H^+-ATPase activity but not Rhcg mediated NH_3 permeability.

Rhcg deficient mice have reduced H^+-ATPase activity as evident from more alkaline urine and in vitro microperfusion experiments demonstrating lower H^+-fluxes. Similar findings have been made in *Atp6v1b1*$^{-/-}$ and *Atp6voa4*$^{-/-}$ mouse models with genetic deletion of single subunits of the H^+-ATPase in intercalated cells (19,23,28,43). H^+-ATPase activity is regulated by different mechanisms including phosphorylation of the A subunit, trafficking of pumps into and out of the membrane, and possibly changes in composition of distinct subunit isoforms and their abundance (15-16,44-46). However, subcellular localization of H^+-ATPase was not different between genotypes. Moreover, the abundance of several H^+-ATPase subunits was similar for both groups of animals. Only the abundance of the intercalated cell enriched B1 isoform was higher and the expression of the B2 isoform reduced. This is in contrast to mice lacking the B1 isoform (*Atp6v1b1*$^{-/-}$), which have an upregulation of the B2 isoform but a decrease of several H^+-ATPase subunits in intercalated cells. The B1 and B2 isoform may serve different roles and B2 cannot replace B1 as evident from lack of stimulation of H^+-ATPases containing only the B2 isoform (28,43). The upregulation of B1 protein abundance may thus rather reflect an attempt to compensate for the loss of H^+-ATPase function in *Rhcg*$^{-/-}$ than cause reduced H^+-ATPase activity.

In order to gain more insights into the effect of Rhcg on H^+-ATPase function, we used the renal HEK293 cell line stably transfected with human RhCG (5). We have previously shown that these cells express a functional H^+-ATPase at the plasma membrane and that H^+-extrusion in the absence of extracellular sodium and bicarbonate is only mediated by H^+-ATPases (41). *In vitro*overexpression of RhCG demonstrated higher H^+ extrusion. Furthermore, several H^+-ATPase subunits were detected at mRNA level in untransfected and RhCG expressing HEK293 cells and only *ATP6V1B1* mRNA was increased. Thus, overexpression of RhCG stimulates membrane-associated H^+-ATPase activity in a heterologous system similar to the *in vivo* situation.

To study reciprocally the effect of H^+-ATPases on RhCG activity in the collecting duct, we employed a pharmacological and genetic approach. In a first series of experiments, we used concanamycin A, an inhibitor of H^+-ATPase activity (47-48). Concanamycin A reduced pH_i-recovery rates in intercalated cells in microperfused collecting ducts by more than 50 % in agreement with previous studies (28,49). However, apical NH_3 permeability mediated by Rhcg was also drastically reduced. This reduction was not due to altered pH gradients that could potentially affect the rate of deprotonation of NH_4^+ to NH_3 and the driving force of NH_3 transport through Rhcg. Thus, these results suggested that either H^+-ATPase activity modulates Rhcg activity or that concanamycin A acts directly or indirectly on Rhcg independent from its inhibitory effect on H^+-ATPases. Therefore, we used in a second

series of experiments, mice lacking the B1 isoform of H^+-ATPases (*Atp6v1b1*$^{-/-}$) that is specifically enriched in intercalated cells. H^+-ATPase function in the intercalated cells from these mice is reduced but not totally abolished (19,28,50). Microperfusion of collecting ducts confirmed reduced H^+-ATPase activity but found not evidence for altered apical or basolateral Rhcg mediated NH_3 permeability. In agreement with these data, we found also only a minor reduction in urinary ammonium excretion in acid-loaded *Atp6v1b1*$^{-/-}$ mice after 4 days. This reduction may be explained by the reduced driving force for NH_3 secretion and decreased trapping of NH_4^+ due to the less acidic urine. Thus, the effect of concanamycin A on NH_3 permeability is most likely the result of unspecific inhibition of Rhcg activity. Concanamycin A is a highly lipophilic substance accumulating in the plasma membrane and may thereby interact with Rhcg independent from its effects on H^+-ATPases. Moreover, our results provide no evidence for modulation of Rhcg activity by H^+-ATPases beyond the generation of pH gradients favorable for NH_3 transport.

In summary, we show that Rhcg functionally interacts withthe activity of the vacuolar H^+-ATPase and enables intercalated cell to enhance the secretion of protons.Absence of Rhcg reduces H^+-ATPase activity and fully explains the excretion of more alkaline urine by *Rhcg*$^{-/-}$ even in the absence of ammonium, a major urinary buffer.

REFERENCES

1. Weiner, I. D., and Hamm, L. L. (2007) *Annu Rev Physiol***69**, 317-340
2. Wagner, C. A., Devuyst, O., Bourgeois, S., and Mohebbi, N. (2009) *Pflugers Arch***458**, 137-156
3. Wagner, C. A., Devuyst, O., Belge, H., Bourgeois, S., and Houillier, P. (2011) *Kidney Int***79**, 154-161
4. Gruswitz, F., Chaudhary, S., Ho, J. D., Schlessinger, A., Pezeshki, B., Ho, C. M., Sali, A., Westhoff, C. M., and Stroud, R. M. (2010) *Proc Natl Acad Sci U S A***107**, 9638-9643
5. Mouro-Chanteloup, I., Cochet, S., Chami, M., Genetet, S., Zidi-Yahiaoui, N., Engel, A., Colin, Y., Bertrand, O., and Ripoche, P. (2010) *PLoS One***5**, e8921
6. Zidi-Yahiaoui N, C. I., Genetet S, Le Van Kim C,, and Cartron JP, C. Y., Ripoche P, Mouro-Chanteloup I. (2009) *Am J Physiol Cell Physiol***297**, 537-547
7. Han, K. H., Croker, B. P., Clapp, W. L., Werner, D., Sahni, M., Kim, J., Kim, H. Y., Handlogten, M. E., and Weiner, I. D. (2006) *J Am Soc Nephrol***17**, 2670-2679
8. Kim, H. Y., Verlander, J. W., Bishop, J. M., Cain, B. D., Han, K. H., Igarashi, P., Lee, H. W., Handlogten, M. E., and Weiner, I. D. (2009) *Am J Physiol Renal Physiol*
9. Verlander, J. W., Miller, R. T., Frank, A. E., Royaux, I. E., Kim, Y. H., and Weiner, I. D. (2003) *Am J Physiol Renal Physiol***284**, F323-337
10. Eladari, D., Cheval, L, Quentin, F, Bertrand, O, Mouro, I, Cherif-Zahar, B, Cartron, J P, Paillard, M, Doucet, A, Chambrey, R. (2002) *J Am Soc Nephrol***13**, 1999-2008
11. Bourgeois, S., Bounoure, L., Christensen, E. I., Ramakrishnan, S. K., Houillier, P., Devuyst, O., and Wagner, C. A. (2013) *J Biol Chem***288**, 5518-5529
12. Biver, S., Belge, H., Bourgeois, S., Van Vooren, P., Nowik, M., Scohy, S., Houillier, P., Szpirer, J., Szpirer, C., Wagner, C. A., Devuyst, O., and Marini, A. M. (2008) *Nature***456**, 339-343
13. Lee, H. W., Verlander, J. W., Bishop, J. M., Nelson, R. D., Handlogten, M. E., and Weiner, I. D. (2010) *Am J Physiol Renal Physiol***299**, F369-379
14. Lee, H. W., Verlander, J. W., Bishop, J. M., Igarashi, P., Handlogten, M. E., and Weiner, I. D. (2009) *Am J Physiol Renal Physiol***296**, F1364-1375
15. Wagner, C. A., Finberg, K E, Breton, S, Marshansky, V, Brown, D, Geibel, J P. (2004) *Physiol Rev***84**, 1263-1314
16. Breton, S., and Brown, D. (2013) *Physiology (Bethesda)***28**, 318-329
17. Forgac, M. (2007) *Nat Rev Mol Cell Biol***8**, 917-929
18. Karet, F. E., Finberg, K E, Nelson, R D, Nayir, A, Mocan, H, Sanjad, S A, Rodriguez-Soriano, J, Santos, F, Cremers, C W, Di Pietro, A, Hoffbrand, B I, Winiarski, J, Bakkaloglu, A, Ozen, S, Dusunsel, R, Goodyer, P, Hulton, S A, Wu, D K, Skvorak, A B, Morton, C C, Cunningham, M J, Jha, V, Lifton, R P. (1999) *Nat Genet***21**, 84-90
19. Finberg, K. E., Wagner, C A, Bailey, M A, Paunescu, T G, Breton, S, Brown, D, Giebisch, G, Geibel, J P, Lifton, R P. (2005) *Proc Nat Acad Sci USA***102**, 13616-13621
20. Schulz, N., Dave, M. H., Stehberger, P. A., Chau, T., and Wagner, C. A. (2007) *Cell Physiol Biochem***20**, 109-120
21. Stehberger, P., Schulz, N, Finberg, K E, Karet, F E, Giebisch, G, Lifton, R P, Geibel, J P, Wagner, C A. (2003) *J Am Soc Nephrol***14**, 3027-3038
22. Smith, A. N., Skaug, J, Choate, K A, Nayir, A, Bakkaloglu, A, Ozen, S, Hulton, S A, Sanjad, S A, Al-Sabban, E A, Lifton, R P, Scherer, S W, Karet, F E. (2000) *Nat Genet***26**, 71-75
23. Hennings, J. C., Picard, N., Huebner, A. K., Stauber, T., Maier, H., Brown, D., Jentsch, T. J., Vargas-Poussou, R., Eladari, D., and Hubner, C. A. (2012) *EMBO Mol Med***4**, 1057-1071
24. Norgett, E. E., Golder, Z. J., Lorente-Canovas, B., Ingham, N., Steel, K. P., and Karet Frankl, F. E. (2012) *Proc Natl Acad Sci U S A***109**, 13775-13780

25. Stettner, P., Bourgeois, S., Marsching, C., Traykova-Brauch, M., Porubsky, S., Nordstrom, V., Hopf, C., Koesters, R., Sandhoff, R., Wiegandt, H., Wagner, C. A., Grone, H. J., and Jennemann, R. (2013) *Proc Natl Acad Sci U S A***110**, 9998-10003
26. Bourgeois, S., Bounoure, L., Christensen, E.I., Ramakrishnan, S.K., Houillier, P., Devuyst, O., Wagner, C.A. (2013) *The Journal of biological chemistry***288**, 5518-5529
27. Finberg, K. E., Wagner, C.A., Bailey, M.A., Paunescu, T.G., Breton, S., Brown, D., Geibisch, G., Geibel, J.P., Lifton, R.P. (2005) *PNAS***102**, 13616-13621
28. Rothenberger, F., Velic, A., Stehberger, P. A., Kovacikova, J., and Wagner, C. A. (2007) *J Am Soc Nephrol***18**, 2085-2093
29. Seaton, B., and Ali, A. (1984) *Med Lab Sci***41**, 327-336
30. Berthelot, M. (1859) *Rep Chim App* **1**, 284
31. McLean, I. W., Nakane, P K. (1974) *J Histochem Cytochem***22**, 1077-1083
32. Wagner, C. A., Lukewille, U, Valles, P, Breton, S, Brown, D, Giebisch, G H, Geibel, J P. (2003) *Pflugers Arch***446**, 623-632
33. Peng, S. B., Li, X, Crider, B P, Zhou, Z, Andersen, P, Tsai, S J, Xie, X S, Stone, D K. (1999) *J Biol Chem***274**, 2549-2555
34. Mohebbi, N., Benabbas, C., Vidal, S., Daryadel, A., Bourgeois, S., Velic, A., Ludwig, M. G., Seuwen, K., and Wagner, C. A. (2012) *Cell Physiol Biochem***29**, 313-324
35. Thomas, J. A., Buchsbaum, R N, Zimniak, A, Racker, E. (1979) *Biochemistry***18**, 2210-2218
36. Watts, B. A., 3rd, and Good, D. W. (1994) *J Biol Chem***269**, 20250-20255
37. Roos, A., and Boron, W. F. (1981) *Physiol Rev***61**, 296-434
38. Chambrey, R., Goossens, D., Bourgeois, S., Picard, N., Bloch-Faure, M., Leviel, F., Geoffroy, V., Cambillau, M., Colin, Y., Paillard, M., Houillier, P., Cartron, J. P., and Eladari, D. (2005) *American journal of physiology. Renal physiology***289**, F1281-1290
39. Milton, A. E., Weiner, I.D. . (1998) *Am J Physiol* **274**, 1086-1094
40. Roos, A., Boron, W F. (1981) *Physiol Rev***61**, 296-434
41. Lang, K., Wagner, C A, Haddad, G, Burnekova, O, Geibel, J. (2003) *Cell Physiol Biochem***13**, 257-262
42. Winter, C., Schulz, N, Giebisch, G, Geibel, J P, Wagner, C A. (2004) *Proc Nat Acad Sci USA***101**, 2636-2641
43. Paunescu, T. G., Russo, L. M., Da Silva, N., Kovacikova, J., Mohebbi, N., Van Hoek, A. N., McKee, M., Wagner, C. A., Breton, S., and Brown, D. (2007) *Am J Physiol Renal Physiol***293**, F1915-1926
44. Nishi, T., Forgac, M. (2002) *Nat Rev Mol Cell Biol***3**, 94-103
45. Alzamora, R., Thali, R. F., Gong, F., Smolak, C., Li, H., Baty, C. J., Bertrand, C. A., Auchli, Y., Brunisholz, R. A., Neumann, D., Hallows, K. R., and Pastor-Soler, N. M. (2010) *J Biol Chem***285**, 24676-24685
46. Paunescu, T. G., Ljubojevic, M., Russo, L. M., Winter, C., McLaughlin, M. M., Wagner, C. A., Breton, S., and Brown, D. (2010) *Am J Physiol Renal Physiol***298**, F643-654
47. Dröse, S., Bindseil, K U, Bowman, E J, Siebers, A, Zeeck, A, Altendorf, K. (1993) *Biochemistry***32**, 3902-3906
48. Dröse, S., Altendorf, K. (1997) *J Exp Biol***200**, 1-8
49. Wagner, C. A., Mohebbi, N., Uhlig, U., Giebisch, G. H., Breton, S., Brown, D., and Geibel, J. P. (2011) *Cell Physiol Biochem***28**, 513-520
50. Gueutin, V., Vallet, M., Jayat, M., Peti-Peterdi, J., Corniere, N., Leviel, F., Sohet, F., Wagner, C. A., Eladari, D., and Chambrey, R. (2013) *J Clin Invest***123**, 4219-4231

Acknowledgements - This study was supported by a grant from the Swiss National Science Foundation to C.A. Wagner (31003A_138143). The use of the Zurich Integrative Rodent Physiology (ZIRP) Core Facility is gratefully acknowledged.

Disclosures - None.

FIGURE LEGENDS

FIGURE 1.*H^+-secretion from cortical collecting duct cells of Rhcg$^{-/-}$ mice is reduced*. Cortical collecting duct were isolated from kidneys of *Rhcg*$^{+/+}$ and *Rhcg*$^{-/-}$ mice after 2 days of HCl-loading, microperfused in vitro, and intracellular pH (pH_i) monitored in cortical collecting duct with BCECF-AM. NH_4Cl (20 mM) was applied from the luminal perfusate. (A) Original pH_i tracing from a CCD exposed to a luminal NH_4Cl pulse. The arrow indicates the rate of pH_i changing measured and calculated. Exposure to an NH_4Cl pulse caused a large acidification of the cells followed by pH_i recovery. The initial slope ($\Delta pHi/\Delta t$) of the alkalinization phase was measured and H^+ fluxes were calculated based on intracellular buffering power (see methods section). (B) Bar graph summarizing H^+ fluxes after removal of the luminal NH_4Cl pulse (n = 8-12 tubules/genotype).

FIGURE 2.*mRNA expression of the B1, B2 and a4 subunits of the H^+-ATPase in Rhcg$^{+/+}$ and Rhcg$^{-/-}$ mice is unchanged.* RT-qPCR was performed in total kidney to determine relative mRNA levels of several H^+-ATPase relevant for intercalated cell H^+-ATPase function. None of the mRNA values measured of the B1 (A), B2 (B) and a4 (C) isoforms was different between the 2 genotypes. Values are mean ± SEM (n= 5 mice/genotype).

FIGURE 3.*Increased B1 and decreased B2 H^+-ATPases protein levels in Rhcg$^{-/-}$ mice.* Protein expression of the B1 (A), B2 (B), E2 (C), a1 (D) and a4 (E) subunits of the H^+-ATPase was assessed by Western blotting in the medullary kidney tissue. In *Rhcg*$^{-/-}$ mice, B1-H^+-ATPase protein abundance was upregulated (A), while B2 H^+-ATPase was downregulated (B). Protein expression of the a1, a4, and E subunits remained unchanged (C-E). Values are mean ± SEM (n= 5 mice/genotype), ***$p \leq 0.001$.

FIGURE 4.*Subcellular localization of the vacuolar H^+-ATPase in type A intercalated cells of kidney collecting ducts from Rhcg$^{+/+}$ and Rhcg$^{-/-}$ mice is similar.*
(A,B) Immunogold staining for the A subunit of the H^+-ATPase revealed a similar density of H^+-ATPases at the apical membrane and in apically localized vesicles of type A intercalated cells in *Rhcg*$^{+/+}$ (A) and *Rhcg*$^{-/-}$ (B) mice. Scale bars: 2µm. (A',B') Magnification of the respective area of the overview electron micrograph in A and B. Scale bars: 0.5 µm. The asterisk indicates the luminal side. A dashed line indicates the lateral cell borders.

FIGURE 5.*RhCG overexpression in renal HEK293 cells increases H^+ excretion*.
H^+-ATPase activity was measured in untransfected HEK293 cells and HEK293 cells stably transfected with human RhCG using the NH_4Cl (20 mM) prepulse after loading cells with BCECF. (A) Overexpression of RhCG was confirmed by RT-qPCR. (B) Original pH_i tracings from untransfected HEK293 (WT) and RhCG overexpressing HEK293 cells. Dashed lines indicate the slope measured to calculate pH_i changes over time.(C) Bar graph summarizes the H^+ extrusion rate of HEK-WT compared to HEK-RhCG after NH_4Cl pulse (n = 5 cells/plate, 3 dishes/condition). Data are mean ± SEM, **$p \leq 0.01$,

FIGURE 6.*ATP6V1B1 mRNA is increased in HEK293 cells overexpressing RhCG.*
mRNA expression of ATP6V1B1 (A), ATP6V1B2 (B) and ATP6V0A1 (C) were measured by RT-qPCR in untransfected HEK293 (HEK-WT) and HEK293 overexpressing RhCG (HEK-RhCG) cells. ATP6V1B1 mRNA was higher in HEK-RhCG cells versus HEK-WT. The mRNA abundance of the other H^+-ATPase subunits, ATP6V1B2 (B) and ATP6V0A1 (C), were unchanged. Values are mean ± SEM (n= 5 dishes/cell type), *$p \leq 0.05$

FIGURE 7. *Concanamycin A reduces H^+-ATPase activity and apical NH_3 permeability in CCDs from wildtype mice.* Cortical collecting duct were isolated from kidneys of wildtype mice after 2 days of NH_4Cl-loading and microperfused in vitro. Intracellular pH (pH_i) was monitored with BCECF-AM and cells were challenged with a luminal NH_4Cl (20 mM) prepulse in the presence or absence of 200 nM Concanamycin A in the lumen. (A)Bar

graphsummarizing the rate of realkalinization after NH_4Cl removing from the lumen corresponding to H^+ secretion.. (B)Bar graphsummarizing the rate of alkalinization after addition of NH_4Cl corresponding to NH_3entry into the cells. (controln = 10 tubules;concanamycin n = 5 tubules). *, $p<0.05$; C : control, ConA : Concanamycin A.

FIGURE 8.*Atp6v1b1$^{-/-}$ mice lacking the B1 H^+-ATPase subunit have decreased H^+-ATPase activity but preserved apical and basolateral NH_3 permeabilities.*
Widltype (*Atp6v1b1$^{+/+}$*) and *Atp6v1b1$^{-/-}$* mice were observed in metabolic cages and urinary pH (A) and urinary ammonium excretion normalized to creatinine (B) monitored during baseline and an acid-load (HCl) for 4 days (n = 7/genotype). Cortical collecting ducts from mice acid-loaded for 2 days were microperfused in vitro and H^+ secretion (C) and apical NH_3 permeability (D) measured after a luminal NH_4Cl prepulse (20 mM) (n = 10 tubules/genotype). (E) Similarly, basolateral NH_3 permeability assessed after an NH_4Cl prepulse from the bath (6 mM) was not different between genotypes (n = 6 tubules/genotype). *$p \leq 0.05$

SUPPLEMENTS

Supplementary table 1. Sequences of the primers and probes of the gene expressions evaluated by RT-qPCR

Supplementary table 2. Blood values in *Atp6v1b1$^{+/+}$* mice and *Atp6v1b1$^{-/-}$* mice under normal diet and HCl load for 4 days. Data are presented as mean ± SEM, n = 5-9 animals/ group, * $p<0.05$ vs baseline period in same genotype, $^{\#}$ $p<0.05$ vs C57BL6 mice during the same period.

Supplementary table 3. Weight, food intake and urinary values in *Atp6v1b1$^{+/+}$* mice and *Atp6v1b1$^{-/-}$* mice under normal diet and during an HCl load for 4 days. Data are presented as mean ± SEM, n = 5-9 animals/ group, * $p<0.05$ vs baseline period in same genotype, $^{\#}$ $p<0.05$ vs C57BL6 mice during the same period.

Figure 1

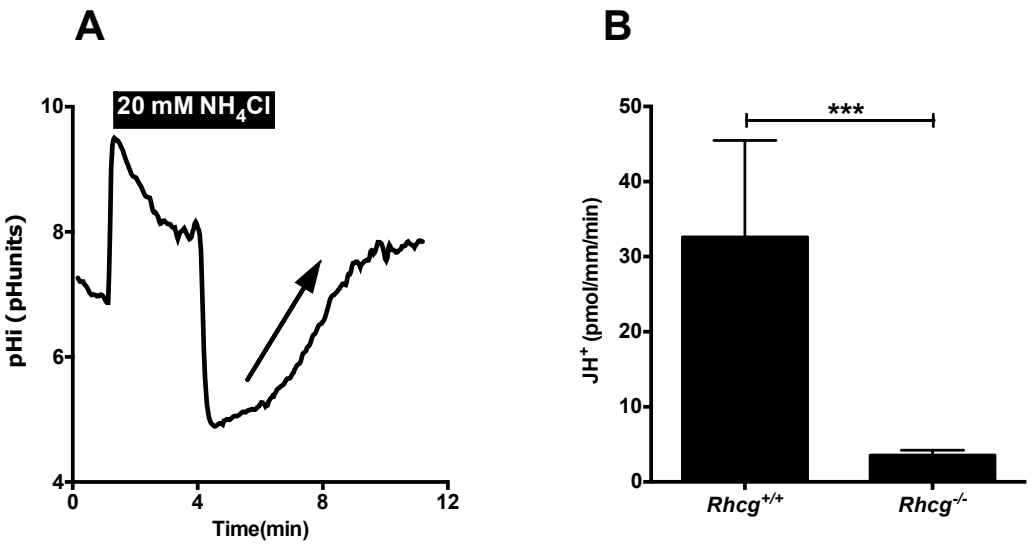
A
20 mM NH4Cl
pHi (pHunits)
10
8
6
4
0
4
8
12
Time(min)
B
***
JH+ (pmol/mm/min)
50
40
30
20
10
0
Rhcg+/+
Rhcg-/-

Figure 2

A

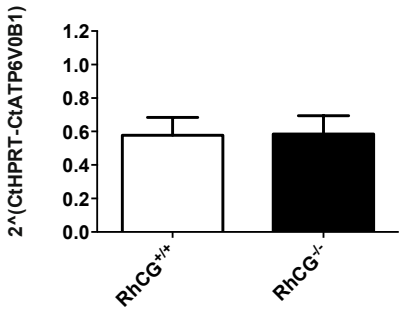
2^(CtHPRT-CtATP6V0B1)
1.2
1.0
0.8
0.6
0.4
0.2
0.0
RhCG+/+
RhCG-/-

B

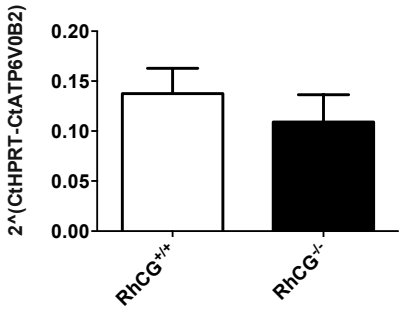
2^(CtHPRT-CtATP6V0B2)
0.20
0.15
0.10
0.05
0.00
RhCG+/+
RhCG-/-

C

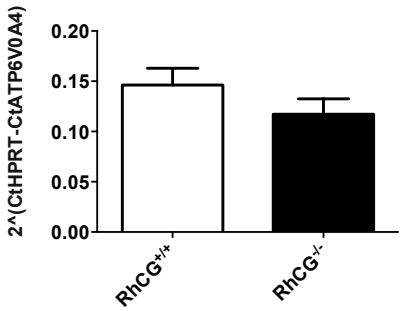
2^(CtHPRT-CtATP6V0A4)
0.20
0.15
0.10
0.05
0.00
RhCG+/+
RhCG-/-

Figure 3

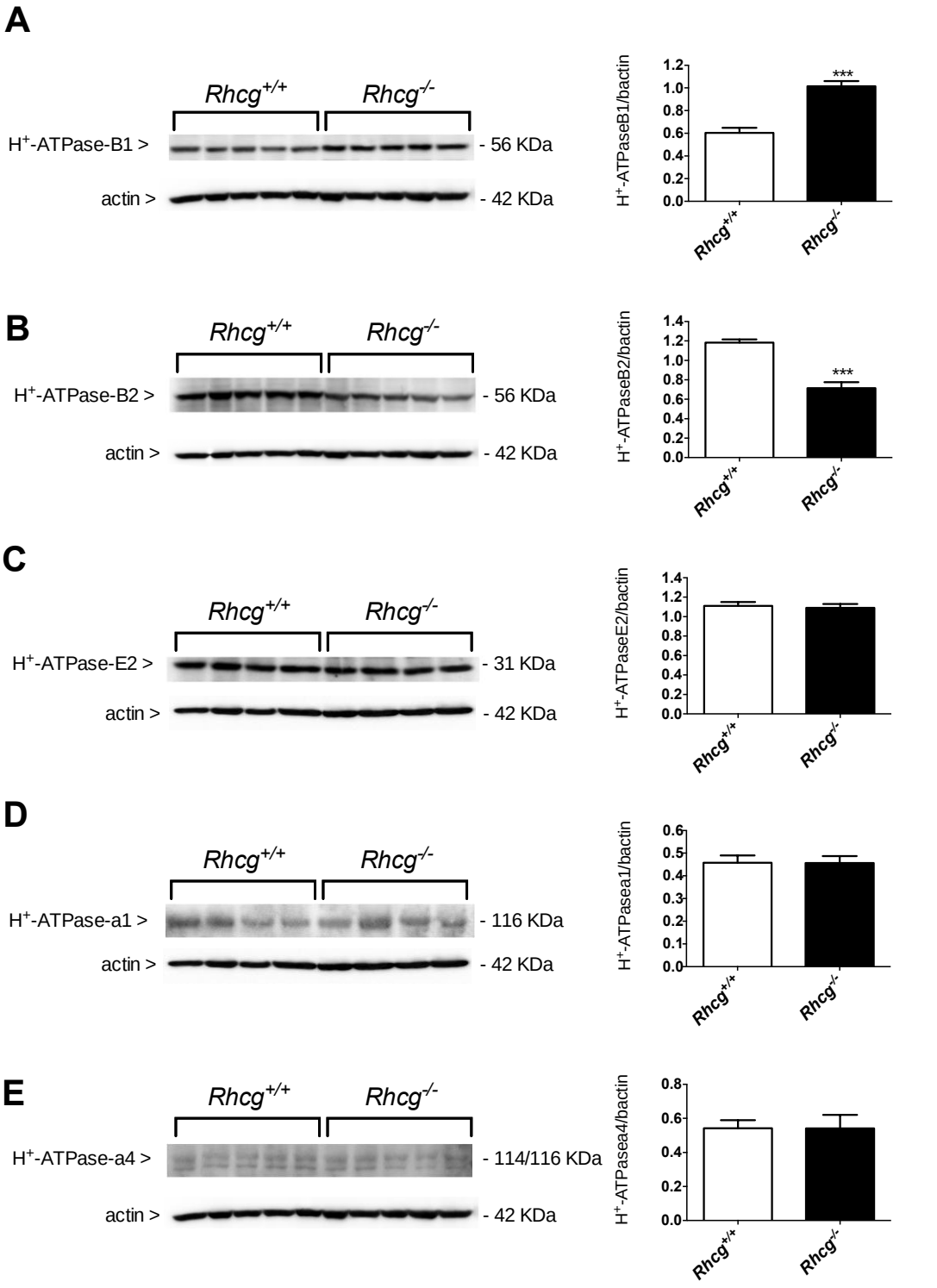
A
Rhcg+/+
Rhcg-/-
H+-ATPase-B1 >
- 56 KDa
actin >
- 42 KDa
H+-ATPaseB1/bactin
***
B
H+-ATPase-B2 >
- 56 KDa
actin >
- 42 KDa
H+-ATPaseB2/bactin
***
C
H+-ATPase-E2 >
- 31 KDa
actin >
- 42 KDa
H+-ATPaseE2/bactin
D
H+-ATPase-a1 >
- 116 KDa
actin >
- 42 KDa
H+-ATPasea1/bactin
E
H+-ATPase-a4 >
- 114/116 KDa
actin >
- 42 KDa
H+-ATPasea4/bactin

Figure 4

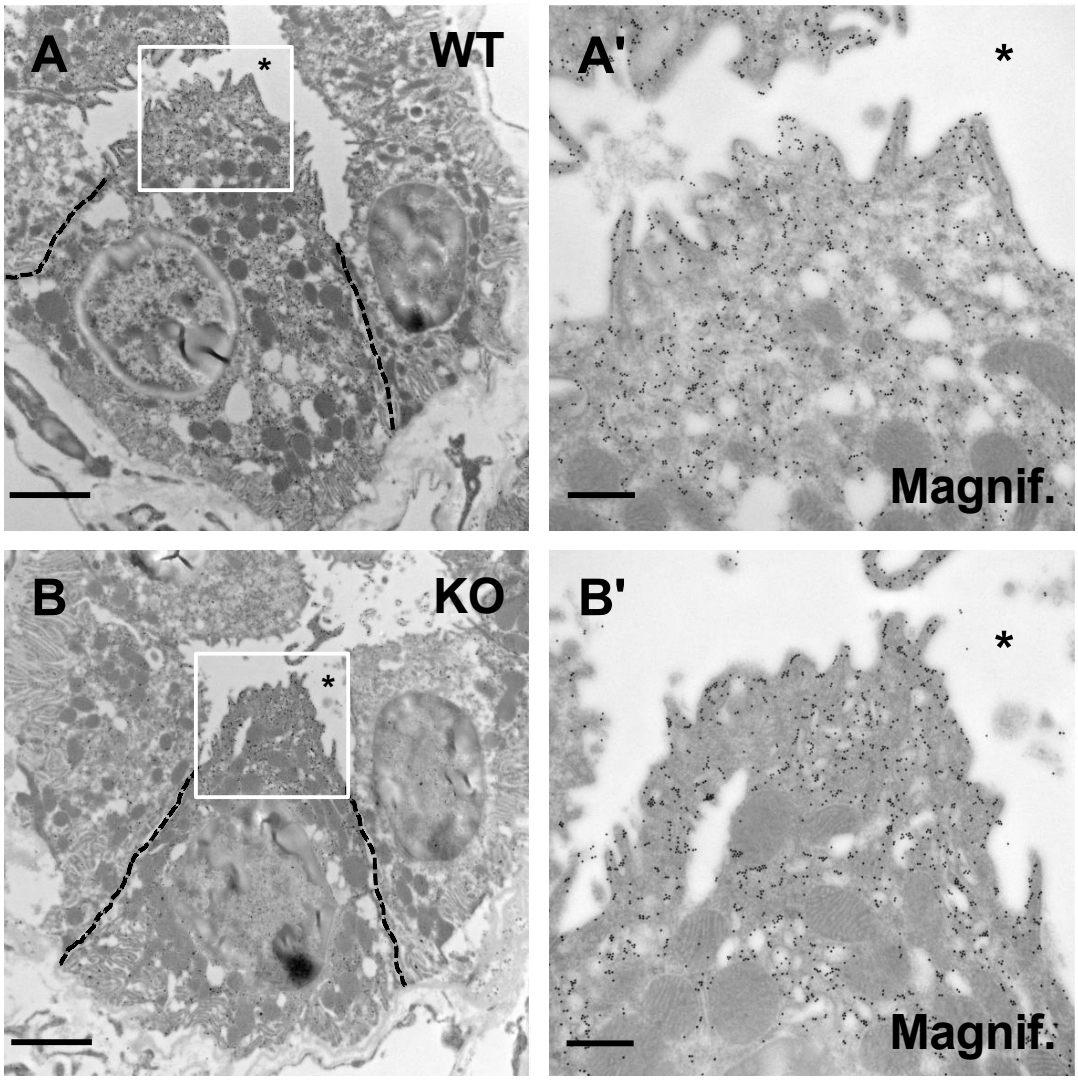

Figure 5

A

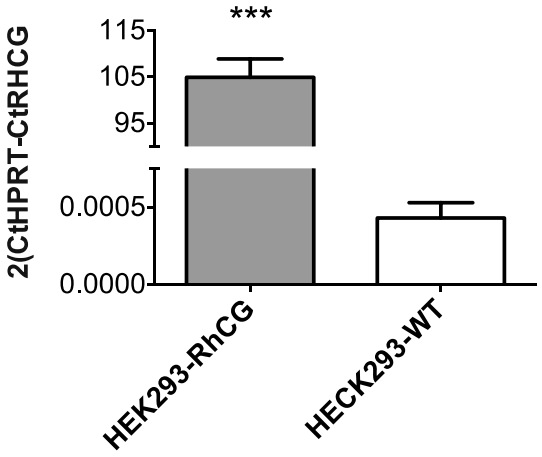
***
115
105
95
0.0005
0.0000
2(CtHPRT-CtRHCG
HEK293-RhCG
HECK293-WT

B

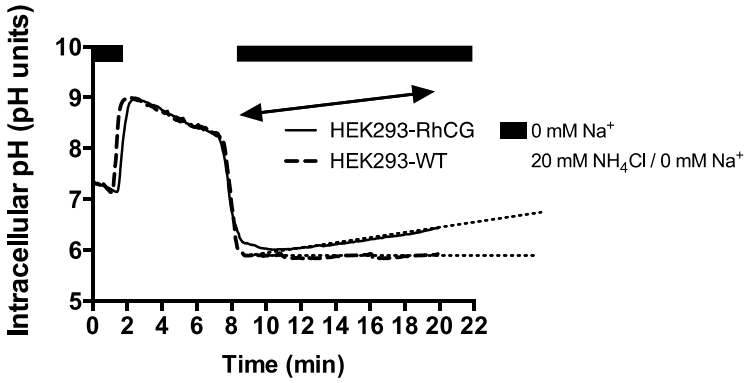
Intracellular pH (pH units)
10
9
8
7
6
5
0 2 4 6 8 10 12 14 16 18 20 22
Time (min)
HEK293-RhCG
HEK293-WT
0 mM Na+
20 mM NH4Cl / 0 mM Na+

C

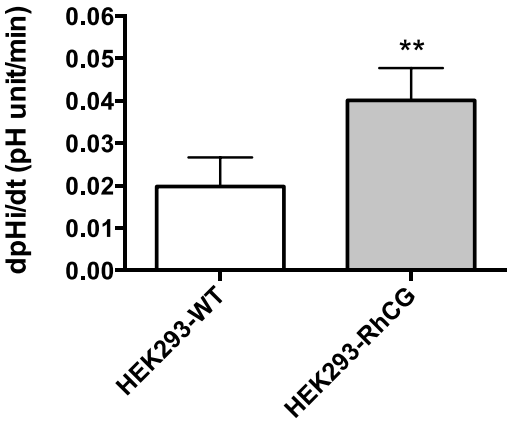
dpHi/dt (pH unit/min)
0.06
0.05
0.04
0.03
0.02
0.01
0.00
**
HEK293-WT
HEK293-RhCG

Figure 6

A

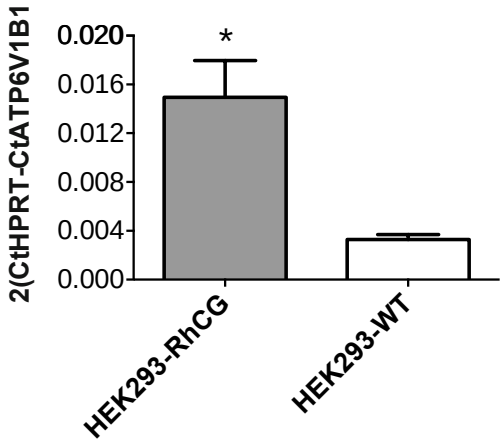
2(CtHPRT-CtATP6V1B1
0.020
0.016
0.012
0.008
0.004
0.000
*
HEK293-RhCG
HEK293-WT

B

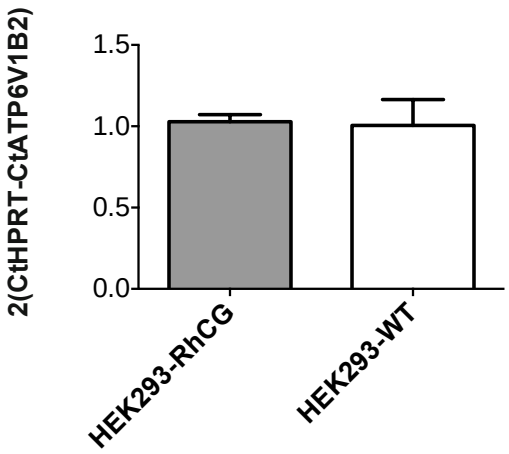
2(CtHPRT-CtATP6V1B2)
1.5
1.0
0.5
0.0
HEK293-RhCG
HEK293-WT

C

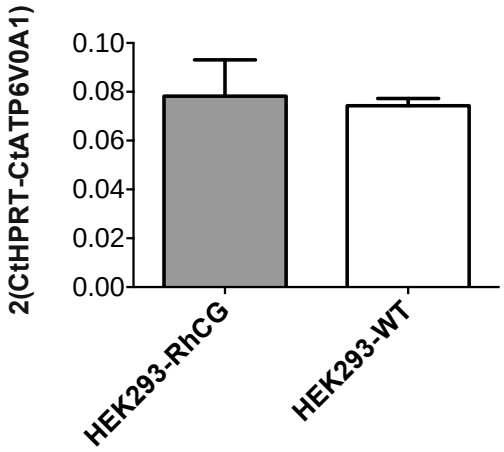
2(CtHPRT-CtATP6V0A1)
0.10
0.08
0.06
0.04
0.02
0.00
HEK293-RhCG
HEK293-WT

Figure 7

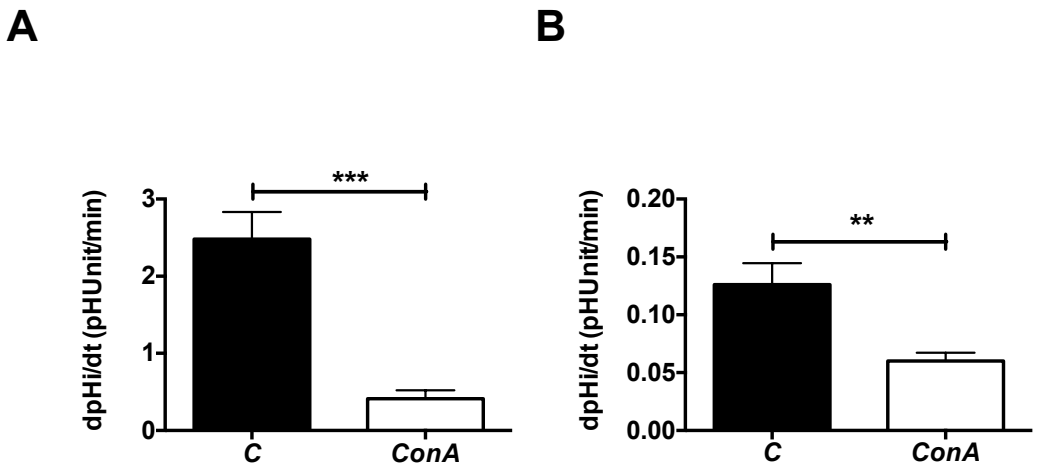
A
B
dpHi/dt (pHUnit/min)
3
2
1
0
***
C
ConA
dpHi/dt (pHUnit/min)
0.20
0.15
0.10
0.05
0.00
**
C
ConA

Figure 8

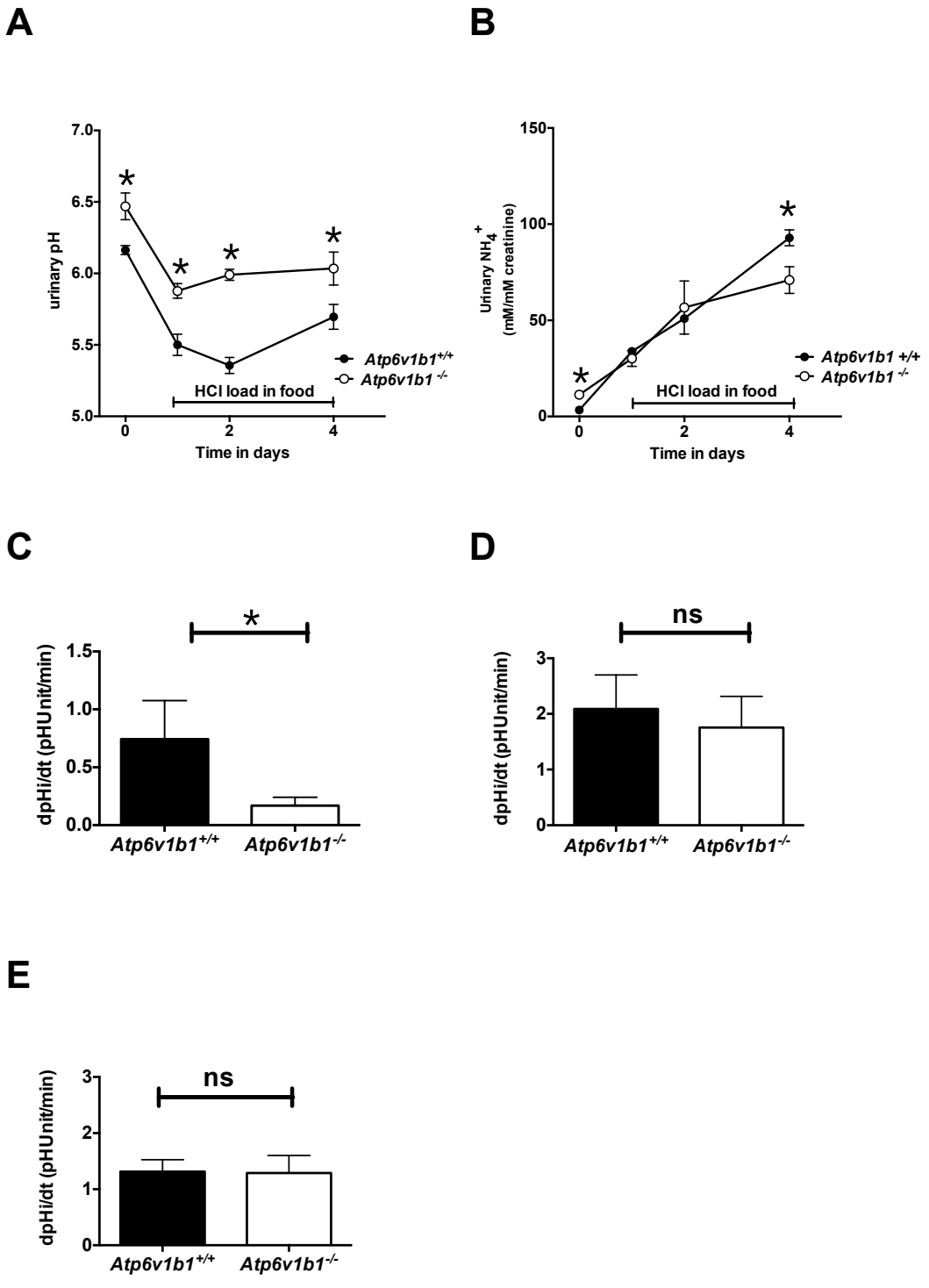
A
B
C
D
E
urinary pH
Time in days
HCl load in food
Atp6v1b1+/+
Atp6v1b1 -/-
Urinary NH4+ (mM/mM creatinine)
dpHi/dt (pHUnit/min)
ns
*

Supplementary data

Supplementary table 1. Primers and probes sequences of the gene expressions evaluated by RT-qPCR

Gene	Accession number	Forward primer	Reverse primer	Probe
Mouse *Atp6v1b1*	NM_134157	5'-CCCAGTATGCTGAGATTGTCAACTTTACCCTCC -3'	5'-CCTGAACAATGGCCTTGGTC-3'	5'-CCCAGTATGCTGAGATTGTCAACTTTACCCTCC-3'
Mouse *Atp6v1b2*	NM_007509	5'-GCTGGTGATCCTGACGGACATGAG-3'	5'-CGTGCCGGTCGAGTGGAAGGTAGAAACGG-3'	5'-CTGCGAGAGGTTTCAGCTG-3'
Mouse *Atp6V0a4*	NM_080467	5'-GACGGTGTCTCATCTATGGTTTGA-3'	5'-TTTGCCCTGCATGGTCTTGTC-3'	5'-TCTCTCCATTATCAAGAGCTCATGCCA-3'
Mouse *Hprt*	NM_013556	5′-TTATCAGACTGAAGAGCTACTGTAAGATC-3′	5′-TTACCAGTGTCAATTATATCTTCAACAATC-3'	5'-TGAGAGATCATCTCCACCAATAACTTTTATGTCCC-3'
Human *RhCG*	NM_016321	5'- CTACCGACGCAACCTAGAGC-3'	5'-GCTGTCCCCATGGTAGGATA-3	5'-CTTTGCCATGATTGGCACCC-3'
Human *ATP6V1B1*	NM_001692	5'-GAGATGATTCAGACGGGCATTT-3'	5'-CTGGTGAAGAAGTCCAAGGC-3'	5'-AATGAGATTGCCGCTCAGAT-3'
Human *ATP6V1B2*	NM_001693	5''-TGAAGGGACTTCAGGTATAGATGC-3'	5'-GGAAGTCTTCGGCCAGTACA-3'	5'-TGGTCGGGTATTCAATGGAT-3'
Human *ATP6V0A1*	NM_001130020	5'-TTCCTGGAACTGACCGAATTA-3'	5'-AGGAGTGCCTCTTCCCATCT-3'	5'-GAGGCTGAATTGCATCATCA-3'
Human *HPRT*	NM_000185	5'-AAGGGTGTTACGTTTAT-3'	5'-TATTTCCTGTGCGTGAT-3'	5'- ACCTCCTTGGGATCTATTTCACCG -3'

Supplementary table 2. Blood values in *Atp6v1b1*$^{+/+}$ *mice* and *Atp6v1b1*$^{-/-}$ *mice* under normal diet and HCl load for 4 days

	Basal status		2 days HCl		4 days HCl	
	C57BL6 (n=9)	*Atp6v1b1*$^{-/-}$ (n=7)	*C57BL6* (n=7)	*Atp6v1b1*$^{-/-}$ (n=6)	*C57BL6* (n=7)	*Atp6v1b1*$^{-/-}$ (n=5)
pH	7.35 ± 0.01	7.40 ± 0.01	7.11 ± 0.02*	7.15 ± 0.02*	7.24 ± 0.02	6.87 ± 0.12*$^{\#}$
pCO_2 (mmHg)	40.0 + 0.6	40.6 ± 1.2	37.3 ± 1.2	39.3 ± 1.5	39.4 ± 1.5	45.4 ± 2.5$^{\#}$
HCO_3 (mM)	21.6 + 0.7	24.8 ± 1.2	11.5 ± 0.8*	12.8 ± 0.6*	16.4 ± 0.9*	8.7 ± 1.8*$^{\#}$
pO_2	52.1 ± 2.2	48.8 ± 2.0	60.4 ± 2.4	62.6 ± 3.4	58.4 ± 2.5	83.8 ± 8.7*$^{\#}$
Na^+ (mM)	144.6 ± 0.5	145.4 ± 0.3	148.0 ± 1.1*	147.8 ± 1.5	151.4 + 0.5*	150.8 ± 2.4*
Cl^- (mM)	109.7 ± 0.6	108.3 ± 0.7	123.4 ± 1.6*	121.0 ± 1.5*	120.0 ± 1.6*	133.6 ± 2.8*$^{\#}$
Ca^{2+} (mM)	1.26 ± 0.01	1.23 ± 0.01	1.34 ± 0.01*	1.33 ± 0.02*	1.36 ± 0.02*	1.60 ± 0.1*$^{\#}$
Hb (g/dl)	15.1 ± 0.2	15.7 ± 0.2	15.6 ± 0.3	16.7 ± 0.2*$^{\#}$	15.3 ± 0.2	18.8 ± 1.2*$^{\#}$

* $p<0.05$ vs baseline period in same genotype, $^{\#}$ $p<0.05$ vs *Atp6v1b1*$^{+/+}$ mice during the same period.

Supplementary table 3. Weight, food intake and urinary values in *Atp6v1b1*$^{+/+}$ *mice* and *Atp6v1b1*$^{-/-}$ mice under normal diet and during an HCl load for 4 days

	Basal status		2 days HCl		4 days HCl	
	C57BL6 (n=7)	*Atp6v1b1*$^{-/-}$ (n=7)	*C57BL6* (n=7)	*Atp6v1b1*$^{-/-}$ (n=7)	*C57BL6* (n=7)	*Atp6v1b1*$^{-/-}$ (n=5)
Weight (g)	22.7 ± 0.28	28.1 ± 0.5$^{\#}$	20.4 ± 0.2*	24.6 ± 0.3*$^{\#}$	20.5 ± 0.3*	23.0 ± 0.3*$^{\#}$
Weight lose in % of body weight under basal status	0.1 ± 0.6	0.4 ± 0.9	10.3 ± 0.5*	13.0 ± 1.6*$^{\#}$	11.9 ± 3.4*	18.8 ± 2.7*$^{\#}$
Food intake (g/24hrs/body weight)	0.36 ± 0.01	0.36 ± 0.02	0.28 ± 0.01*	0.22 ± 0.03*	0.34 ± 0.04	0.26 ± 0.01*$^{\#}$
Water intake (ml/24hrs/body weight)	0.17 ± 0.05	0.05 ± 0.01$^{\#}$	0.20 ± 0.05	0.20 ± 0.04*	0.18 ± 0.03	0.23 ± 0.06*
Urine values						
volume (ml/24 h)	2.6 ± 0.4	3.0 ± 0.1	2.1 ± 0.2	4.7 ± 0.8$^{\#}$	3.1 ± 0.2	3.9 ± 1.2
creatinine excretion (µmol/24 h)	3.7 ± 0.6	3.4 ± 0.2	3.4 ± 0.4	1.8 ± 0.3*$^{\#}$	1.9 ± 0.2*	1.9 ± 0.7*
Urinary pH	6.2 ± 0.0	6.5 ± 0.1$^{\#}$	5.4 ± 0.1*	6.0 ± 0.0*$^{\#}$	5.7 ± 0.1*	6.0 ± 0.1*$^{\#}$
UNH_4/UCr (mEq/mmol)	3.4 ± 0.3	11.3 ± 1.2$^{\#}$	51.0 ± 2.0*	56.7 ± 13.8*	88.9 ± 6.2*	76.6 ± 7.2*$^{\#}$
UPi/UCr (mEq/mmol)	13.1 ± 1.1	11.6 ± 0.7	14.3 ± 2.4	18.8 ± 3.2	16.4 ± 2.6	22.7 ± 5.2

* $p<0.05$ vs baseline period in same genotype, $^{\#}$ $p<0.05$ vs *Atp6v1b1*$^{+/+}$ mice during the same period.

V Discussion

V.1 Implications of RhCG in disease

When RhCG-mediated NH_3 secretion was demonstrated*in vivo*by Biver and co-workers in 2008 asa critical pathway enabling final urinary acid excretion, RhCG appeared as a promising candidate involved in orphan dRTA[7]. Since then, the phenotype of *Rhcg*$^{+/-}$ mice was studied and revealed that one missing copyof the *Rhcg* gene is enough to induce incomplete metabolic acidosis[39]. This data reinforced our interest for looking for mutations of*RhCG* in dRTA patients who might more likely harbour heterozygous abnormalities of RhCG. However, the spectrum of severity found in dRTA is large ranging from the absence of symptoms when not challenged,to major effects in infancy with severe acidosis, impaired growth, and early nephrocalcinosis causing eventually renal insufficiency[47]. To date, no mutation of *RhCG* in humans has been linked to dRTA despite directly sequencing *RhCG* in a cohort of more than 50 patients with orphan dRTA (personal communication Vargas, R., Wagner, C.A., Houillier, P.). Furthermore, the two studies that raised the hypothesis of *RhCG* mutations in dRTA were performed on mice receiving NH_4Cl or HCl acid treatment, both considered as strong experimental acid-loads which are unlike physiological conditions[7,39]. Hence, it became of major interest to study*Rhcg* mutant animals in more commonly occurringconditions of increased urinary NH_4^+ excretion resembling what potential *RhCG* mutant patients could face.

Rhcg$^{-/-}$mice receiving a dietary acid-load of high animal protein diet, which approximated the typical western diet, were able to implement compensatory mechanisms in order to adapt the acid-load created by the metabolism of high protein. *Rhcg* heterozygous mice acid-base status was not affected by high protein intakes. Considering these data, it is tempting to speculate that the effect of *RhCG*mutations in humans would also be

compensated in physiological acid-loading conditions, preventing the apparition of a disturbance of the acid-base status in the mutation carriers, therefore decreasing further the chances to correlate *RhCG* to a pathological setting.

Nevertheless, the relevance of RhCG for the clinics may apply for other aspects. In normal kidneys, diets rich in animal proteins have been linked to the development of tubular-interstitial injury[63], and are generally suspected to have several negative impacts on renal function[68].In *Rhcg*$^{-/-}$ mice fed western diet-like high casein, the compensation mechanisms observed in the kidney proximal tubule and TAL were amplified compared to the response of normal kidneysto the same diet. Hence, one can speculate that human kidneys lacking *RhCG*or having reduced expression, in the long term, could develop chronic kidney disease from compensating their defect. The ability of normal kidneys to excrete acids progressively decreases with increasing age[84]. This phenotype might appear earlier or be more severe in humans harbouring a mutation of *RhCG*compared to a normally aging population.

Moreover, we observed in *Rhcg*$^{-/-}$an exaggerated bone resorption compared to the effect of high protein diet in animals with normal kidneys. Although the effect of the absence of *Rhcg* on bone measured in *Rhcg*$^{-/-}$ mice was not severe in these 3 months old animals, further experiments conducted on older animals receiving a longer high protein treatment than 9 days might reveal a stronger effect. This data raisealso the possibility of the implication of RhCG in bone pathologies. Among bone diseases, osteoporosis, which is characterized by a reduction in bone mass and a deterioration of bone architecture, appearing after the age of fourty[85] could constitute a possible consequence of *RhCG* impairment. Multiple causes lead to osteoporosis such as estrogene deficiency found in post-menauposal women, reduced vitamin D and increased PTH production or local factors and signalling molecules reducing bone formation or increasing resorption[86]. In *Rhcg*$^{-/-}$, higher levels of the bone resorption marker deoxypyrydinoline were paralleled by hypercalcemia, suggesting a possible altered status of vitamin D/PTH axis in the mice.

V.2 Regulation of RhCG expression and activity

Following analysis and interpretation of the data presented in three aimsof this dissertation we can suppose that different types of regulation of RhCG might exist.

Wildtype mice receiving 9 days high protein diet acid-load showed a transient increase in *Rhcg* mRNA levels suggesting that acidosis might induce a transcriptional regulation of Rhcg expression or an increase in *Rhcg* mRNA stabilization. The forkhead transcription factor Foxi1 is highly expressed in intercalated cells of kidneys and mice deficient for Foxi1 develop dRTA[87]. Furthermore, in intercalated cells of kidneys, Foxi1 is required for the expression of the A1, E2 and a4 subunits of the vacuolar H^+-ATPase[88]. RhCG, which is necessary to the normal function of vaculoar H^+-ATPasesin type-A intercalated cells of kidney CCDs, could also be a potential target of Foxi1. However, preliminary data indicate that *Foxi1*$^{-/-}$mice do not show reduced expression of *Rhcg* mRNA (Kampik N.B., unpublished results). In *Foxi1*$^{-/-}$ total kidney, the level of *Atp6v1b1* mRNA is highly reducedand no B1 protein can be detected by immunofluorescence in the distal nephron epithelia.The effect ofFoxi1on Rhcg protein expression is not known but it is likely that Rhcg protein abundance is not altered.

Studies in rat receiving a chronic HCl acid-load revealed that apical membrane abundance of Rhcg in OMCDs and in the base of the inner medulla are increased[89]. In the OMCD, this enhanced staining resulted from both increased total protein and changes in the subcellular distribution of Rhcg[90]. Hence, Rhcg function might also be regulated by trafficking, enabling a sustained adaptation to chronic metabolic acidosis. However, the exact mechanisms underlying this regulation have not been investigated yet.

As discussed before, metabolic acidosis alters gene expression and cellular localization of proteins involved in renal acid elimination but can also influence hormonalpathways as well as paracrine signalling. In response to

metabolic acidosis, the angiotensin II-aldosterone axis, as well as endothelin, show an increased production.

While glucocorticosteroids enhance ammoniagenesis in the proximal tubule, the distal tubule is the recognized site for the action of mineralocorticoids. In type-A intercalated cells of kidneys, aldosterone, but also angiotensin II[91], which stimulates aldosterone release in the adrenal gland, are strong stimuli for the activity of vacuolar H^+-ATPases[91,92]. The effect of both hormones appears to be mediated by intracellular Ca^{2+} increases activating H^+-ATPases in a Protein Kinase C dependent manner[93,94]. A similar pathway involving either aldosterone, angiotensin II or both could possibly regulate Rhcg activity and enhance the functional partnership observed between Rhcg and vacuolar H^+-ATPases in the collecting duct of kidney following an acid-load. Furthermore, in high protein acid-loaded kidneys, enhanced activity of H^+-ATPases by aldosterone was also reported following increased levels of the vasoactive substance endothelin[63].

Endothelin 1 was first discoveredas a potent endothelial-derived vasoconstrictor as well as a sodium-regulating peptide[95]. In kidneys, epithelial cells of the collecting duct are able to synthetize endothelin (ET_1)[95] and express endothelin receptors B (ET_B)[97]. Systemic but also paracrine production of endothelin 1 is increased during metabolic acidosis. Interestingly, ET1 paracrine production is also increased during a high protein diet, which leads to an acid load without blood gas disturbance[63]. In the proximal tubule, the apical Na^+/H^+ exchanger NHE3, which is involved in NH_4^+secretion and HCO_3^- reabsorption in this nephron segment, is increased by ET_1/ET_B receptors in response to metabolic acidosis[98]. RhCG activation mediated by ET_1/ET_B receptor inthe kidney collecting duct cells might exist and explain, at least in part, the origin of higher NH_4^+ excretion observed in mice after a high protein acid-load.

More paracrine factors such as nitric oxide (NO) or prostaglandinscould constitute plausible regulators of RhCG function. Nitric oxide is synthetized

endogenously from from L-arginine by various nitric oxide synthase (NOS) enzymes and is a powerful vasodilatator, a central nervous system neurotransmitter and plays also a role in immunity[99]. In intercalated cells of kidney CCDs, NO is produced by an inducible form of NOS and responsible for the inhibition of vacuolar H^+-ATPases activity[100], which might decrease the driving force of Rhcg mediated NH_3 passage. Prostaglandins are derived from the metabolism of arachidonic acid and produced by the action of the cyclooxygenase (COX) enzyme. In the kidney, they are produced in various nephron segments but thecollecting duct is the major site of renal prostaglandin production. Most of the available evidence indicates that the predominant effect of prostaglandins on renal function involves salt and water transport. Prostaglandin E2 (PGE2) appears to be involved in both water excretion and absorption but the underlying mechanisms are not fully understood and likely depend on which receptor is activated under a particular physiologic condition[101]. Studies in rat also revealed that prostaglandinsinhibit NH_3 synthesis in normal and mild metabolic acidosis conditions[102]. However, the role of prostaglandins in acid excretion by the renal collecting duct system has not been yet investigated. Our study of the response of *Rhcg*$^{+/+}$, *Rhcg*$^{+/-}$ *and Rhcg*$^{-/-}$miceto acidogenic high protein diet revealed altered urine concentration and urinary NH_4^+ excretion in *Rhcg*$^{-/-}$ versus wildtype. This response could reflect a particular action of PGE2 on Rhcg.

V.3 Molecular pathways of urinary NH_4^+ excretion in intercalated cells of kidney

In the third aim of the dissertation, we tried to detail the molecular pathway leading to the excretion of NH_4^+ in the intercalated cells of kidneys. Our first hypothesisof a potential partnership between Rhcg and the vacuolar H^+-ATPase was based on the evidence of the predominant role of Rhcg and H^+-ATPases in achieving urinary NH_4^+ excretion and the fact that *Rhcg*$^{-/-}$ mice excrete more alkaline urine. Our data in microperfused CCDs of *Rhcg*$^{+/+}$ and $^{-/-}$ mice and in the in vitro model of HEK cells overexpressing RhCG and wildtypetested this hypothesis and indicate that Rhcg enhances the activity of

the vacuolar H^+-ATPase. However, the mechanism underlying this effect is still unclear. In microperfused CCD of rabbit kidneys, intracellular NH_3levelsincrease H^+-K^+-ATPase-mediated proton secretion, and not vacuolar H^+-ATPase-mediated proton secretion[103]. This stimulus of the H^+/K^+-ATPase activitymost likely worksthrough increased insertion of the H^+/K^+-ATPase at the apical membrane mediated by vesicule associatedsoluble N-ethylmaleimide-sensitive fusion attachment receptor proteins (vSNARE)[104].In metabolic acidosis, the role of H^+/K^+-ATPases in acid excretion by collecting ducts becomes minor compared to vacuolar H^+-ATPases[105]. However, the more alkaline urine of *Rhcg*$^{-/-}$ mice is also detected at baseline[7]. Further experiments assessing the activity of the H^+/K^+-ATPase in *Rhcg*$^{-/-}$ mice in different conditions (baseline or following an acid-load) might help to understand better the mechanisms underlying the reduced proton excretion observed in *Rhcg*$^{-/-}$ mice.

The study performed on *Rhcg*$^{-/-}$ mice challenged with high casein acidogenic protein diet detailed further the mechanisms involvedin the renal collecting duct to manage a physiological acid-load. We showed that in the absence of Rhcg, a compensation of its lack exists,from the increased production of NH_4^+ to theshunting of its accumulation in the renal interstitium, whichis enough to allow a proper urinary NH_4^+ excretion. We described in *Rhcg*$^{-/-}$mice a mechanism of shunting interstitial NH_4^+ reabsorption prior to distal tubule transepithelial passage to enable a direct elimination of NH_4^+. However, this process might not fully explain how the lack of Rhcg mediated NH_3 transport does not impair final NH_4^+ formation in the lumen. The passive NH_3 diffusion across kidney CD cells might be different, or, another protein involved in NH_3 permeability in the collecting duct might exist.Genome-wide studies performed in mice receiving either 0, 4 or 7 days NH_4Cl acid-load enabled to uncover genes involved at various levels of the response to metabolic acidosis, including SNAT3, PDG and PEPCK[106]. A similar approach comparing the expression levels of the collecting duct genes of *Rhcg*$^{-/-}$ in conditions where the potential candidate involved in *Rhcg* compensation seems to be highly expressed such as chronic high casein protein diet, with conditions where increased urinary NH_4^+ excretion is not required such as

non-acidogenic high soy protein diet, might reveal unknown genes involved in urinary NH_4^+ excretion in the collecting duct.

VI Conclusion and perspectives

The present study confirmed that RhCG has a pivotal role in renal management of metabolic acid loads, revealed the importance of the protein in physiological acid-loading conditions and provided evidence for its concerted action with renal vacuolar H^+-ATPases in urine acidification.Notwithstanding, the question of RhCG relevance in pathology remains open. Likewise, the regulation of RhCGexpression and activity remains to be further elucidated and might provide a further molecular explanation for the collecting duct response to acid-base disturbances, a response obviously involving NH_3 permeability mechanisms still unknown.

VII References

1 Priestley, J. *Experiments and Observations on Different Kinds of Air*. (1774).

2 Goodwin, J. *A Dyer's Manual*. (1982).

3 Nash, T. P. J., Benedict, S.R. The ammonia content of the blood, and its bearing on the mechanism of acid neutralization in the animal organism. *J Biol Chem.***48**, 463-488 (1921).

4 Pitts, R. F., Lotspeich, W.D., Schiess, W. A., Ayer, J.L. The renal regulation of acid-base balance in man. I.The nature of the mechanism for acidifying the urine *J Clin Invest.***27**, 48-56 (1948).

5 Pitts, R. F. The renal regulation of acid base balance with special reference to the mechanism for acidifying the urine. *Science.***102**, 49-54 (1945).

6 Marini, A. M., Matassi, G., Raynal, V., André, B., Cartron, J.P., Chérif-Zahar, B. The human Rhesus-associated RhAG protein and a kidney homologue promote ammonium transport in yeast. *Nat Genet.***26**, 341–344 (2000).

7 Biver, S., Belge, H., Bourgeois, S., Van Vooren, P., Nowik, M.. Scohy, S., Houillier, P., Szpirer, J., Szpirer, C., Wagner, C. A., Devuyst, O., Marini, A. M. A role for Rhesus factor Rhcg in renal ammonium excretion and male fertility. *Nature.***456**, 339-343 (2008).

8 Wagner, C. A., Devuyst, O., Bourgeois, S., Mohebbi, N. Regulated acid-base transport in the collecting duct. *Pflugers Arch EJP.* **458**, 137-156 (2009).

9 Boron, W. F. *Medical Physiology,* 2nd edition, 851-866(2008).

10 Brenner and Rector's, *The Kidney*, 9th edition, 202-226 (2011).

11 Boron, W. F. Acid-base transport by the renal proximal tubule. *J Am Soc Neph.* **17**, 2368-2382 (2006)

12 Preisig, P., Hamm, L.L., Alpern, R. J., Cellular Mechanisms of Renal Tubular Acidification in Seldin and Giebisch's The Kidney: Physiology and Pathophysiology, 4th edition, 1539-1587 (2008).

13 Indiveri, C., Abruzzo, G., Stipani, I., Palmieri, F. Identification and purification of the reconstitutively active glutamine carrier from rat kidney mitochondria. *Biochem J.***333**, 285-290 (1998).

14 Sastrasinh, S., Sastrasinh, M. Glutamine transport in submitochondrial particles. *Am J Physiol.***257**, 1050-1058 (1989).

15 Curthoys, N. P. *Renal Ammonium Ion Production and Excretion*in Seldin and Giebisch's The Kidney: Physiology and Pathophysiology, 4th edition, 1601-1621(2008).

16 Nagami, G. T.Luminal secretion of ammonia in the mouse proximal tubule perfused in vitro.*J Clin Invest.* **81**(1): 159–164(1988).

17 Häussinger, D., Lamers, W.H., Moorman, A.F. Hepatocyte heterogeneity in the metabolism of amino acids and ammonia. *Enzyme.***46**, 72-93 (1992).

18 Buerkert, J., Martin, D., Trigg, D. Ammonium handling by superficial and juxtamedullary nephrons in the rat. Evidence for an ammonia shunt between the loop of Henle and the collecting duct. *J. Clin Invest.***70**, 1-12 (1982).

19 Good, D. W. Ammonium transport by the thick ascending limb of Henle's loop. *Ann Rev Physiol.***56**, 623-647 (1994).

20 Bourgeois, S., Meer, L.V., Wootla, B., Bloch-Faure, M., Chambrey, R., Shull, G.E., Gawenis, L.R., Houillier, P. NHE4 is critical for the renal ammonia handling in rodents. *J Clin Invest*. **120**(6):1895-904 (2010).

21 Houillier P., Bourgeois, S. More actors in ammonia absorption by the thick ascending limb. *Am J Physiol Renal Physiol*. **302**(3):F293-7 (2012).

22 Wagner, C. A., Finberg, K. E., Breton, S., Marshansky, V., Brown, D., Geibel, J. P. Renal vacuolar H+-ATPase. *Physiol rev.***84**, 1263-1314 (2004).

23 Star, R. A., Kurtz, I., Mejia, R., Burg, M.B., Knepper, M.A. Disequilibrium pH and ammonia transport in isolated perfused cortical collecting ducts. *Am J Physiol.***253**, 1232-1242 (1987).

24 Weiner, I. D. & Hamm, L. L. Molecular mechanisms of renal ammonia transport. *Ann rev physiology.***69**, 317-340 (2007).

25 Busque, S. M. The role and regulation of the Slc38a3 (SNAT3) glutamine transporter in the mouse, 2009.

26 Marini, A. M., Vissers, S., Urrestarazu, A., Andre, B. Cloning and expression of the MEP1 gene encoding an ammonium transporter in Saccharomyces cerevisiae. *EMBO.***13**(15): 3456-3463 (1994).

27 Ninnemann, O., Jauniaux, J. C., Frommer, W. B. Identification of a high affinity NH4+ ransporter from plants. *EMBO.***13**(15): 3464-3471 (1994).

28 Marini, A. M., Matassi, G., Raynal, V., André, B., Cartron, J.P., Chérif-Zahar, B. The human Rhesus-associated RhAG protein and a kidney homologue promote ammonium transport in yeast. *Nat Genet.***26**, 341-344 (2000).

29 Cherif-Zahar, B. Le Van Kim, C., Rouillac, C., Raynal, V., Cartron, J.P., Colin, Y. Organization of the gene (RHCE) encoding the human blood group RhCcEe antigens and characterization of the promoter region. *Genomics.***19**, 68-74 (1994).

30 Le van Kim, Mouro, I., Chérif-Zahar, B., Raynal, V., Cherrier, C., Cartron, J.P., Colin, Y.Molecular cloning and primary structure of the human blood group RhD polypeptide. *Proc Natl Acad Sci USA.***89**, 10925-10929 (1992).

31 Verlander, J.W., Miller, R.T., Frank, A.E., Royaux, I.E., Kim, Y.H., Weiner, I.D. Localization of the ammonium transporter proteins RhBG and RhCG in mouse kidneys. *Am J Physiol Renal Physiol.* **284**(2):F323-37 (2003)

32 Han, K.H., Lee, H.W., Handlogten, M.E., Whitehill, F., Osis, G., Croker, B.P., Clapp, W.L., Verlander, J.W., Weiner, I.D. Expression of the ammonia transporter family member, Rh B Glycoprotein, in the human kidney. *Am J Physiol Renal Physiol*. **304**(7):F972-81(2013).

33 Mak, D. D. O., Dang, B., I., Weiner, D., Foskett, J., Westhoff, C.M. Characterization of ammonia transport by the kidney Rh glycoproteins RhBG and RhCG. *Am J Physiol Renal Physiol.***290**, 297-305 (2006)

34 Chambrey, R., Goossens, D., Bourgeois, S., Picard, N., Bloch-Faure, M., Leviel, F., Geoffroy, V., Cambillau, M., Colin, Y., Paillard, M., Houillier, P.., Cartron, J. P., Eladari, D.Genetic ablation of Rhbg in the

mouse does not impair renal ammonium excretion. *Am J Physiol Renal Physiol.***289**, 1281-90 (2005)

35 Bishop, J.M., Verlander, J.W., Lee, H.W., Nelson, R.D., Weiner, A.J., Handlogten, M.E., Weiner, I.D. Role of the Rhesus glycoprotein, RhB glycoprotein, in renal ammonia excretion. *Am J Physiol Renal Physiol.* **299**(5):F1065-77 (2010).

36 Eladari, D., Cheval, L., Quentin, F., Bertrand, O., Mouro, I, Cherif-Zahar, B., Cartron, J.P., Paillard, M., Doucet, A., Chambrey, R. Expression of RhCG, a new putative NH(3)/NH(4)(+) transporter, along the rat nephron. *J Am Soc Nephrol.***13**(8): 1999-2008 (2002).

37 Yip, K.P., Kurtz, I. NH3 permeability of principal cells and intercalated cells measured by confocal fluorescence imaging.*Am J Physiol.* **269**(4 Pt 2):F545-50 (1995).

38 Lee, H.W., Verlander, J.W., Bishop, J.M., Nelson, R.D., Handlogten, M.E., Weiner, I.D. Effect of intercalated cell-specific Rh C glycoprotein deletion on basal and metabolic acidosis-stimulated renal ammonia excretion. *Am J Physiol Renal Physiol.***299**(2):F369-79 (2010).

39 Bourgeois, S., Bounoure, L., Christensen, E.I., Ramakrishnan, S.K., Houillier, P., Devuyst, O., Wagner, C.A. Haploinsufficiency of the ammonia transporter Rhcg predisposes to chronic acidosis: Rhcg is critical for apical and basolateral ammonia transport in the mouse collecting duct. *J. Biol Chem.***288**, 5518-5529 (2013).

40 Gruswitz, F., Chaudhary, S., Ho, J.D., Schlessinger, A., Pezeshki, B., Ho, C.M., Sali, A., Westhoff, C.M., Stroud, R.M. Function of human Rh based on structure of RhCG at 2.1 A. *Proc Natl Ac Sci USA.***107**, 9638-9643 (2010).

41 Katz, A. L. Renal Na-K-ATPase: its role in tubular sodium and potassium transport. *Am J Physiol.***242**, 207-219 (1982).

42 Haas, M. The Na-K-Cl cotransporters. *Am J Physiol.***267**, 8669-8685 (1994).

43 Alper, S. L. Molecular physiology and genetics of Na+-independent SLC4 anion exchangers. *J Exp Biol***212**, 1672-1683 (2009).

44 Wagner C.A., Devuyst, O., Belge, H., Bourgeois, S., Houillier, P. The rhesus protein RhCG: a new perspective in ammonium transport and distal urinary acidification. **79**(2):154-61 (2011)

45 Kraut, J. A., Madias, N. E. Metabolic acidosis: pathophysiology, diagnosis and management. *Nature rev Nephrol.***6**, 274-285 (2010).

46 Fry, A. C., Karet, F.E. Inherited renal acidosis. *Physiology.***22**, 202-211 (2007).

47 Karet, F. E. Inherited Distal Renal Tubular Acidosis. *J Am Soc Nephrol.***13**, 2178-2184 (2002)

48 Karet, F.E., Gainza, F.J., Györy, A.Z., Unwin, R.J., Wrong, O., Tanner, M.J., Nayir, A., Alpay, H., Santos, F., Hulton, S.A., Bakkaloglu, A., Ozen, S., Cunningham, M.J., di Pietro, A., Walker, W.G., Lifton, R.P. Mutations in the chloride-bicarbonate excnager AE1 cause autosomal dominant but non autosomal recessive distal renal tubular acidosis. *Proc Natl Acad Sci U S A*. **26**;95(11):6337-42 (1998).

49 Vargas-Poussou, R., Houillier, P., Le Pottier, N., Strompf, L., Loirat, C., Baudouin, V., Macher, M.A., Déchaux, M., Ulinski, T., Nobili, F., Eckart, P., Novo, R., Cailliez, M., Salomon, R., Nivet, H., Cochat, P., Tack, I., Fargeot, A., Bouissou, F., Kesler, G.R., Lorotte, S., Godefroid, N, Layet, V., Morin, G., Jeunemaître, X., Blanchard, A. Genetic investigation of autosomal recessive distal renal tubular acisosis: veidence for early sensorineural hearing loss associate with mutaion in the ATP6V0 gene. *J Am Soc Nephrol.***17**(5):1437-43 (2006).

50 Mohebbi, N., Vargas-Poussou, R., Hegemann, S.C., Schuknecht, B., Kistler, A.D., Wüthrich, R.P., Wagner, C.A. Homozygous and compound heterozygous mutations in the ATP6V1B1 gene in patients with renal tubular acidosis and sensorineural hearing loss. *Clin Genet.***83**, 274-278 (2013)

51 Stover, E.H., Borthwick, K.J., Bavalia, C., Eady, N., Fritz, D.M., Rungroj, N., Giersch, A.B., Morton, C.C., Axon, P.R., Akil, I., Al-Sabban, E.A., Baguley, D.M., Bianca, S., Bakkaloglu, A., Bircan, Z, Chauveau, D., Clermont, M.J., Guala, A., Hulton, S.A., Kroes, H., Li Volti, G., Mir, S., Mocan, H., Nayir, A., Ozen, S., Rodriguez Soriano, J., Sanjad, S.A., Tasic, V., Taylor, C.M., Topaloglu, R., Smith, A.N.,

Karet,F.E. Novel ATP6V1B1 and ATP6V0A4 mutations in auotsomal recessive distal renal tubular acidosis with new evidence for hearing loss. *J Med Genet.* **39**(11):796-803 (2002).

52 Kim, H.Y., Verlander, J.W., Bishop, J.M., Cain, B.D., Han, K.H., Igarashi, P., Lee, H.W., Handlogten, M.E., Weiner, I.D. Basolateral expression of the ammonia transporter family member Rh glycoprotein in mouse kidney. *Am J Physiol Renal Physiol.***296**(3):F543-55 (2009).

53 Jaeger, P., Karlmark, B., Giebisch, G. Ammonium transport in rat cortical tubule: relationship to potassium metabolism. *Am J Physiol.***245**, 593-600 (1983).

54 McKinney, T. D., Davidson, K.K. Effect of potassium depletion and protein intake in vivo on renal tubular bicarbonate transport in vitro. *Am J Physiol.***252**, 509-516 (1987).

55 Tannen, R. L., McGill, J. Influence of potassium on renal ammonia production. *Am J Physiol.***11**, 1178-1184 (1976).

56 Tannen, R. L. Relationship of renal ammonia production and potassium homeostasis. *Kidney Int.***11**, 453-465 (1977).

57 Busque, S. M., Wagner, C. A. Potassium restriction, high protein intake, and metabolic acidosis increase expression of the glutamine transporter SNAT3 (Slc38a3) in mouse kidney. *AmJ Physiol Renal physiol.***297**, F440-450 (2009).

58 Han, K. H., Lee, H.W., Handlogten, M.E., Bishop, J.M., Levi, M., Kim, J., Verlander, J.W., Weiner, I.D. Effect of hypokalemia on renal expression of the ammonia transporter family members, Rh B Glycoprotein and Rh C Glycoprotein, in the rat kidney. *Am J Physiol Renal physiol.***301**, 823-832 (2011).

59 Marieb, E. N., Hoehn, K. *Human Anatomy & Physiology*, 7th edition, 612-636 (2004).

60 Welbourbe, T. C., Givens, G., Joshi, S. Renal ammoniagenesis response to chronic acid loading: Role of glucocorticoids. *Am J Physiol.***254**, 134-138 (1988).

61 Waybill, M. M., Clore, J.N., Emerick, R.A., Watlington, C.O., Schoolwerth, A.C. Effects of corticosteroids on urinary ammonium excretion in humans. *J Am Soc Nephrol.***4**, 1531-1537 (1994).

62 Higashlhara, E., Carter, N.W., Pucacco, L., Kokko, J.P. Abdosterone effects on papillary collecting duct pH profile of the rat. *Am J Physiol.***246**, 725-731 (1984).

63 Wesson, D. E., Nathan, T., Rose, T., Simoni, J., Tran, R. M. Dietary protein induces endothelin-mediated kidney injury through enhanced intrinsic acid production. *Kidney Int.***71**, 210-217 (2007).

64 Remer, T. Influence of nutrition on acid-base balance-metabolic aspects. *Eur J Nutr.***40**, 214-220 (2001).

65 Nakamura, H., Ito, S., Ebe, N., Shibata, A. Renal effects of different types of protein in healthy volunteer subjects and diabetic patients. *Diabetes care.***16**, 1071-1075 (1993).

66 Friedman, A. N. High-protein diets: Potential effects on the kidney in renal health and disease. *Am J Kidney Dis.***44**, 950-962 (2004).

67 Bernstein, A. M., Treyzon, L., Li, Z. Are high-protein, vegetable-based diets safe for kidney function? A review of the literature. *J Am Diet Assoc.***107**, 644-650 (2007).

68 Odermatt, A. The Western-style diet: a major risk factor for impaired kidney function and chronic kidney disease. *Am J Physiol Renal Physiol.***301**, F919-931 (2011).

69 Foundation, T. N. K. KDOQI Clinical Practice Guidelines and Clinical Practice Recommendations for Diabetes and Chronic Kidney Disease (2007).

70 Pedrini, M. T., Levey, A.S., Lau, J., Chalmers, T.C., Wang, P.H. The effect of dietary protein restriction on the progression of diabetic and nondiabetic renal diseases: a meta-analysis. *Ann Intern Med.***124**, 627-632 (1996).

71 Khanna, A., Simoni, J., Hacker, C., Duran, M. J., Wesson, D. E. Increased endothelin activity mediates augmented distal nephron acidification induced by dietary protein. *J Am Soc Neph.***15**, 2266-2275 (2004).

72 Wesson, D. E., Simoni, J. Increased tissue acid mediates a progressive decline in the glomerular filtration rate of animals with reduced nephron mass. *Kidney Int.***75**, 929-935 (2009).

73 Khanna, A., Simoni, J., Wesson, D. E. Endothelin-induced increased aldosterone activity mediates augmented distal nephron acidification as a result of dietary protein. *J AmSoc Nephrol.***16**, 1929-1935, (2005).

74 Remer, T., Manz, F. Dietary protein as a modulator of the renal net acid excretion capacity: Evidence that an increased protein intake improves the capability of the kidney to excrete ammonium. *Nutr Biochem.***6**, 431-437 (1995).

75 Barzel, U. S., Massey, L.K. Excess dietary prot can adversely affect bone. *J Nutr.* 128, 1051–1053 (1998).

76 Darling, A. L., Millward, D. J., Torgerson, D. J., Hewitt, C. E., Lanham-New, S. A. Dietary protein and bone health: a systematic review and meta-analysis. *Am J Clin Nutr.***90**, 1674-1692 (2009).

77 Doucet, A. H+, K(+)-ATPASE in the kidney: localization and function in the nephron. *Exp Nephrol.***5**, 271-276 (1997).

78 Forgac, M. Structure, mechanism and regulation of the clathrin-coated vesicle and yeast vacuolar H+-ATPases. *J Exp Biol.***203**, 71-80 (2000).

79 Couloigner, V., Teixeira, M., Hulin, P., Sterkers, O., Bichara, M., Escoubet, B., Planelles, G., Ferrary, E. Effect of locally applied drugs on the pH of luminal fluid in the endolymphatic sac of guinea pig. *Am J Physiol Regul Integr Comp Physiol.***279**, 695-700 (2000).

80 Brown, D., Smith, P.J., Breton, S. . Role of V-ATPase-rich cells in acidification of the male reproductive tract. *J Exp Biol.***200**, 257-262 (1997).

81 Nelson, H., Nelson, N. Disruption of genes encoding subunits of yeast vacuolar H+-ATPase causes conditional lethality. *Proc NatlAcad Sci USA.***87**, 3503-3507 (1990).

82 Schulz, N., Dave, M.H., Stehberger, P.A., Chau, T., Wagner, C.A. Differential localization of vacuolar H+-ATPases containing a1, a2, a3, or a4 (ATP6V0A1-4) subunit isoforms along the nephron. *Cell Physiol Biochem.***20**, 109-120 (2007).

83 Forgac, M., Vacuolar ATPases: rotary proton pumps in physiology and pathophysiology. *Nat rev Mol Cell Biol,***8**(11): 917-29 (2007)

84 Frassetto, L. A., Morris, R.C. Sebastian, A. Effect of age on blood acid-base composition in adult humans: role of age-related renal functional decline. *Am J Physiol.***271**, 1114-1122 (1996).

85 Rodan, G. A., Martin, T.J. Therapeutic Approaches to Bone Diseases. *Science.***289**, 1508-1514 (2000).

86 Raisz, L. G. Pathogenesis of osteoporosis: concepts, conflicts, and prospects. *J Cli Invest.***115**, 3318-3325 (2005).

87 Blomqvist, S. R., Vidarsson, H., Fitzgerald, S., Johansson, B.R., Ollerstam, A, Brown, R., Persson, A.E., Bergström, G. Gö., Enerbäck, S,. Distal renal tubular acidosis in mice that lack the forkhead transcription factor Foxi1. *J Clin Invest.***113**, 1560-1570 (2004).

88 Vidarsson, H., Westergren, R., Heglind, M., Blomqvist, S.R., Breton, S., Enerbäck, S. The forkhead transcription factor Foxi1 is a master regulator of vacuolar HATPase proton pump subunits in the inner ear, kidney and epididymis. *PloS one.***4**, e4471 (2009).

89 Seshadri, R. M., Klein, J.D., Smith, T., Sands, J.M., Handlogten, M.E., Verlander, J.W., Weiner, I.D. Changes in subcellular distribution of the ammonia transporter, Rhcg, in response to chronic metabolic acidosis. *Am J Physiol Renal Physiol.***290**, 1443-1452 (2006).

90 Seshadri, R.M., Klein, J.D., Kozlowski, S., Sands, J.M., Kim, Y.H., Han, K.H., Handlogten, M.E., Verlander, J.W., Weiner, I.D. Renal expression on the ammonia transporters, Rhbg and Rhcg, in response to chronic metabolic acidosis. Am J Physiol Renal Physiol 290(2):F397-408 (2006)

91 Rothenberger, F., Velic, A., Stehberger, P.A., Kovacikova, J., Wagner, C.A. Angiotensin II stimulates vacuolar H+ -ATPase activity in renal acid-secretory intercalated cells from the outer medullary collecting duct. *J AmSoc Nephrol.***18**, 2085-2093 (2007).

92 Hays, S. R. Mineralocorticoid modulation of apical and basolateral membrane H+/OH-/HCO 3- transport processes in the rabbit inner stripe of outer medullary collecting duct. *J Clin Invest.***90**, 180-187 (1992).

93 Winter, C., Schulz, N., Giebisch, G., Geibel, J. P., Wagner, C.A. Nongenomic stimulation of vacuolar H+-ATPases in intercalated renal

tubule cells by aldosterone. *Proc Nat Acad Sci USA.***101**, 2636-2641 (2004).

94 Winter, C., Kampik, N.B., Vedovelli, L., Rothenberger, F., Paunescu, T.G., Stehberger, P.A., Brown, D., John, H., Wagner, C.A. Aldosterone stimulates vacuolar H(+)-ATPase activity in renal acid-secretory intercalated cells mainly via a protein kinase C-dependent pathway. *American journal of physiology. Cell Physiol.***301**, 1251-1261 (2011).

95 Yanagisawa, M., Kurihara, H., Kimura, S. A novel potent vasoconstrictor peptide produced by vascular endothelial cells. *Nature*.**332**, 415-441 (1988)

96 Kohan, D.E, Endothelins in the normal and diseased kidney.*Am J Kidney Dis.* **29**: 2–26 (1997).

97 Terada, Y., Ktomita, H., Nonoguchi, H., Marumo F. Different localization of two types of endothelin receptor mRNA in microdissected rat nephron segments using reverse transcription and PCR assay. *J Clin Inves.t***90**: 107–112 (1992).

98 Laghmani, K., Preisig, P.A., Moe, O.W., Yanagisawa, M., Alpern, R.J. Endothelin-1/endothelin-B receptor-mediated increases in NHE3 activity in chronic metabolic acidosis.*J Clin Invest*. **107**(12):1563-9 (2001).

99 Röszer, T. The biology of subcellular Nitric Oxide.*Springer* (2012).

100 Tojo, A., Guzman, N.J., Garg, L.C., Tisher, C.C., Madsen, K.M. Nitric oxide inhibits bafilomycin-sensitive H(+)-ATPase activity in rat cortical collecting duct. *Am J Physiol***267**(4 Pt 2): F509-15 (1994)

101 Olesen, E.T., Fenton, R.A., Is there a role for PGE2 in urinary concentration? *J Am Soc Nephrol***24**(2): 169-178 (2013)

102 Jones, E.R., Beck, T.R., Kapoor, S., Shay, R., Narins, R.G. Prostaglandins inhibit renal ammoniagenesis in the rat *J Clin Invest*. **74**(3): 992–1002 (1984)

103 Frank, A.E., Wingo, C.S., Weiner, I.D. Effect of ammonia on bicarbonate transport in the collecting duct. *Am J Physiol Renal Physiol*. **278**(2):F219-26 (2000)

104 Frank, A. E., Wingo, C.S., Andrews, P.M., Ageloff, S., Knepper, M.A., Weiner, I.D. Mechanisms through which ammonia regulates cortical collecting duct net proton secretion. American journal of physiology. Renal physiology **282,** 1120-1128 (2002)

105 Tsuruoka, S., Schwartz, G. J. Adaptation of rabbit cortical collecting duct HCO−3 transport to metabolic acidosis in vitro.*J. Clin. Invest***97**, 1076-1084 (1996).

106 Nowik, M., Lecca, M.R., Velic, A., Rehrauer, H., Brändli, A.W., Wagner, C.A. Genome-wide gene expression profiling reveals renal genes regulated during metabolic acidosis. Physiol Genomics **32**(3): 322-34 (2008)

VIII Acknowledgements

I would like to thank Prof. Dr. Carsten Alexander Wagner for giving me the chance to accomplish my PhD studies with quality projects that I enjoyed to contribute to.
I also thank him for his supervision and financial support throughout my PhD studies.

I would like to thank Dr. Soline Bourgeois for all the technical and intellectual knowledge she shared with me with patience. Without her great supervision, I would not have been able to complete my PhD studies in the same way.

I would also like to thank my colleagues in the lab for their fruitful ideas and discussions and the joyful working ambiance they created. For the later, I address a special thank to Kessara Chan.

I thank my fiancé, Dr. Nicolas Perony for his constant encouragements and for making my life fantastic.

To Okko who supported me more than he realises during the time I was writing this dissertation.

The biggest acknowledgement goes finally to my parents who always did everything they could to encourage and support me to study. They gave me the most important advise to succeed: “Do whatever you like, as long as you do it with love and passion”.